

Principles of Protein Folding

Rudi Glockshuber

Institute of Molecular Biology and Biophysics

ETH Zurich

HS 2019

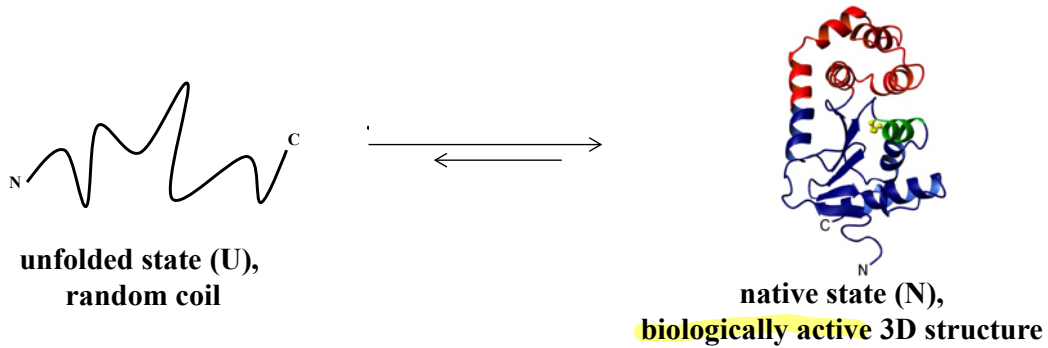
Table of content

| | | |
|------|--|----|
| 1. | Anfinsen's principle and the protein folding problem | 3 |
| 2. | Spectroscopic techniques for studying protein folding and conformational transitions in proteins | 8 |
| 2.1. | Absorption spectroscopy | 8 |
| 2.2. | Fluorescence spectroscopy | 11 |
| 2.3. | Circular dichroism spectroscopy | 14 |
| 3. | The two-state model of protein folding and the experimental determination of thermodynamic protein stability | 18 |
| 4. | The temperature dependence of protein stability | 26 |
| 5. | Kinetics of protein folding | 34 |
| 5.1. | Direct folding from the unfolded to the native state via a single transition state | 34 |
| 5.2. | Folding intermediates and their consequences for protein folding kinetics | 45 |
| 6. | Slow reactions in protein folding | 52 |
| 6.1. | Proline <i>cis/trans</i> isomerization as the rate-limiting step in protein folding | 52 |
| 6.2. | Disulfide bond formation as the rate-limiting step in protein folding | 56 |
| 7. | Analysis of complex folding reactions: Test for native molecules by interrupted refolding experiments | 65 |
| 8. | References | 70 |

1. Anfinsen's principle and the protein folding problem

Average length 350 Å

Protein folding is the process in which an unstructured (unfolded) polypeptide chain reacts to its unique, biologically active (three-dimensional structure, the native state N. This reaction is spontaneous and reversible (Scheme 1):



Scheme 1: Two-state equilibrium of protein folding

The protein folding reaction is a miraculous product of molecular evolution: Assume that you are analyzing the folding reaction of a specific protein at a protein concentration of $1 \mu\text{M}$ in a 1 mL test tube. The starting point of the reaction will then be a mixture of $6 \cdot 10^{14}$ flexibly disordered (unfolded) polypeptide chains with identical covalent structure (identical amino acid sequence). Prior to folding, each of these unfolded polypeptide chains will adopt a different three-dimensional structure due to different combinations of φ, ψ angles at each peptide bond and different dihedral angles in the amino acid side chains that all rapidly fluctuate in the unfolded state. These different structures of the unfolded protein are very similar in their free energies and thus can be treated as a single state, the unfolded state U. Under physiological conditions, each of these $6 \cdot 10^{14}$ molecules with different structures will then spontaneously fold to exactly the same tertiary structure! The following conclusions can be drawn from this intriguing observation:

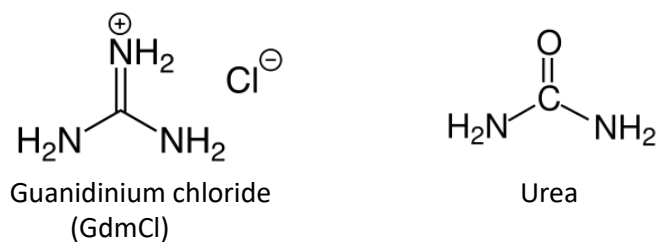
1. The entire information for the unique three-dimensional structure of the native state of a protein is completely contained in its amino acid sequence (Anfinsen principle) [1]. In other words: The covalent structure of a protein contains its folding code. Without this folding code, the genetic code would be meaningless, because only the native state is biologically active.
2. The folding code is a product of molecular evolution and evolved via multiple, successive, random amino acid replacements that eventually enabled a polypeptide chain to spontaneously adopt a defined tertiary structure with a specific activity that provided an advantage under selective pressure.
3. The biologically active, native state N is the thermodynamically most stable state under physiological conditions.

Condition in the cell
(pH, temperature ...)

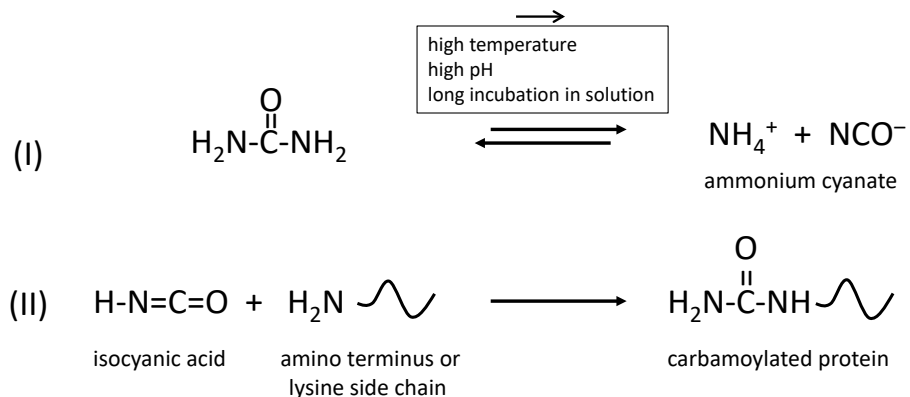
Condition for unfolding: urea
guanidium chloride
often used now

Despite the fact that the amino acid sequence of a polypeptide chain defines its native tertiary structure, it is still impossible to date to calculate the three-dimensional structure of a protein from its primary structure. This unsolved problem is termed the “**protein folding problem**” [2]. The solution of the protein folding problem would have dramatic consequences for basic and applied research and medicine! It would not only make protein structure determination by X-ray crystallography, NMR spectroscopy or electron microscopy obsolete, but would allow the prediction of the amino acid sequences of novel proteins with prescribed binding properties, catalytic properties or even novel folds and thus revolutionize the development of therapeutic proteins or new catalysts for biotechnology. There is no simple answer to the question of why the protein folding problem is so difficult, but it is evident that multiple unknown factors contribute to its complexity. These include the energetics of site-specific contributions of noncovalent intramolecular interactions (H-bonds, electrostatic and van der Waals interactions and hydrophobic interactions) in the native and unfolded state of proteins, the exact mechanisms that allow proteins to fold extraordinarily fast, and computer algorithms for structure prediction [2].

In the following, we focus on experimental strategies for characterizing the protein folding reaction *in vitro*. Analysis of protein folding *in vitro* makes use of the fact that certain organic molecules, termed **denaturants**, shift the folding equilibrium towards the unfolded state in a concentration-dependent manner. The most common denaturants are guanidinium chloride (GdmCl) and urea:



GdmCl is the most frequently used denaturant used in protein folding studies. It is a stronger denaturant than urea (see below) and its use avoids the irreversible carbamoylation of primary amino groups in proteins than may occur upon prolonged incubation of proteins with urea due to the slow dissociation of urea to ammonium cyanate (Scheme 2).



Scheme 2: Carbamoylation of primary amino groups in proteins by isocyanic acid formed after dissociation of urea to ammonium cyanate

For the analysis of the protein folding reaction *in vitro*, the protein of interest is first converted to its fully unfolded state by mixing it with high concentrations of GdmCl or urea. The refolding reaction is then initiated by rapid dilution (10–100fold) of the unfolded protein solution with a physiological buffer to a final (low) denaturant concentration at which the native state is more stable than the unfolded state.

It turns out that spontaneous folding of small, one-domain proteins occurs surprisingly fast, which is maybe best illustrated by the **Levinthal Paradox** [3]: If we assume *in a thought-experiment* that a small protein of 100 amino acids has three possible conformations per amino acid residue (different *phi* and *psi* angles of the polypeptide backbone and different side chain conformations), this translates into $3^{100} = 5.2 \cdot 10^{47}$ possible structures that the polypeptide chain can adopt. How long would it take to find the single structure of the native state N in a random search for N? If we assume that a single conformational change occurs with a half-life of the rotation around a C-C bond ($\sim 10^{-13}$ s), the molecule would require $5.2 \cdot 10^{47} \times 10^{-13}$ s = $1.6 \cdot 10^{27}$ years to find N, which is many orders of magnitude longer than the age of the universe ($13.8 \cdot 10^9$ years). However, the *experimentally observed* half-lives of protein folding are in the range of 10^{-3} s for small one-domain proteins to several hours for some large proteins and protein assemblies. Consequently, proteins do not need to probe all possible conformations in their search for N. Instead, the folding reaction is cooperative. This means that once a contact between a pair of residues that also occurs in N (native contact) is established in an initial stage of the folding process, it favors the formation of neighboring native contacts. This mechanism i) stabilizes native contacts so that they are not dissolved again but maintained during the further search for N ii) makes native interactions the more favorable the more native interactions are already formed and iii) dramatically reduces the number of conformational states that need to be probed to find N. In addition, the cooperativity of folding indicates that the folding pathway is mainly dictated by interactions that are also present in N. As the folding reaction can start from any possible unstructured state U, there is however not a single, unique folding pathway that any molecule needs to

follow. Instead, multiple pathways are leading to the thermodynamically most stable state N. A frequent and useful graphical representation of the existence of multiple folding pathways is the funnel-shaped energy landscape model of the protein folding process (Figure 1):

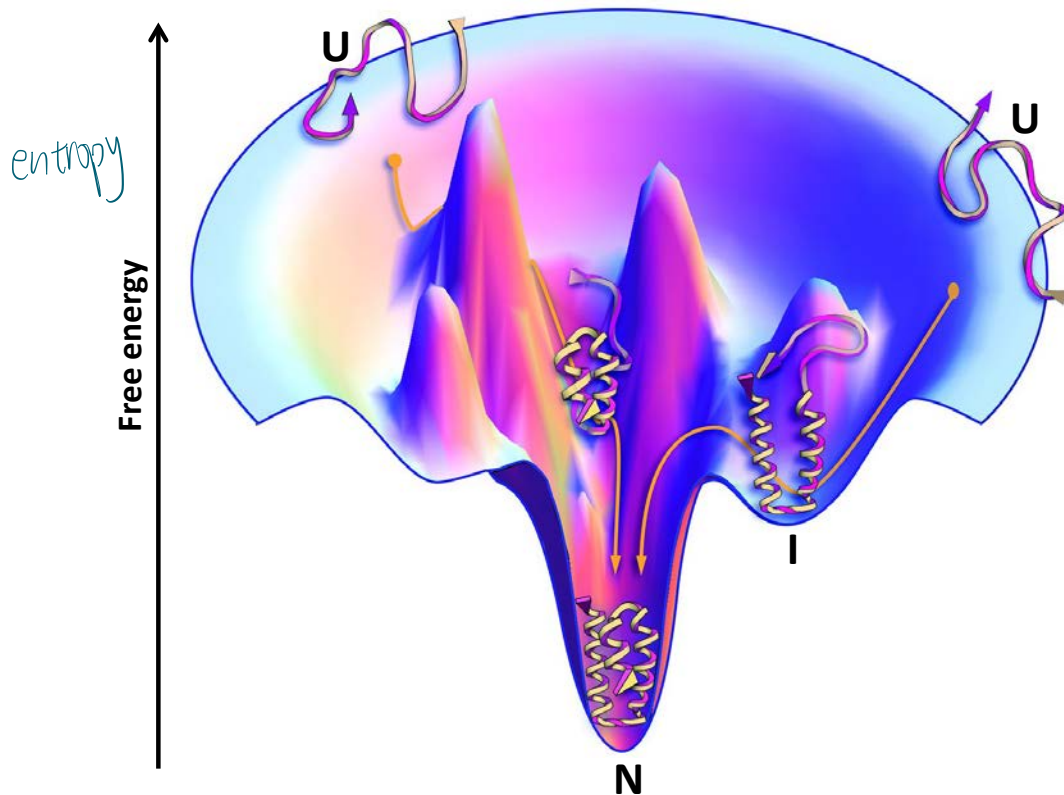


Figure 1: The protein folding funnel: Proteins have a huge number of unfolded, high-energy states (U), but only a few low-energy, folded structures (structured intermediates I and N) of which N is the thermodynamically most stable state under physiological conditions (adapted from Dill and MacCallum, Science 2012; 338, 1042-1046).

The protein folding reaction can start from any unfolded structural state. All these states are very similar in their free energy. In some cases (left pathway in Figure 1), the folding reaction is mainly downhill on the energy landscape (without population of structured intermediates), in other cases (right pathway in Figure 1), the folding molecule may fall into a local minimum on the energy landscape and transiently populate a (partially) structured intermediate I that further reacts to N. As will be discussed below, the formation of a structured intermediate slows the folding reaction because a larger activation energy barrier needs to be overcome in the reaction from I to N. Consequently, a protein folding reaction is not necessarily uniform (with a single folding half-life for all molecules), but may be a mixture of fast and slow folding species. The folding funnel model also nicely illustrates the cooperativity of the folding process because the funnel becomes the steeper the closer the folding molecule approaches N. This is because the more native interactions are formed during folding, the more they favor the formation of further native interactions. In the simplest case, when no structured intermediates are populated during the folding of a specific protein (smooth energy landscape), the consequence is that the folding reaction becomes an *all-or-nothing reaction*,

so that the protein is either completely unfolded or completely folded under physiological conditions. This simplest case of protein folding and more complex cases will be discussed below in detail.

Let us consider another “thought experiment” that illustrates the cooperativity of folding of a polypeptide in which the native state is stabilized by n hydrogen bonds. We make the following assumptions:

- Formation of the first H-bond is energetically unfavorable ($K = [1H]/[U] = 10^{-4}$).
- Formation of every additional H-bond becomes 10 times more favorable than formation of the previous one.

$$K_{eq} = \frac{[N]}{[U]} = \frac{K_F}{K_U}$$

Under these prerequisites, only 1 in 10^7 molecules would be native after attainment of the **folding equilibrium** if N only contained 2 H-bonds, because $[N]/[U] = [2H]/[U] = 10^{-4} \cdot 10^{-3} = 10^{-7}$. If N contained 3 H-bonds, only 1 in 10^9 molecules would be native: $[N]/[U] = 10^{-4} \cdot 10^{-3} \times 10^{-2} = 10^{-9}$. Eventually, however, N will become more stable than U when the number of H-bonds that stabilize N reaches a critical threshold:

N has 9 H bonds: $K = [N]/[U] = 10^{-4} \cdot 10^{-3} \cdot 10^{-2} \cdot 10^{-1} \cdot 10^{-0} \cdot 10^1 \cdot 10^2 \cdot 10^3 \cdot 10^4 = 10^0 = 1:1$;

N has 10 H bonds: $K = [N]/[U] = 10^{-4} \cdot 10^{-3} \cdot 10^{-2} \cdot 10^{-1} \cdot 10^{-0} \cdot 10^1 \cdot 10^2 \cdot 10^3 \cdot 10^4 \cdot 10^5 = 10^5:1$.

In more general terms, this theoretical example shows that

- many mutually stabilizing, intramolecular interactions are required for a significant population of N after attainment of the folding equilibrium and
- partially structured states are not significantly populated after attainment of the folding equilibrium.

This is in full agreement with the observation that short peptides composed of e.g. 10–30 amino acids are not capable for forming a defined three-dimensional structure and remain intrinsically disordered under physiological conditions. They are simply too small for formation of enough mutually stabilizing interactions. Indeed, the minimum length of a polypeptide chain required for formation of a defined three-dimensional structure is about 30–50 amino acids.

2. Spectroscopic techniques for studying protein folding and conformational transitions in proteins

The main spectroscopic techniques used for studying protein folding in solution are fluorescence and circular dichroism (CD) spectroscopy, and sometimes absorption spectroscopy [4]. Absorption and CD spectroscopy in protein folding make use of the fact that native and unfolded proteins interact differently with electromagnetic radiation in the ultraviolet (UV) range between 180 and 310 nm, while native and unfolded proteins emit light with different intensity in the range of 300–450 nm.

2.1. Absorption spectroscopy

Absorption is the process in which a photon is absorbed by a molecule and the absorbed energy is converted to heat. Upon absorption of a photon, the molecule is converted from its electronic singlet ground state S_0 to its excited electronic singlet state S_1 . This process is extremely rapid and occurs within $\sim 10^{-15}$ seconds. Depending on the absorbing molecule, the lifetime of S_1 is in the range of $\sim 10^{-13}$ to $\sim 10^{-9}$ seconds before it again reaches the ground state S_0 . In absorption spectroscopy, the sample in a cuvette with the pathlength d is excited with monochromatic light with the intensity I_0 , and the intensity of the light that passes the sample, I , is detected (Figure 2).

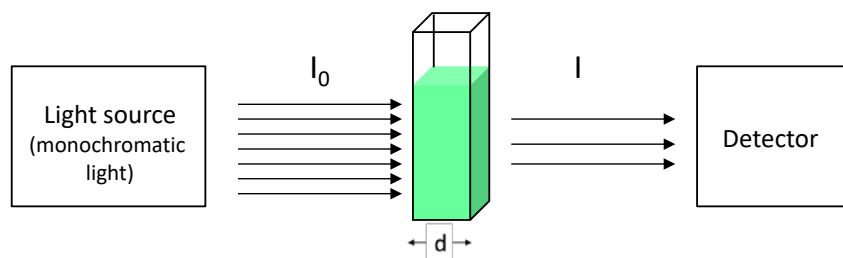


Figure 2: Schematic representation of an absorption measurement.

The absorption A of the sample is given by equation 1:

$$A = \frac{I_0}{I} \quad (\text{dimensionless}) \quad (1)$$

The Lambert-Beer law describes the dependence of the measured absorption A on the concentration c of the absorbing substance, the pathlength d and the molar extinction coefficient ε of the substance (eq. 2):

$$A = \varepsilon \cdot c \cdot d \quad (2)$$

The molar extinction coefficient ε (unit: $M^{-1}cm^{-1}$) corresponds to the absorption of a 1 M solution of the substance in a cuvette with a pathlength of 1 cm at a given wavelength. The absorbance is thus directly proportional to the concentration of the substance.

The absorption spectrum of a substance is obtained when its absorption is recorded at different wavelengths. Figure 3 shows the typical UV absorption spectrum of a protein that does not contain chromogenic cofactors (e.g. FAD or heme):

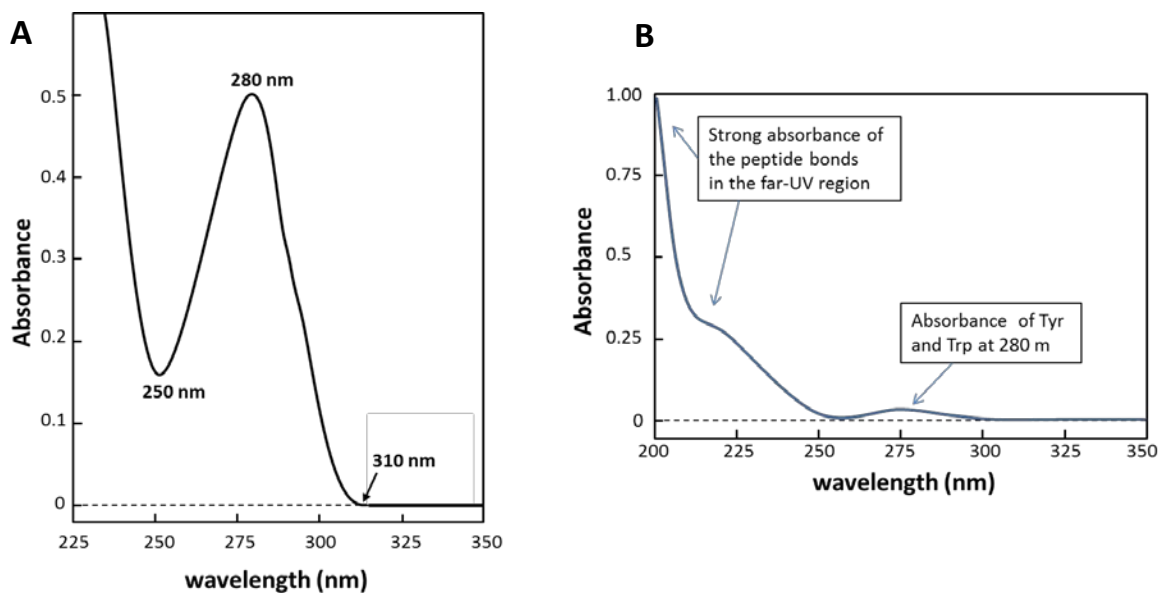


Figure 3: Typical absorption spectrum of a protein lacking chromogenic cofactors. A) Spectrum recorded between 225 and 350 nm. B) Spectrum of the same protein recorded between 200 and 350 nm and at 15-fold lower concentration compared to A).

Absorption spectra of proteins show a maximum at 280 nm, a minimum around 250 nm and no absorption above 310 nm (Figure 3A). The maximum at 280 nm comes from the sum of the individual absorption contributions of all tyrosine (Tyr) and tryptophan (Trp) residues in the protein (Figure 4). In addition, disulfide bonds also contribute to the maximum at 280 nm to a small extent.

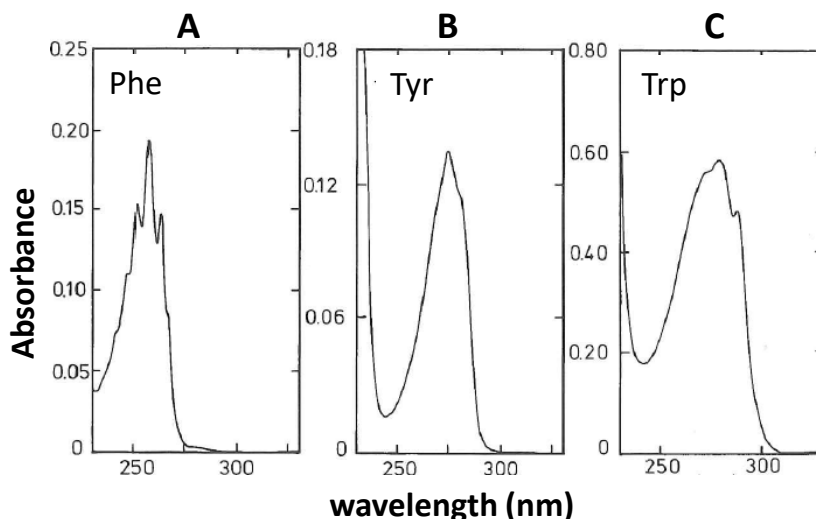


Figure 4: Absorption spectra of the three aromatic amino acids at pH 7.0. A) 1 mM Phe; B) 0.1 mM Tyr; C) 0.1 mM Trp. Note that phenylalanine (Phe) does not absorb at 280 nm, and that Tyr does not absorb light above 295 nm. Adapted from Schmid FX, The protein folding handbook, 22-44, Wiley, 2005).

Consequently, the molar extinction coefficient of a protein can be calculated from the number n of its tyrosines, tryptophans and disulfide bonds, and the molar extinction coefficients of

Tyr, Trp and disulfide bonds, which have values of 1490, 5500 and 125 M⁻¹cm⁻¹, respectively (eq. 3):

$$\epsilon_{280 \text{ nm, calculated}} = (n_{\text{Tyr}} \cdot 1490 + n_{\text{Trp}} \cdot 5500 + n_{\text{SS}} \cdot 125) \text{ M}^{-1}\text{cm}^{-1} \quad (3)$$

Trp not only shows a 3.7-fold higher absorption at 280 nm than Tyr. It also still absorbs light between 295 and 310 nm, while Tyr shows no absorption above 295 nm. As Trp is a rare amino acid compared to Tyr, it may occur that a small protein of e.g. 100 residues does not contain a single Trp residue. This can be readily seen from its lacking absorption above 295 nm. As an example, Figure 5 shows the absorption spectra of the enzyme ribonuclease T1, which has a single Trp residue, and its Trp-free variant. The fact that Trp is the only amino acid that still absorbs light at 295 nm can be used in fluorescence spectroscopy: Excitation of the protein at 295 nm will only excite its Trp residues and thus allow selective monitoring of conformational changes around these Trp residues (see below).

The absorption spectra of native and unfolded proteins are generally very similar. Thus, although Tyr and Trp residues are often buried in the hydrophobic core of folded proteins compared to their exposure to solvent in the unfolded state, this has no strong influence on their absorption properties. The spectra of unfolded proteins are often only shifted by ~2 nm towards lower wavelengths relative to the native protein and show similar absorption values. It is found empirically that the absorption at 280 nm of a native protein does not differ by more than 10% from that of the unfolded protein (Figure 5). As the absorption at 280 nm can either increase or decrease upon unfolding, the calculated molar extinction coefficient of the protein needs to be corrected for obtaining the exact extinction coefficient of the native protein. For this purpose, the absorption spectrum of the native protein in physiological buffer is compared with the spectrum of the unfolded protein (identical concentration) in buffer containing a high concentration of denaturant (e.g. 8 M GdmCl). The measured absorption values at 280 (A_{native} and A_{unfolded}) are then used to determine the molar extinction coefficient of the native protein according to (eq. 4):

$$\epsilon_{280 \text{ nm, native protein}} = \epsilon_{280 \text{ nm, calculated}} \cdot \frac{A_{280 \text{ nm, native}}}{A_{280 \text{ nm, unfolded}}} \quad (4)$$

The most important application of absorption spectroscopy in protein biochemistry is the termination of protein concentration via the molar extinction coefficient of the native protein at 280 nm (eq. 4). At protein concentrations that are too low for very accurate determination of A_{280 nm}, the absorption at 205 nm can be used because protein absorption at 205 is much higher than at 280 nm (Figure 3B), dominated by peptide bond absorption and almost independent of Tyr and Trp content. Indeed, all protein solutions of 1 mg/mL show specific absorptions of 28.5-33 (1 cm path length). On the average, A_{205 nm} is about 30 times more sensitive compared to concentration measurements via A_{280 nm}. Equation (5) allows protein concentration determination with less than 5% error:

$$A_{205 \text{ nm}}^{1 \text{ mg/mL}} = 27.0 + 120 \cdot \frac{A_{280 \text{ nm}}}{A_{205 \text{ nm}}} \quad (5)$$

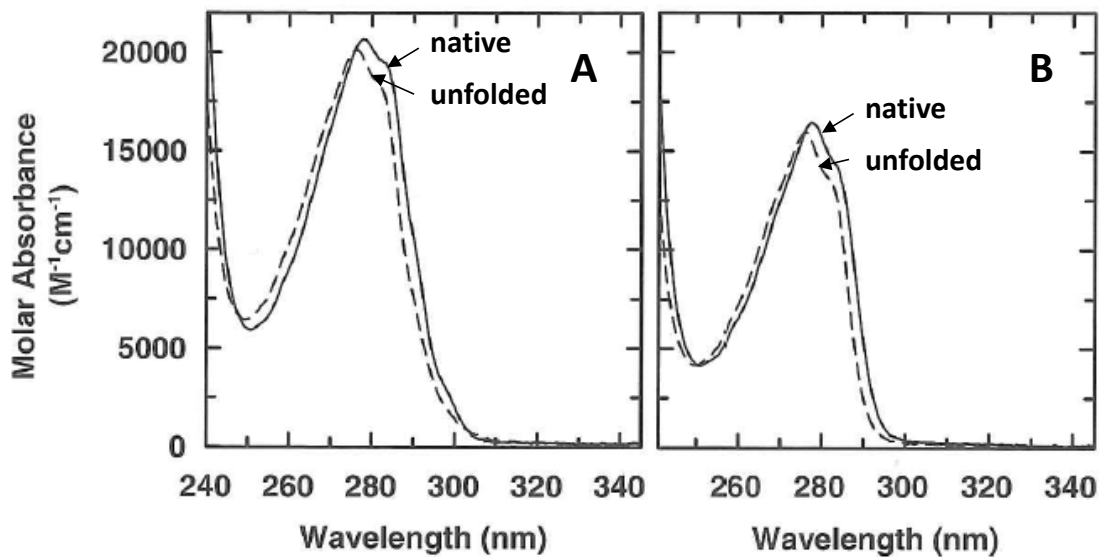


Figure 5: UV Absorption spectra of a native (solid lines) and unfolded (dashed lines) protein at identical concentrations. A) Spectra of ribonuclease T1; B) spectra of the Trp-free ribonuclease T1 variant Trp59Tyr in which the single Trp was replaced by Tyr. Note that the variant has zero absorption between 295 and 310 nm. Adapted from Schmid FX, The protein folding handbook, 22-44, Wiley, 2005).

Although the absorption spectra of native and unfolded proteins are quite similar (Figure 5), the small absorption differences between native and unfolded proteins at certain wavelengths can be used to monitor the folding process. Compared to fluorescence and CD spectroscopy, absorption changes during folding are however relatively small. In addition, absorption spectroscopy is less sensitive than fluorescence and CD spectroscopy and thus requires higher protein concentrations. For these reasons, CD and fluorescence spectroscopy have become the most frequently used spectroscopic techniques for recording protein folding in solution.

2.2. Fluorescence spectroscopy

The property of a compound to absorb light of a certain energy and to then re-emit light of lower energy is called fluorescence. Here, in contrast to pure absorption, the absorbed energy is only partially converted to heat and the rest of the absorbed energy is released as light with a higher wavelength (lower energy) relative to the energy of the absorbed light. This is illustrated by Jablonski diagram (Figure 6): Upon light absorption of a fluorescent molecule, different vibrational states of the electronically excited state S_1 are first populated, followed by radionless relaxation to the vibrational ground state of S_1 . The S_1 life time of a fluorescent molecule is typically in the nanosecond range. From the vibrational ground state of S_1 , the molecule can then relax to different vibration states (including rotation sub-states) of the electronic ground state S_0 under emission of a photon. There are different transition probabilities for these transitions to the electronic ground state that give rise to the

fluorescence spectrum of the molecule, in which the intensity of the emitted light is plotted against the wavelength of the emitted light.

The mechanism underlying the fluorescence of molecules has the following consequences:

- The shape of a fluorescence spectrum of an individual chromophore is independent of the wavelength at which the chromophore was excited. This is because all molecules relax to the vibration ground state of the 1st electronically excited state prior to light emission.
- The intensity of fluorescence spectra is highest when the excitation of the molecules is most efficient. This is at the wavelength of the absorption maximum.
- One can also record excitation spectra where one detects the intensity of emitted light at constant wavelength and varies the excitation wavelength. Excitation spectra have the same shape as the absorption spectrum of the excited chromophore.

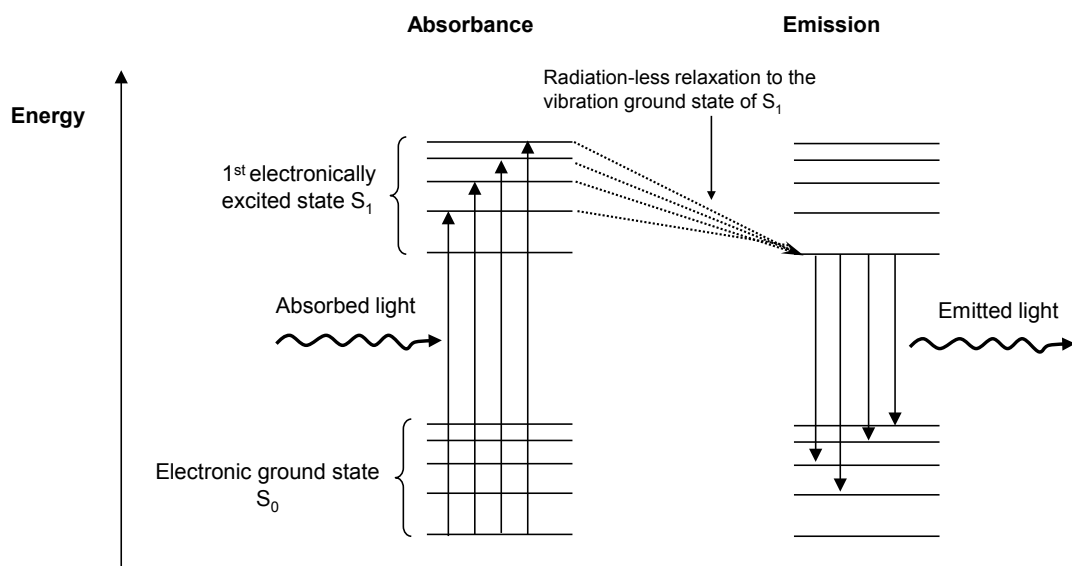


Figure 6: Jablonski Diagram

The wavelength and the intensity of the light emitted by a fluorescent molecule is detected perpendicular to the excitation beam (Figure 7).

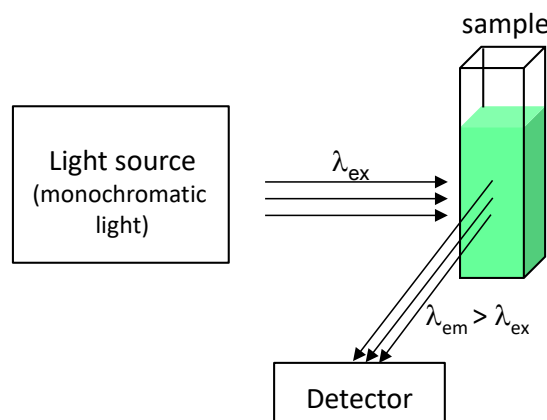


Figure 7: Detection of the intensity and wavelength of light emitted by a fluorescent molecule in fluorescence spectroscopy

As in absorption spectra of proteins, the fluorescence properties of proteins are dominated by their aromatic amino acids tyrosine and tryptophan, the only amino acids showing fluorescence. A big advantage of fluorescence spectroscopy of proteins is its high sensitivity. Protein concentrations of about 1 μM are generally sufficient for sensitive recording of fluorescence spectra or conformational changes. To measure the fluorescence spectrum of a protein, one typically excites the protein at 280 nm, where both Tyr and Trp absorb strongly. The intensity of the light emitted by the protein is then measured at wavelengths between 290 nm and 450 nm.

The ratio between the number of emitted photons and the number of absorbed photons is the quantum yield ϕ_F . Tyr and Trp have similar quantum yields of 0.14 and 0.13, respectively. Due to the much higher absorbance of Trp compared to Tyr, Trp is however a more than 3.5 times stronger fluorophore than tyrosine when an excitation wavelength of 280 nm is used (see Table 1).

Table 1: Fluorescence properties of tyrosine and tryptophan residues

| Amino acid | Absorbance maximum | Fluorescence maximum | Quantum yield (ϕ_F) | Molar extinction coefficient | Sensitivity relative to tryptophan |
|----------------|--------------------|----------------------|----------------------------|-------------------------------------|------------------------------------|
| Tryptophan (W) | 280 nm | 355 nm | 0.13 | $5500 \text{ M}^{-1}\text{cm}^{-1}$ | 1 |
| Tyrosine (Y) | 275 nm | 304 nm | 0.14 | $1400 \text{ M}^{-1}\text{cm}^{-1}$ | 0.29 |

In addition to its high sensitivity, a particular advantage of fluorescence spectroscopy is that the fluorescence properties of Tyr and in particular Trp residues can respond strongly to the changes in their local environment occurring during protein folding or when proteins adopt an alternative conformation. In native proteins, Tyr and Trp residues are often buried in the hydrophobic core of the protein, while they are completely solvent exposed in the unfolded state. In addition, changes in fluorescence intensity upon unfolding (fluorescence can either increase or decrease, depending on the respective protein), the tryptophan emission maximum is shifted from 320–335 nm (native) to 355 nm (unfolded) (Figure 8). Proteins that only contain Tyr but no Trp residues show smaller changes in their fluorescence properties during unfolding, which are generally still sufficient to follow unfolding (Figure 8). Overall, fluorescence spectroscopy very sensitively reports changes in the tertiary structure of proteins. Fluorescence-sensitive structural changes are not restricted to unfolding reactions. Even small local conformational changes as they e.g. may occur upon ligand binding, can often be detected by fluorescence spectroscopy. To selectively observe structural changes around Trp side chains only, one makes use of the fact that tyrosine shows no absorbance at 295 nm. Excitation of a protein that contains both Tyr and Trp residue at 295 nm thus allows selective

monitoring of the structural changes around the Trp residues independently of structural changes around the Tyr residues.

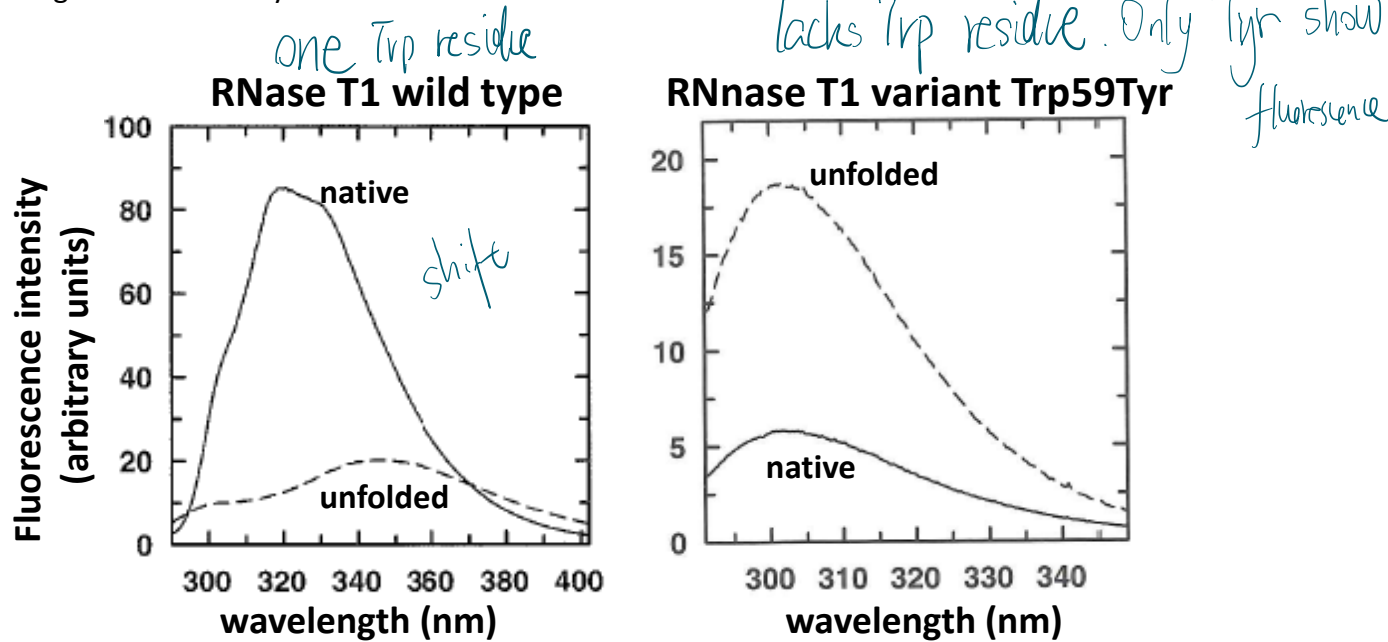


Figure 8: Fluorescence spectra of native and unfolded (in 6 M GdmCl) ribonuclease (RNase) T1 (left panel) and its tryptophan-free variant Trp59Tyr (right panel). Proteins were excited at 280 nm. Note that the fluorescence spectra of wild type RNase T1 (left panel) are dominated by the single Trp59 which shows a fluorescence maximum at 320 nm in the native and 355 nm in the unfolded state. The folding reaction can be recorded sensitively at 320 nm, where the fluorescence intensity increases about 6-fold upon folding. In the case of the Trp-free variant Trp59Tyr (right panel), only the tyrosines contribute to the recorded fluorescence spectra. Although the fluorescence maximum (305 nm) is identical for the native and unfolded protein, folding can still be recorded sensitively by the about 3-fold decrease in fluorescence intensity at 305 nm upon folding. Adapted from Schmid FX, The protein folding handbook, 22-44, Wiley, 2005).

2.3 Circular dichroism spectroscopy

Linearly polarized light (all E vectors are parallel) can be viewed as the sum of left and right circularly polarized waves of equal amplitude and phase. The projection of the amplitudes perpendicular to the propagation direction shows a line. *Proteins are chiral molecules and absorb right and left circularly polarized light with different molar extinction coefficients.* As a consequence of the difference in amplitudes, the transmitted light is elliptically polarized, that is the projection of the amplitudes perpendicular to the propagation direction no longer moves on a line, but describes an ellipse (see figure below). The CD spectrometer measures the difference in the intensities of left and right circularly polarized light after passing through the sample and expresses this as the **ellipticity** θ , the angle measuring the extent to which the transmitted light is elliptical (Figure 9). The larger the difference between the amplitudes of left and right circularly polarized light, the larger the ellipticity. The ellipticity is proportional to ΔA , the difference in absorption of left and right circularly polarized light. Since the

difference between the two components is usually very small, on the order of 0.0001, the ellipse that is described by the E vector is very narrow, corresponding to an ellipticity of only a few 1/100th of a degree.

From Figure 9 below it can easily be seen that the angle characterizing the ellipse, θ , is dependent on the large (b) and small (a) axis of the ellipse: $\tan\theta = \frac{a}{b}$

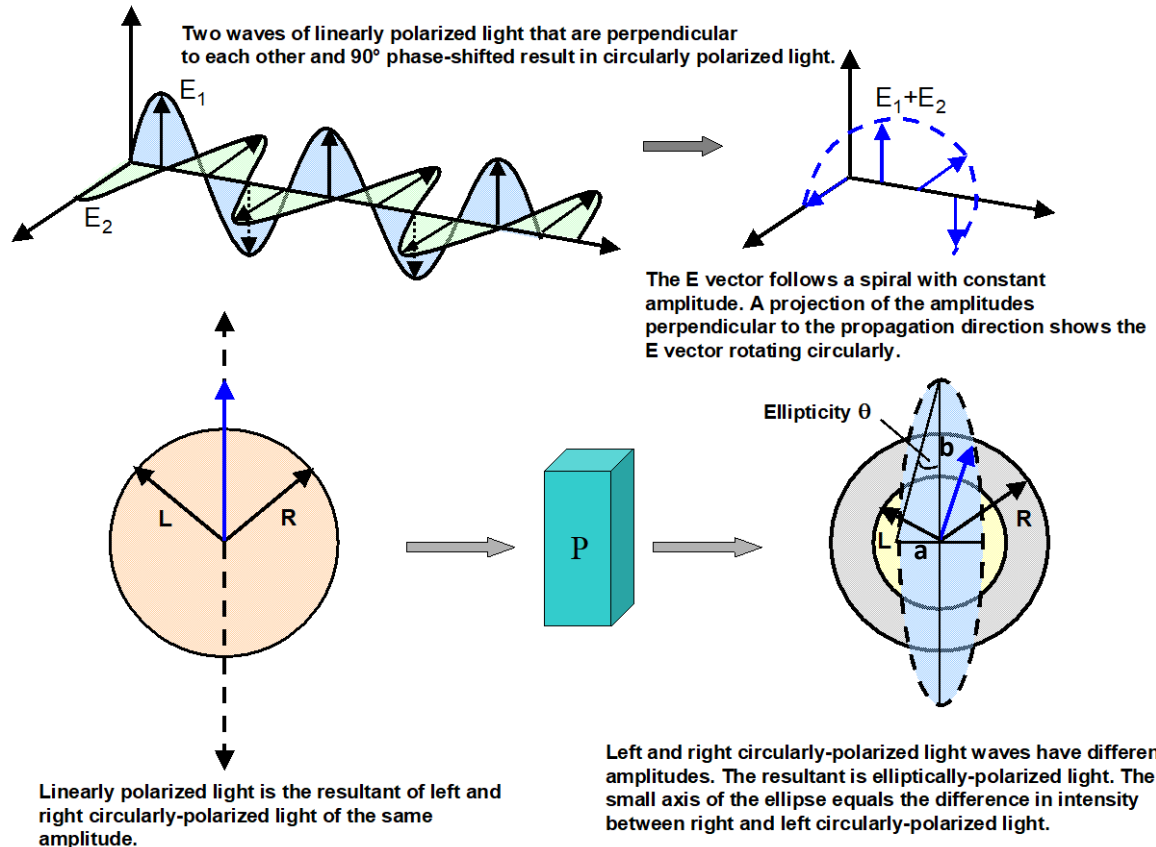


Figure 9: Circular dichroism spectroscopy of proteins is based on differences in the extinction coefficients of proteins for right and left circularly polarized light at a given wavelength.

The small axis a of the ellipse is equal to the difference in the intensities of left and right circularly-polarized light, and b is equal to the sum of the intensities of left and right circularly polarized light. Through simple geometrical calculations the following relationship between ΔA and θ follows (eq. 5):

$$\theta = 33 \cdot \Delta A \quad (5)$$

Analogous to the difference in the extinction coefficients, $\Delta \epsilon = \epsilon_L - \epsilon_R$, one can define the molar ellipticity, $[\theta]$. This parameter is expressed per decimole, and not per mole. This unit is used by CD spectroscopists for historical reasons. The relationship between $[\theta]$ and $\Delta \epsilon$ is therefore:

$$[\theta] = 3300 \cdot \Delta \epsilon \quad (\text{unit: grad cm}^2 \text{ dmol}^{-1}) \quad (6)$$

Analogous to Beer's law, the measured ellipticity θ (in degrees) depends on the sample concentration c , the thickness of the cuvette d (in cm) and the *molar* ellipticity $[\theta]$.

$$\Theta = \frac{[\theta] \cdot c \cdot d}{100} \quad (\text{unit: grad cm}^2 \text{ dmol}^{-1}) \quad (7)$$

It is even more common to measure the mean molar ellipticity per amino acid of a protein $[\theta]_{\text{MRW}}$. Particularly in the far-UV CD range (180–250 nm), this value gives a good estimate of the extent of secondary structure formation in a protein. The molar mean residue ellipticity $[\theta]_{\text{MRW}}$ of a protein can be obtained by dividing the measured molar ellipticity by the number of amino acids in the protein (n) (eq. 8):

$$[\theta]_{\text{MRW}} = [\theta] / n \quad (\text{unit: Grad cm}^2 \text{ dmol}^{-1}) \quad (8)$$

Figure 10 shows that CD spectra of proteins with different secondary structure components are characteristically distinct in the far-UV range between 190 and 250 nm where the peptide bond absorbs light. Remember that $[\theta]_{\text{MRW}}$ values are absolute and reproducible values, analogous to absorbance spectroscopy.

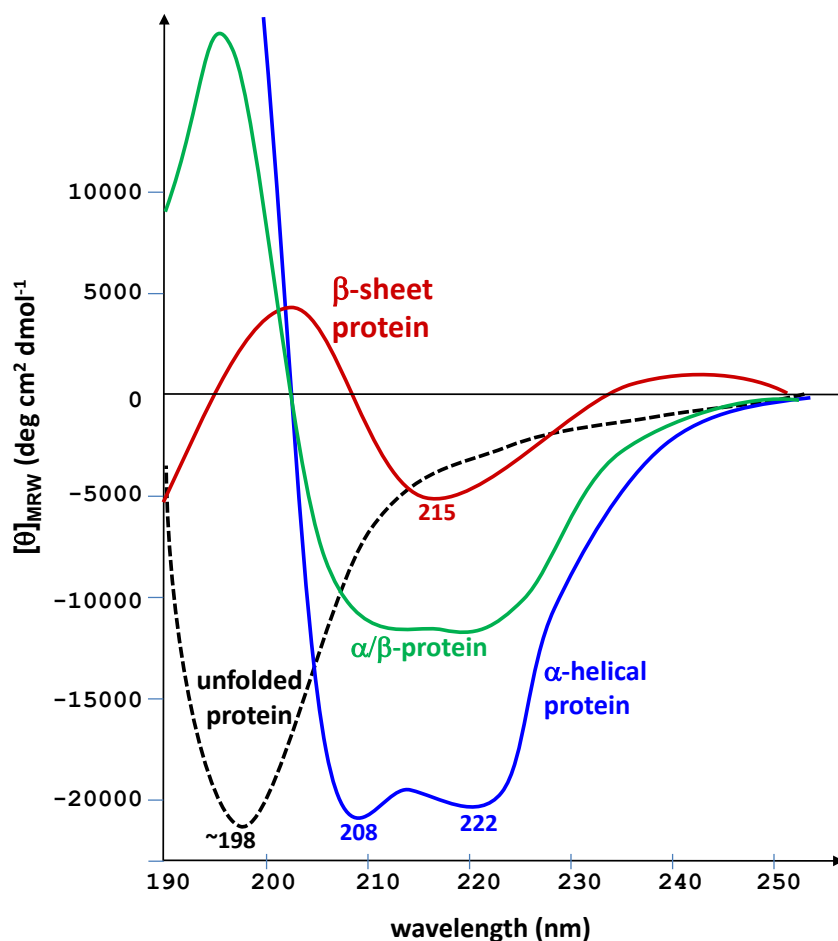
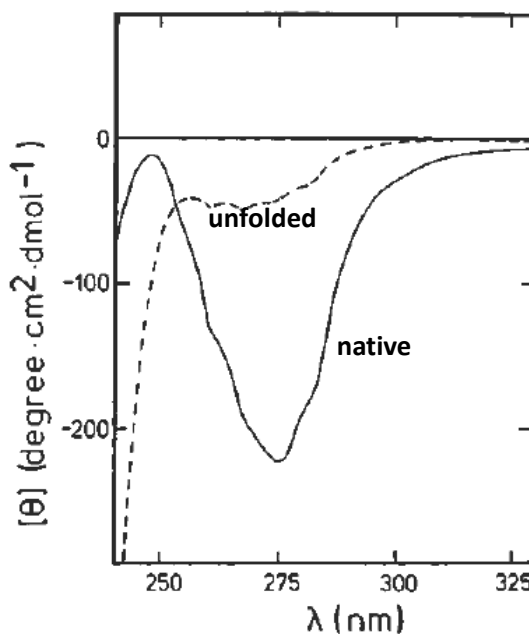


Figure 10: Far-UV CD spectra of proteins (recorded between 190 and 250 nm) report on their secondary structure content. Proteins only containing α -helical secondary structure (blue line) show characteristic minima at 208 and 222 nm, all- β -sheet proteins (red line) exhibit a minimum at 215 nm, and unfolded proteins (random coil structure) show a minimum around 198 nm (dashed black line). Note that α -helices show a more negative CD signal than β proteins and thus dominate the shape of CD spectra of proteins containing both α -helices and β -sheets (green line).

Proteins that only contain α -helices as regular secondary structures show a strongly negative CD signal with minima at 208 and 222 nm and values of about $-20000 \text{ degree cm}^2 \text{ dmol}^{-1}$, while all- β -sheet proteins have a weaker negative signal ($-5000 \text{ degree cm}^2 \text{ dmol}^{-1}$) with a minimum at 215 nm. Thus, the shape of the far-UV CD spectrum of a protein is, at least to a certain extent, predictable from its three-dimensional structure. Since the far-UV CD spectra of native and unfolded proteins are generally very different (the minimum of unfolded proteins is at about 198 nm, see Figure 10), far-UV CD spectroscopy is an excellent tool to measure folding and conformational transitions in proteins that involve changes in secondary structure content. In addition, far-UV CD is quite sensitive and not does not require large amounts of protein. Far-UV CD data are typically recorded at protein concentrations of 0.2 mg/mL in a volume of 0.2 mL (1 mm pathlength), so that only 40 μg of protein are required per measurement.

Also in the near-UV range (250–310 nm) where the aromatic amino acids Trp, Tyr and Phe as well as disulfide bonds absorb light, proteins show characteristic CD spectra (Figure 11). The shapes of these spectra can however not be predicted, because they reflect the asymmetric environment of aromatic residues in the context of an intact tertiary structure, which is different in every protein. In fact, near-UV CD spectra are characteristic for each individual protein. It follows that a characteristic near-UV spectrum is absent in unfolded proteins and conformational states without defined tertiary structure. The main applications of near-UV CD spectroscopy are i) rapid testing for the presence of an intact tertiary structure and ii) monitoring the loss of tertiary structure independently of the loss of secondary structure during protein unfolding.

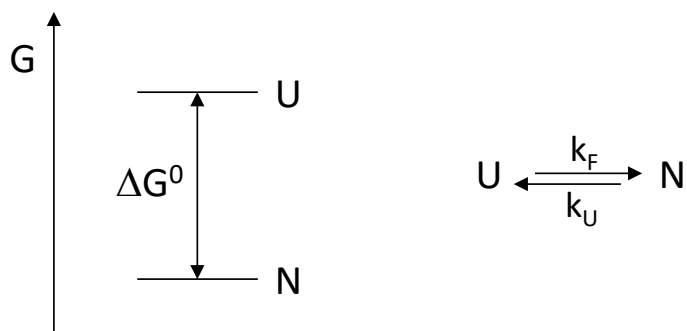


Near-UV CD spectra provide a fingerprint of protein tertiary structure,

Figure 11: Near-UV CD spectra of a native and an unfolded protein. Note that the far-UV CD signal is essentially absent in the unfolded protein. The folded protein shows a spectrum with characteristic shape which is a signature of its intact tertiary structure and the asymmetric environment of its aromatic residues.

3. The two-state model of protein folding and the experimental determination of the thermodynamic stability of proteins

As outlined in chapter 1, most small, one-domain proteins show a cooperative all-or-nothing behavior in their folding reaction. This means that they exist, at any temperature, pH or denaturant concentration, as a mixture of completely folded molecules (N) and completely unfolded molecules (U) under equilibrium conditions, i.e., when the folding equilibrium has been attained. This is exactly the assumption underlying the two-state model folding [5]. It means that the equilibrium between U and N is only determined by the microscopic rate constants of folding and unfolding (k_F and k_U , respectively). Consequently, the thermodynamic stability of the protein, ΔG^0 , can be directly calculated from the Gibbs equation (eq. 9),



$$\Delta G^0 = -R \cdot T \cdot \ln K_{eq} = -R \cdot T \cdot \ln \frac{[N]}{[U]} = -R \cdot T \cdot \ln \frac{k_F}{k_U} \quad (9)$$

where R is the gas constant, T the temperature in Kelvin, K_{eq} is the equilibrium constant of folding, and k_F and k_U are the microscopic rate constants of folding and unfolding, respectively. Equation (9) allows the calculation of $K_{eq} = [N]/[U]$ as a function of ΔG^0 at 25°C. The table below shows that K_{eq} increases 10-fold with a stability increase of 5.7 kJ/mol.

increase
of free
energy

| ΔG^0 (kJ/mol) | $K_{eq} = [N]/[U]$ | Fraction of native molecules |
|-----------------------|--------------------|------------------------------|
| +5.7 | 1:10 | 9% |
| 0 | 1:1 | 50% |
| -5.7 | 10:1 | 91% |
| -11.4 | 100:1 | 99% |
| -17.1 | 1000:1 | 99.9% |
| etc. | etc. | etc. |

The fraction of native molecules (f_N) at equilibrium is calculated from equation (10):

$$f_N = \frac{K_{eq}}{K_{eq} + 1} \quad (10)$$

If a protein folds according to the two-state model, f_N at any condition can be readily determined when the spectroscopic properties of N and U differ. As an example, Figure 12 shows the fluorescence spectra of U and N (identical concentrations) of a specific protein. As the difference between the signals of U and N (S_U and S_N , respectively) is largest at 330 nm unfolding data are recorded at 330 nm. The figure shows the recorded fluorescence signal S at 330 nm (black dot in Figure 12) for conditions where $f_N = 0.6$ (corresponding to $K_{eq} = [N]/[U] = 1.5$). f_N can then be calculated according to equation (11):

$$f_N = \frac{S - S_U}{S_N - S_U} \quad (11)$$

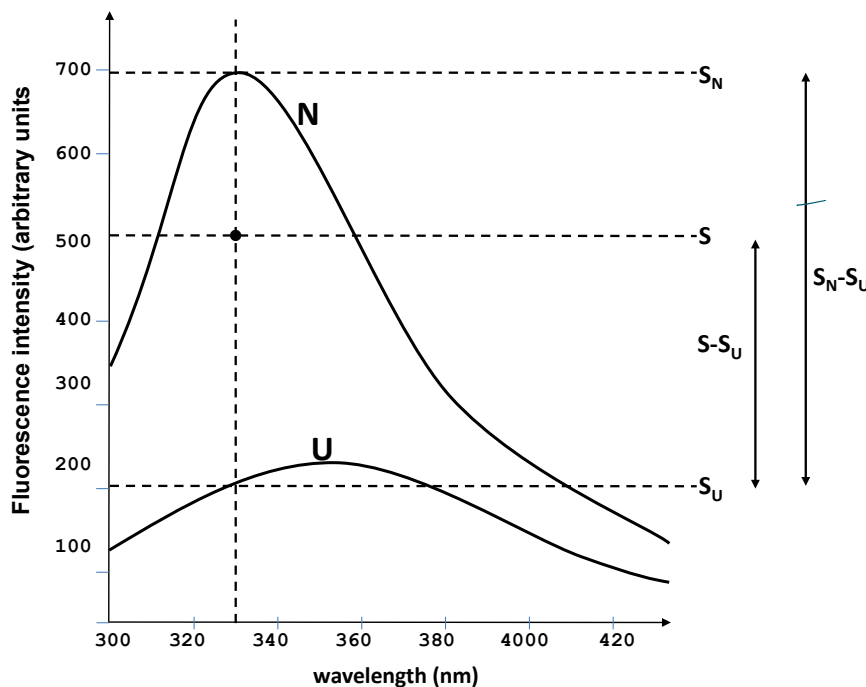


Figure 12: Spectroscopic determination of f_N via the spectroscopic signal at a wavelength where N and U show different signals.

It follows from eq. 9 that either the equilibrium concentrations of U and N need to be known for calculating ΔG^0 under physiological conditions, or k_F and k_U . We first discuss the strategy for determining $[U]$ and $[N]$. Here, the main difficulty is the exact determination of $[U]$. This is because the thermodynamic stabilities of most proteins are higher than -20 kJ/mol so that less than one in thousand molecules will be unfolded at equilibrium under physiological conditions. This is far below the accuracy with which any of the spectroscopic methods discussed in chapter 2 can detect the fraction of unfolded molecules. We therefore make use of the fact that the folding equilibrium can be shifted towards U with increasing denaturant concentration ($[D]$) [6]. The protein is incubated at different denaturant concentrations and the fraction (percentage) of native molecules after attainment of equilibrium is determined

spectroscopically. To confirm that the equilibrium was attained, the experiment is performed in opposite directions: The native protein is mixed with increasing [D] (unfolding transition) and the completely unfolded protein (in the presence of high [D]) is diluted to lower denaturant concentrations (refolding transition). The equilibrium is attained only when the unfolding and refolding transitions coincide. Figure 13A shows a typical example of an equilibrium unfolding/refolding transition of a small one-domain protein folding according to the two-state model. The transition curve is S-shaped and symmetrical. For each data point in the transition region (denaturant concentrations where the fraction of native molecules is between 5 and 95%, indicated with a yellow background in Figure 13) an accurate determination of K_F and thus ΔG^0 is possible. Figure 13B shows that there is a linear dependence of ΔG^0 on denaturant concentration. Linear extrapolation of ΔG^0 to zero denaturant yields the free energy of folding in the absence of denaturant, $\Delta G_{H_2O}^0$, according to equation (12)

$$\Delta G^0 = \Delta G_{H_2O}^0 + m_{eq} \cdot [D] \quad (12)$$

(linear dependent)

where the parameter m_{eq} corresponds to the slope of the dependence of ΔG^0 on [D]. As ΔG^0 is zero at the transition midpoint, the denaturant concentration where 50% of the molecules are native and 50% are unfolded, $[D_{1/2}]$, is given by equation (13)

$$[D_{1/2}] = \Delta G_{H_2O}^0 / m_{eq} \quad (13)$$

Combination of equations 9-11 gives the fraction of native molecules (f_N) as a function of $\Delta G_{H_2O}^0$, m_{eq} , $[D]$ and temperature (eq. 14):

$$f_N = \frac{e^{-(\Delta G_{H_2O}^0 + m_{eq} \cdot [D]) / RT}}{e^{-(\Delta G_{H_2O}^0 + m_{eq} \cdot [D]) / RT} + 1} \quad (14)$$

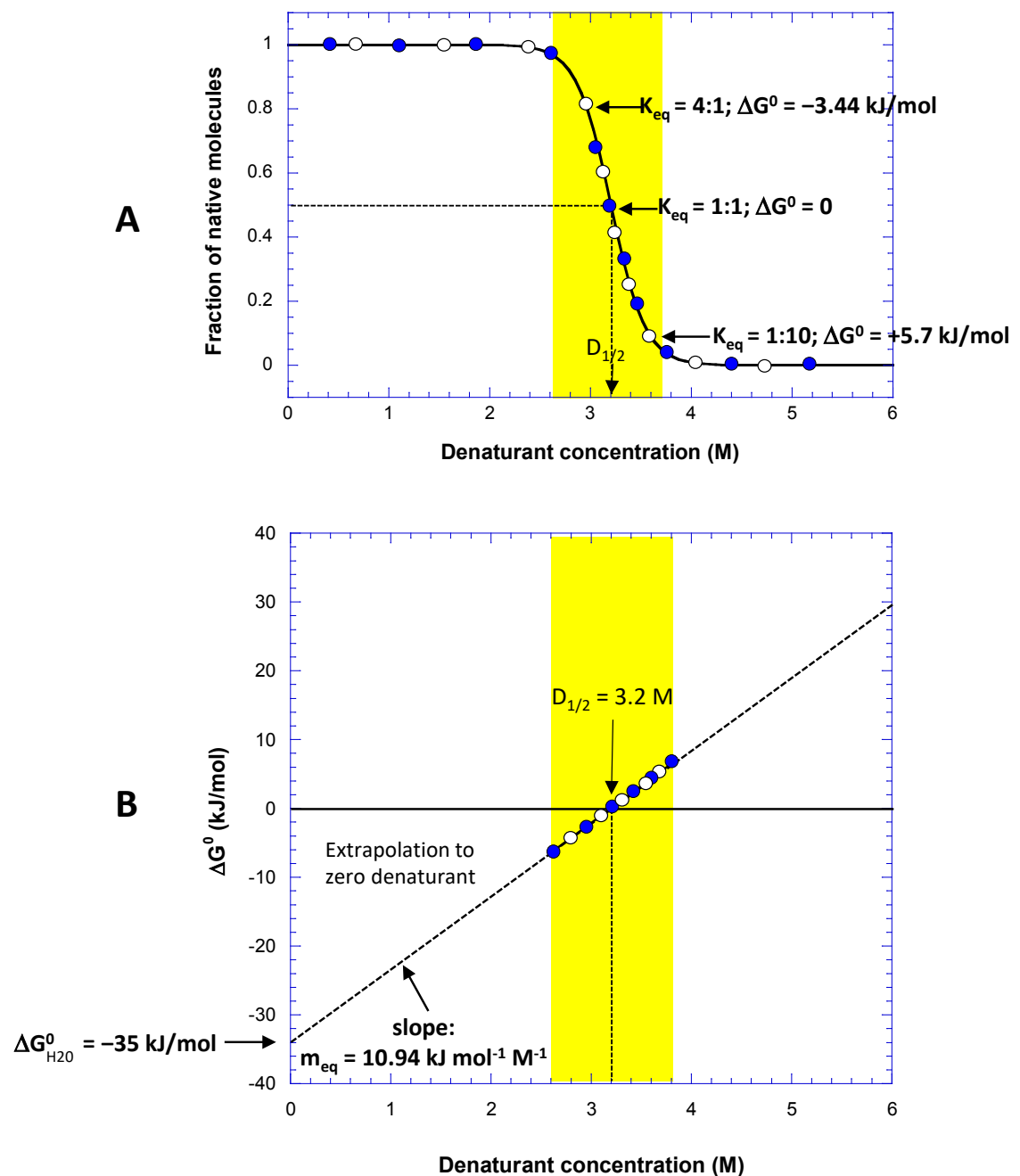


Figure 13: Determination of the free energy of folding of a small protein that follows the two-state model of folding with $\Delta G^0_{H2O} = -35 \text{ kJ/mol}$ by denaturant-induced equilibrium unfolding/refolding experiments.

Top: The fraction of native molecules plotted against denaturant concentration yields a symmetric, S-shaped unfolding curve. The yellow region indicates the range of denaturant concentrations at which K_F and ΔG^0 can be determined accurately (5-95% unfolded molecules). Closed symbols: Refolding experiments; open symbols: unfolding experiments; $D_{1/2}$: midpoint of the unfolding transition (3.2 M denaturant).

Bottom: ΔG^0 linearly depends on denaturant concentration: Linear extrapolation of the ΔG^0 values recorded in the transition region to zero denaturant yields the thermodynamic stability of the proteins under physiological conditions.

The parameter m_{eq} is linked to the *cooperativity* of the folding reaction. It is a measure of the denaturant sensitivity of K_{eq} and ΔG^0 and directly proportional to the *difference in accessible surface area* between U and N, ΔASA_{UN} [7]. In more general terms, it can be stated that the transition between two conformational states of a protein is the more denaturant-sensitive the larger the difference in accessible surface area between the two states is. ΔASA_{UN} itself is linearly dependent on the length of the polypeptide chain if N does not contain unstructured regions and can be calculated from the empirical equation (15).

$$\Delta ASA_{UN} = [-907 + 93 \cdot (\text{number of amino acids})] \text{ Å}^2$$

It follows that m_{eq} is linearly dependent on the mass of the protein (number of amino acids \times 110 Da) and predictable for every protein. In addition, m_{eq} is dependent on the denaturant. The empirical equations (15) and (16) show that GdmCl is an about 2-fold stronger denaturant than urea [7]:

GdmCl: $m_{eq} = [3590 + 0.92 \cdot (\Delta ASA_{UN})] \text{ J mol}^{-1} \text{ M}^{-1}$ (16)

Urea: $m_{eq} = [1560 + 0.46 \cdot (\Delta ASA_{UN})] \text{ J mol}^{-1} \text{ M}^{-1}$ (17)

Figure 14 shows the predicted m_{eq} values in GdmCl and urea as a function of the molecular mass of the protein.

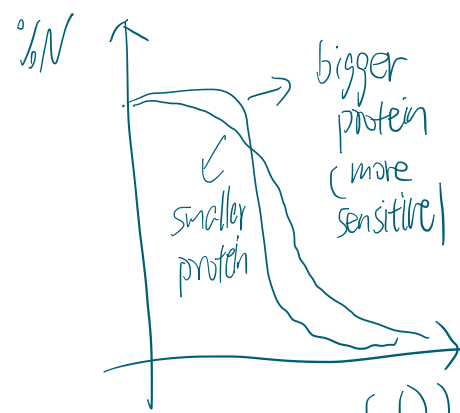
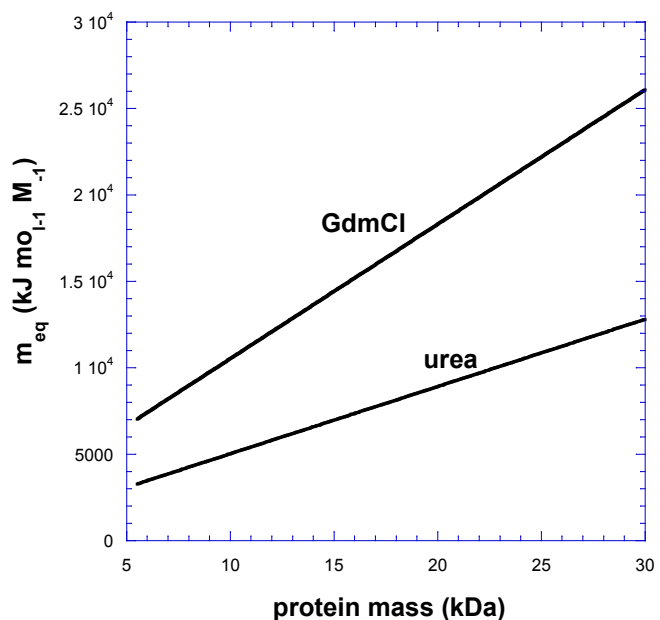


Figure 14: Predicted m_{eq} values in GdmCl and urea as a function of the mass of the protein.

As an example, Figure 15 shows the different effects of GdmCl and urea on the unfolding/refolding equilibrium of a 10 kDa protein with a thermodynamic stability ($\Delta G_{H_2O}^0$) of -20 kJ/mol, assuming that ionic strength introduced by GdmCl has no influence on protein stability:

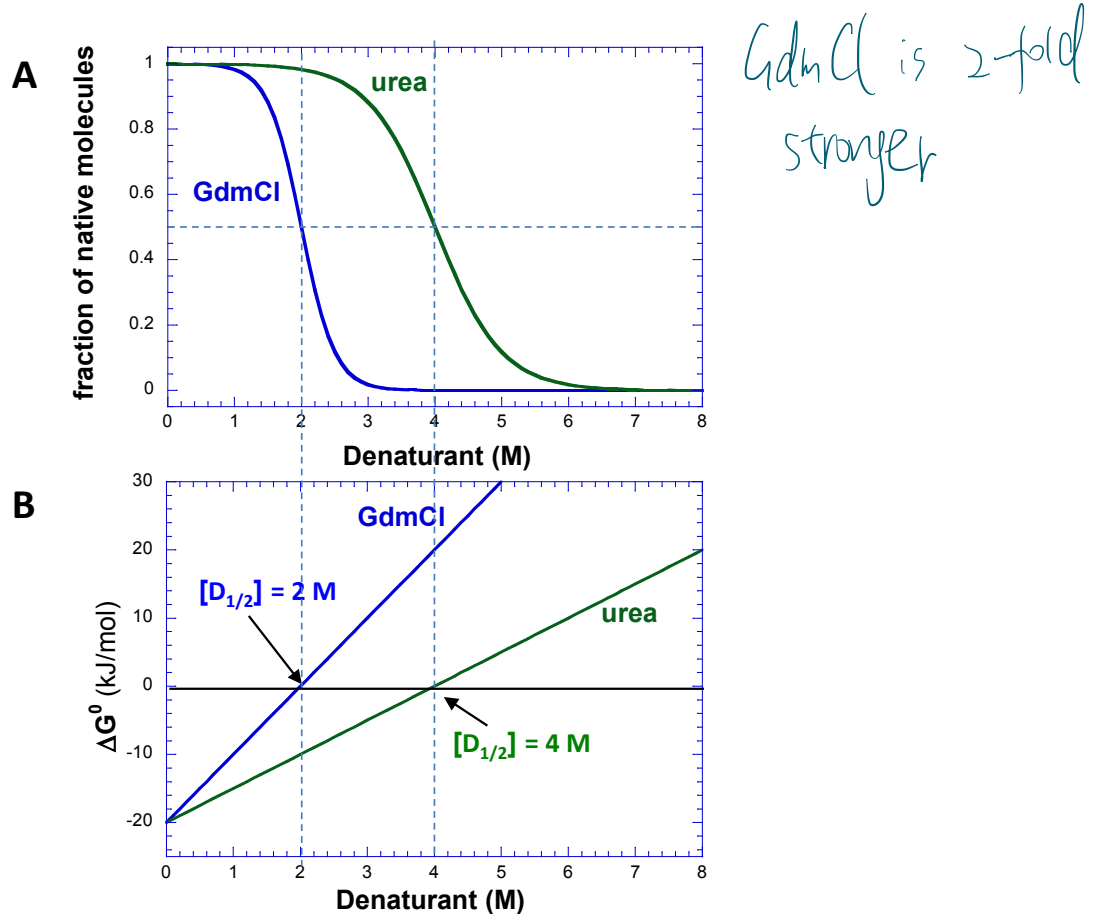


Figure 15: Effect of GdmCl and urea on the equilibrium unfolding transition of a 10 kDa protein with a free energy of folding of -20 kJ mol^{-1} . The m_{eq} values are $10 \text{ kJ mol}^{-1} \text{M}^{-1}$ for GdmCl and $5 \text{ kJ mol}^{-1} \text{M}^{-1}$ for urea. A: Denaturant-dependence of the fraction of native molecules. B: Denturant dependence of ΔG^0 . Note that the transition midpoints differ by a factor of two because the m_{eq} values differ by a factor of two.

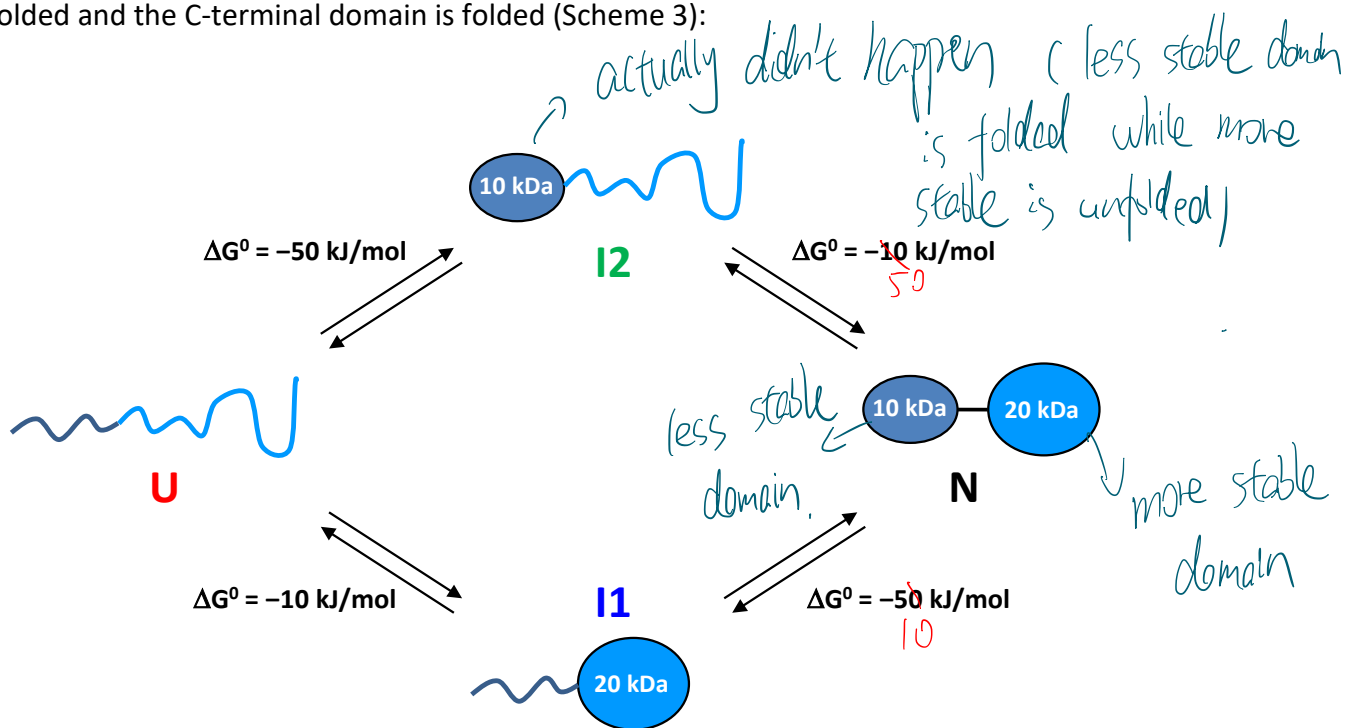
There are two ways to test whether the equilibrium unfolding transition of a protein is consistent with the two-state model of folding, because the two-state model makes the following predictions for denaturant-induced equilibrium unfolding:

- The equilibrium transitions must be independent of the spectroscopic technique used to monitor unfolding, because secondary and tertiary structure is lost simultaneously upon unfolding. Recording of unfolding with far-UV CD (loss of secondary structure) must yield the same result as recording of unfolding with fluorescence (loss of tertiary structure).
- The experimentally determined m_{eq} value must correspond to the m_{eq} value predicted from the mass of the protein (eq. 16, 17).

Note that the determined m_{eq} value is always too low if there is a breakdown of the two-state model! The following example illustrates this: Assume you investigate the denaturant dependent unfolding of a protein that consists of two independently folding domains of similar mass and similar stability. Here, also partially structured forms of the protein can occur at equilibrium in which only one of the domains is folded and the other domain is unfolded

(see also below). Each of the two domains will unfold with a m_{eq} value that corresponds to about 50% of the m_{eq} calculated for the full-length protein. As both domains also have very similar $[D_{1/2}]$ values, a single transition would be observed with a m_{eq} value that is two times lower than the calculated m_{eq} value!

A two-domain protein with independently folding domains can be readily recognized if both domains differ significantly in their stability. As an example, we consider a 30 kDa protein with a 10 kDa N-terminal domain with $\Delta G_{H_2O}^0 = -10 \text{ kJ/mol}$ and a larger and more stable 20 kDa C-terminal domain with $\Delta G_{H_2O}^0 = -50 \text{ kJ/mol}$. If both domains fold and unfold independently according to the two-state model, two partially structured intermediates can be populated in addition to N and U: An intermediate I1 in which the N-terminal domain is unfolded and the C-terminal domain is folded, and an intermediate I2 in which the N-terminal domain is unfolded and the C-terminal domain is folded (Scheme 3):



Scheme 3: Four-state model of folding of a two-domain protein with independently folding domains

Far-UV CD spectroscopy is extremely useful for analyzing protein folding mechanisms in which more than two states occur, because each individual unfolding step is associated with loss of secondary structure and thus detectable by a change in the far-UV CD signal. Figure 16A shows a simulation of the recorded far-UV CD signal of the two-domain protein from scheme 3 using the above stability parameters for the N- and C-terminal domain. Figures 16B and 16C show the relative populations of N, I1, I2 and U at each denaturant concentration after attainment of the folding equilibrium.

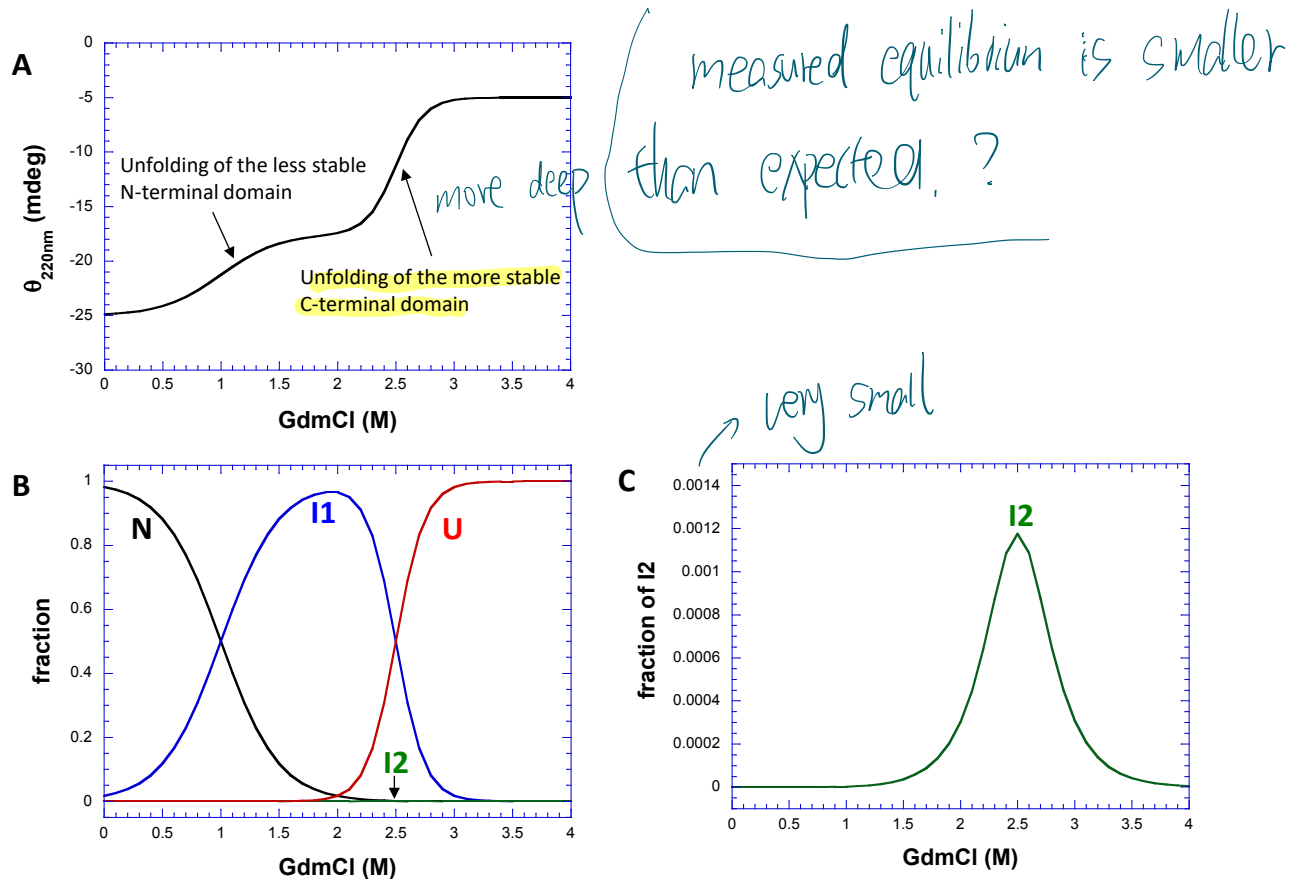


Figure 16: Four-state equilibrium unfolding transition of a two-domain protein with domains that fold independently (scheme 3).

A: GdmCl-dependent equilibrium unfolding recorded via the far-UV CD signal at 220 nm. Note that the larger size of the more stable domain is evident from its steeper unfolding transition.

B,C: Population of N, I1, I2 and U as a function of GdmCl concentration. Note that I2 is maximally populated at 2.5 M GdmCl to only 0.12% because the C-terminal domain is much more stable than the N-terminal domain, which makes the population of a state (I2) in which the C-terminal domain is unfolded and the N-terminal domain is still folded very unlikely.

The following parameters were used to calculate the CD signal at 220 nm and the fraction of N, I1, I2 and U between zero and 4 M GdmCl:

N-terminal domain (10 kDa): $\Delta G_{H_2O}^0 = -10 \text{ kJ/mol}$, $m_{eq} = 10 \text{ kJ mol}^{-1} \text{M}^{-1}$; $[D_{1/2}] = 1.0 \text{ M GdmCl}$; CD_{220} signal of the native N-domain: -10 mdeg; CD signal of the unfolded N-domain: -2.5 mdeg.

C-terminal domain (20 kDa): $\Delta G_{H_2O}^0 = -50 \text{ kJ/mol}$, $m_{eq} = 20 \text{ kJ mol}^{-1} \text{M}^{-1}$; $[D_{1/2}] = 2.5 \text{ M GdmCl}$; CD_{220} signal of the native C-domain: -15 mdeg; CD signal of the unfolded C-domain: -2.5 mdeg.

The fractions of the native and unfolded N- and C-domain for the unfolding of the individual domains ($f_N^{N\text{domain}}$, $f_U^{N\text{domain}}$, $f_N^{C\text{domain}}$, $f_U^{C\text{domain}}$) at each GdmCl concentration can be calculated according to equation (13). The fractions of N, I1, I2 and U in the four-state equilibrium are calculated as follows: $f_N = f_N^{N\text{domain}} \cdot f_N^{C\text{domain}}$; $f_{I1} = f_U^{N\text{domain}} \cdot f_N^{C\text{domain}}$; $f_{I2} = f_N^{N\text{domain}} \cdot f_U^{C\text{domain}}$; $f_U = f_U^{N\text{domain}} \cdot f_U^{C\text{domain}}$; with $f_N + f_{I1} + f_{I2} + f_U = 1$.

4. The temperature dependence of protein stability

because ΔH and ΔS are temp dependent

The thermodynamic stabilities of several hundred one-domain proteins have been determined by denaturant-dependent unfolding equilibria. The obtained $\Delta G_{\text{H}_2\text{O}}^0$ values are in the range of **-10 to -80 kJ/mol**, showing that protein stability is surprisingly low compared to the sum of all interactions that specifically stabilize N [8]. In fact, protein stability typically only corresponds to the energy of a few hydrogen bonds! This means that proteins were not evolved towards maximum thermodynamic stability and that the protein folding reaction also includes an energetically unfavorable component. For a more detailed analysis, we need to consider that the Gibbs free energy difference between two states under equilibrium conditions, ΔG , is composed of an enthalpic and an entropic term according to classical thermodynamics (eq. 18)

$$\Delta G = \Delta H - T\Delta S \quad (18)$$

where ΔH is the enthalpy difference and ΔS is the entropy difference between the two states and T is the temperature (in Kelvin). In protein folding, the term ΔH includes all specific interactions that stabilize N (hydrogen bonds, van der Waals interactions and electrostatic interactions), while ΔS includes the loss of entropy of the polypeptide chain upon folding and the gain in entropy of water molecules from the hydration shell of U that become released to the bulk upon folding and thus less ordered.

4.2. The heat capacity difference between U and N, Δc_p , and its influence on the temperature dependence of thermodynamic protein stability

The Gibbs free energy of folding is temperature dependent because both ΔH and ΔS are temperature dependent according to the following equations (19, 20),

$$\frac{d\Delta H(T)}{dT} = \Delta c_p = C_p^N - C_p^U \quad (19)$$

$$\frac{d\Delta S(T)}{dT} = \Delta c_p/T \quad (20)$$

where Δc_p is the difference in heat capacity between U and N at constant pressure. Heat capacity is defined as the amount of energy required to increase the temperature of one mole of a substance by 1 K and has the unit $\text{J}\cdot\text{mol}^{-1}\cdot\text{K}^{-1}$. In contrast to most other reactions of organic molecules in aqueous solution, the protein folding reaction is associated with a large change in heat capacity because the heat capacity of U is significantly higher than that of N [9, 10]. This is because many additional water molecules are immobilized in the hydration shell of U compared to N. It is assumed that these immobilized water molecules form stronger hydrogen bonds among each other than water molecules in the bulk, in particular around the exposed hydrophobic residues in U, so that more energy is required to increase the temperature of U compared to N. Accordingly, the Δc_p value for the folding reaction, like m_{eq} , is linearly dependent on $\Delta A\text{SA}$ and

thus linearly dependent on the size of the protein (eq.14). The following relationship is found empirically (eq. 21) (Fig. 17) [7]:

$$\Delta c_p = (1.05 - 0.795 \cdot \Delta ASA) \text{ kJ} \cdot \text{mol}^{-1} \cdot \text{K}^{-1} \quad (21)$$

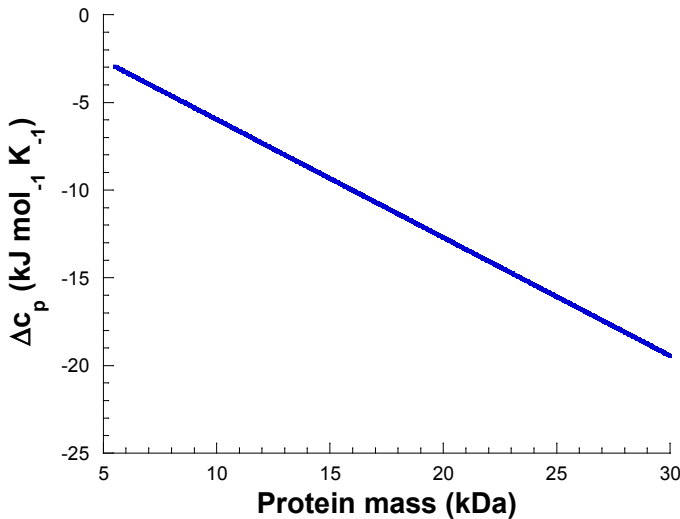


Figure 17: ΔC_p of folding linearly depends on the mass of the protein, because ΔASA linearly depends on the mass. A mean mass per residue of 110 Da was used to predict ΔC_p as a function of protein mass according to the empirical equations 14 and 20.

ΔC_p for *folding* ($\Delta C_p = c_p(N) - c_p(U)$) is negative because $c_p(N) < c_p(U)$. Note that many textbooks describe the thermodynamics of protein stability for the *unfolding* reaction, for which ΔC_p is positive. Integration of equations (19) and (20) and using the melting temperature T_m as reference temperature yields the dependence of ΔH and ΔS on Δc_p , T_m and temperature T (eq. 22, 23):

Inference $\Delta H(T) = \Delta H_m + \Delta c_p \cdot (T - T_m) \quad (22)$

$$\Delta S(T) = \Delta S_m + \Delta c_p \cdot \ln\left(\frac{T}{T_m}\right) \quad (23)$$

where ΔH_m and ΔS_m are the enthalpy and entropy differences between N and U at T_m .

As the equilibrium constant of folding ($K_{eq} = [N]/[U]$) is equal to 1 at T_m and ΔG is zero at T_m (eq. 24),

$$\Delta G_m = \Delta H_m - T_m \Delta S_m = 0 \quad (24)$$

ΔS_m can be calculated from ΔH_m and T_m (eq. 25):

$$\Delta S_m = \frac{\Delta H_m}{T_m} \quad (25)$$

Combination of equations 18, 22, 23 and 25 yields the general equation for the temperature dependence of the free energy of folding (ΔG) (equation 25), in which the term ΔS_m no longer

appears because T_m is used as the reference temperature so that ΔS_m can be replaced by $\Delta H_m/T_m$ (eq. 25) [9-11]:

$$\Delta G(T) = \Delta H_m + \Delta c_p \cdot (T - T_m) - T \left(\frac{\Delta H_m}{T_m} + \Delta c_p \cdot \ln \left(\frac{T}{T_m} \right) \right) \quad (26)$$

Equation (26) shows that three parameters need to be known for calculating the free energy of folding at any temperature: ΔH_m , T_m and Δc_p .

$$\Delta H \quad \Delta c_p \quad T$$

As an example, Figure 18 shows the consequences of equation (26) for the dependence of ΔG , ΔH and $T\Delta S$ of folding of a one-domain protein with $\Delta c_p = -7 \text{ kJ mol}^{-1} \text{ K}^{-1}$, $\Delta H_m = -300 \text{ kJ mol}^{-1}$ and $T_m = 340 \text{ K}$ on temperature:

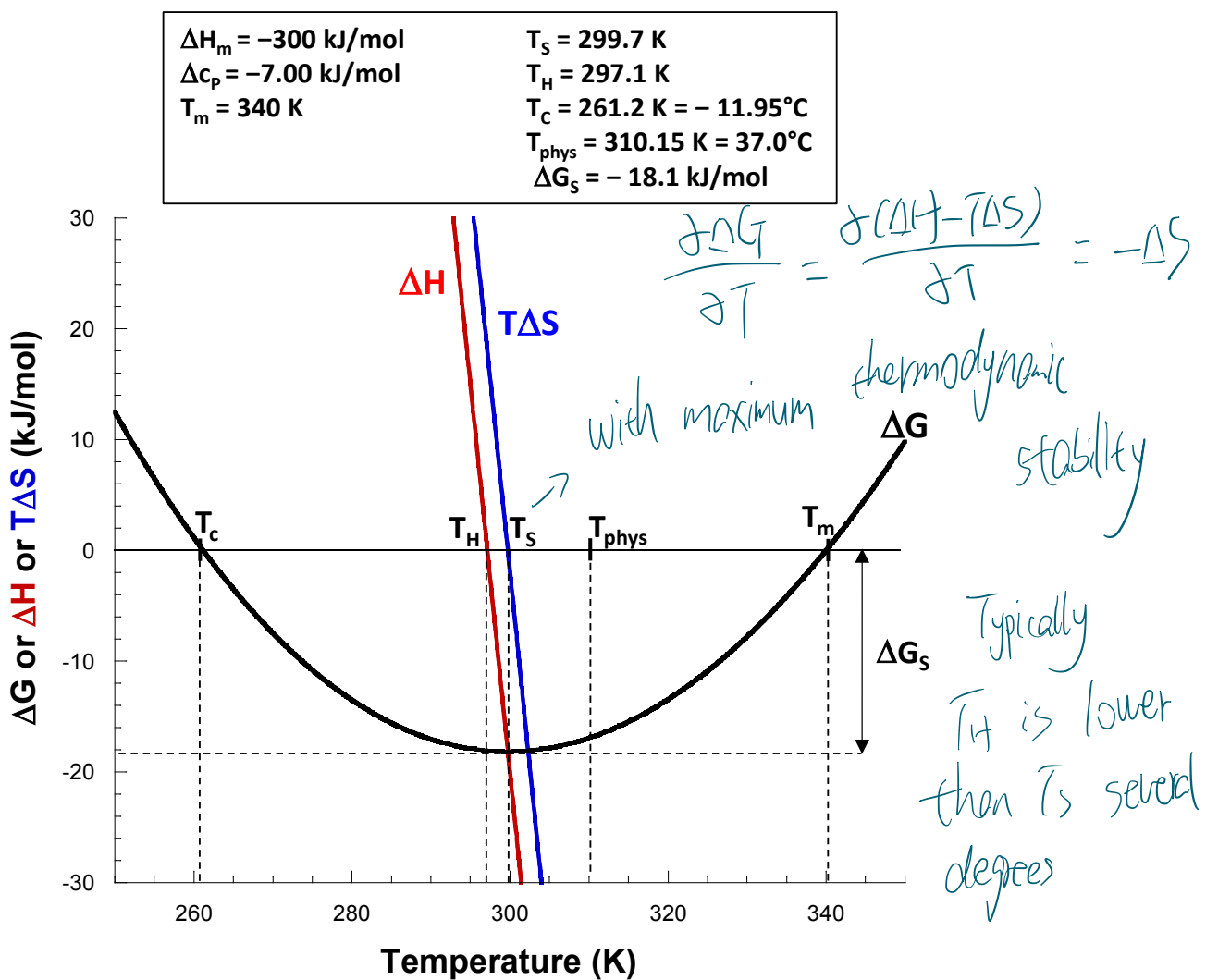


Figure 18: Temperature dependence of ΔG , ΔH and $T\Delta S$ of folding of a small one-domain protein according to the two-state model, with $\Delta c_p = -7 \text{ kJ mol}^{-1} \text{ K}^{-1}$, $\Delta H_m = -300 \text{ kJ mol}^{-1}$ and $T_m = 340 \text{ K}$.

T_c is the temperature of cold denaturation, T_H the temperature at which $\Delta H = 0$ and T_s is the temperature where $\Delta S = 0$ and the protein has its maximum thermodynamic stability ΔG_s . T_{phys} indicates the physiological temperature (temperature of optimum growth of the organism from which the protein was isolated).

in this temp
the absolute value
of ΔH and $T\Delta S$ is much larger than ΔG

The following conclusions can be drawn from equation (25) and Figure 18:

- A direct consequence of the large negative value of Δc_p of protein folding is a curved, v-shaped temperature dependence of ΔG with two unfolding temperatures: the melting temperature T_m and the temperature of cold denaturation, T_c . For most (but not all) proteins, T_c is below zero °C.
- By definition, the slope of the temperature dependence of ΔG equals $-\Delta S$ ($\delta \Delta G(T)/\delta T = -\Delta S(T)$). This slope is zero at the temperature of maximum thermodynamic stability ΔG_s . Consequently, the protein reaches ΔG_s at T_s , the temperature where $\Delta S = 0$ (corresponding to $T\Delta S = 0$) (Figure 18). Combination of equations 23–25 allows calculation of T_s and ΔG_s (eq. 27, 28):

$$T_s = T_m \cdot e^{-\Delta H_m / (\Delta c_p \cdot T_m)} \quad (27)$$

$$\Delta G_s = \Delta H_m + \Delta c_p \cdot (T_s - T_m) \quad (28)$$

- The temperature at which ΔH is zero, T_H (eq. 29), is always lower than T_s , but typically only a few °C.

$$T_H = T_m - \Delta H_m / \Delta c_p \quad (29)$$

- The temperature of cold denaturation T_c can be estimated from equation (30):

$$T_c \approx \frac{T_m^2}{T_m + 2(\frac{\Delta H_m}{\Delta c_p})} \quad (30)$$

It follows that T_c increases with decreasing ΔH_m and increasing T_m and Δc_p . Thus, the probability that T_c is above zero °C also increases with increasing size of the protein.

- T_{phys} is the optimum growth temperature of the organism from which the respective protein originates. For the vast majority of proteins, T_{phys} is *higher* than T_s . Figure 18 shows that both ΔH and $T\Delta S$ of folding are negative at temperatures between T_s and T_m (including T_{phys}), i.e., folding is enthalpically favored and entropically disfavored in this temperature range. In contrast, ΔH and $T\Delta S$ are both positive above T_c and below T_H (Figure 18), so that folding is entropically favored and enthalpically disfavored between T_c and T_H .
- Due to the large negative values of Δc_p of folding, the temperature dependence of ΔH and $T\Delta S$ is very high, and the absolute values of ΔH and $T\Delta S$ are much larger than that of ΔG . In other words, the free energy of folding ΔG is only a small difference of large numbers! This phenomenon is termed *enthalpy/entropy compensation*. Indeed, as a rule of thumb, one can say that ΔH_m is typically one order of magnitude higher than ΔG at temperatures close to T_s .

- To illustrate the enthalpy/entropy compensation in protein folding, Figure 19 shows exactly the same data as Fig. 18, but with a larger y-axis scale so that the values of ΔH and $T\Delta S$ are visible over the entire temperature range. While ΔH linearly depends on temperature (eq. 22), the temperature curve of $T\Delta S$ is bent and intersects the linear ΔH slope twice, namely at T_c and T_m where $\Delta G = 0$ and $\Delta H = T\Delta S$.

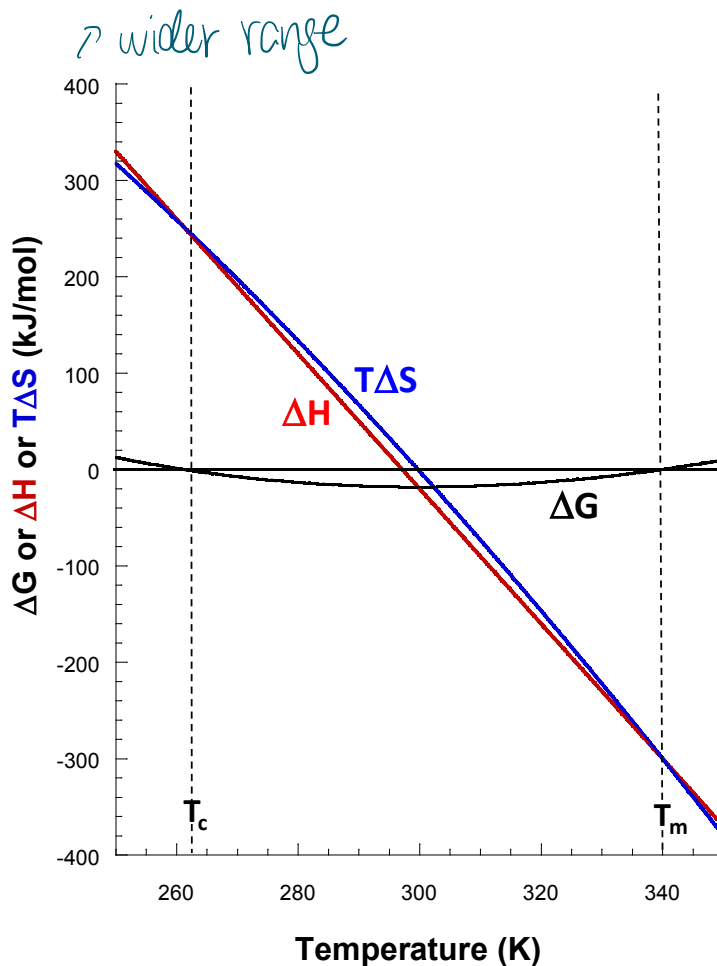


Figure 19: Temperature dependence of ΔG , ΔH and $T\Delta S$ of folding of a small one-domain protein with $\Delta c_p = -7 \text{ kJ mol}^{-1} \text{ K}^{-1}$, $\Delta H_m = -300 \text{ kJ mol}^{-1}$ and $T_m = 340 \text{ K}$. The figure shows the same data set as Figure 17, but with a larger y-axis scale. Note that the absolute values of ΔH and $T\Delta S$ are much larger than the corresponding ΔG values, and that the $T\Delta S$ curve intersects the linear ΔH slope at T_c and T_m .

As mentioned above, ΔH_m , T_m and Δc_p need to be known to calculate the free energy of folding of a protein at any temperature (eq. 26). The heat changes associated with thermal unfolding can be determined directly with *isothermal titration calorimetry (DSC)*. A cell containing protein with buffer and a reference cell with buffer alone are continuously heated and the energy required to keep both cells at constant temperature is recorded. The experiment yields the heat capacity c_p as a function of temperature (Figure 20A). The area under the obtained peak corresponds to ΔH_m of unfolding (ΔH_m (folding) = $-\Delta H_m$ (unfolding)), T_m as well as ΔC_p , which is the difference in the c_p values of the pre- and post-transition baseline (Figure 20A).

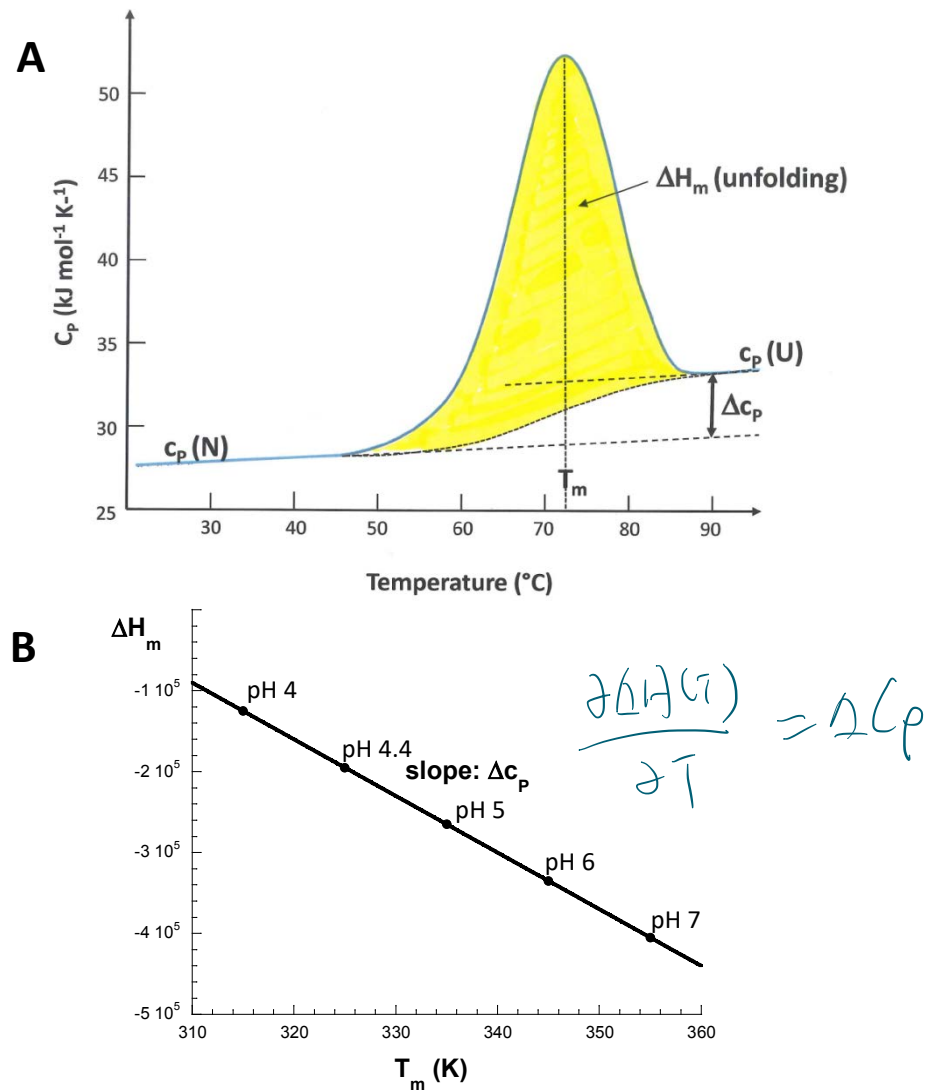


Figure 20: Thermal unfolding of a protein recorded with differential scanning calorimetry (DSC). A: Plot of c_p against temperature. The peak corresponds to the additional heat required for protein unfolding, the pre- and post-transition baselines correspond to the heat capacity of N and U, respectively. The yellow area under the peak corresponds to ΔH_m (unfolding). Note that ΔH_m (folding) = $-\Delta H_m$ (unfolding). In principle, the parameters ΔH_m , T_m and Δc_p thus can be obtained in a single experiment. B: For a more accurate determination of Δc_p , melting curves are recorded at different pH values (between neutral and acidic pH, because T_m usually decreases with decreasing pH). The recorded T_m values are plotted against the corresponding ΔH_m values for folding (filled circles), and the slope of the linear fit corresponds to Δc_p of folding.

The small differences between the pre- and post-transition baselines often make it difficult to determine Δc_p accurately from a single DSC run. For a more accurate determination of Δc_p , the DSC run is repeated at different pH values. As proteins typically become less stable at acidic pH, T_m decreases with decreasing pH, and ΔH_m of folding becomes less negative with decreasing pH. A plot of ΔH_m against T_m (Figure 20B) yields a linear relationship with the slope

of Δc_p (folding). Note that it is important to determine Δc_p experimentally with high precision, even though it can be roughly predicted from the mass of the protein (eq. 21).

An alternative way of measuring ΔH_m is the spectroscopic recording of the fraction of native molecules (f_N) during thermal unfolding. As long as the two-state model of folding is valid and thermal unfolding is fully reversible, the van't Hoff equation (eq. 27) can be applied, which describes the dependence of the equilibrium constant K of a chemical equilibrium on temperature and ΔH :

$$\frac{d(\ln K_{\text{eq}})}{dT} = \frac{\Delta H(T)}{RT^2} \quad (27)$$

Integration with T_m as reference temperature and $K_{\text{eq}} = [N]/[U]$ yields equation (28) which allows the calculation of the fraction of native molecules f_N as a function of temperature, T_m and ΔH_m :

$$f_N = \frac{\exp\left[\left(\frac{T}{T_m} - 1\right) \cdot \Delta H_m / RT\right]}{1 + \exp\left[\left(\frac{T}{T_m} - 1\right) \cdot \Delta H_m / RT\right]} \quad (28)$$

Figure 21 shows that thermal unfolding of a protein obeying the two-state model yields, similar to denaturant-induced unfolding, a symmetrical, S-shaped transition curve from which T_m and ΔH_m can be extracted. In addition, Figure 21 shows that the thermal unfolding transition becomes steeper with increasing ΔH_m .

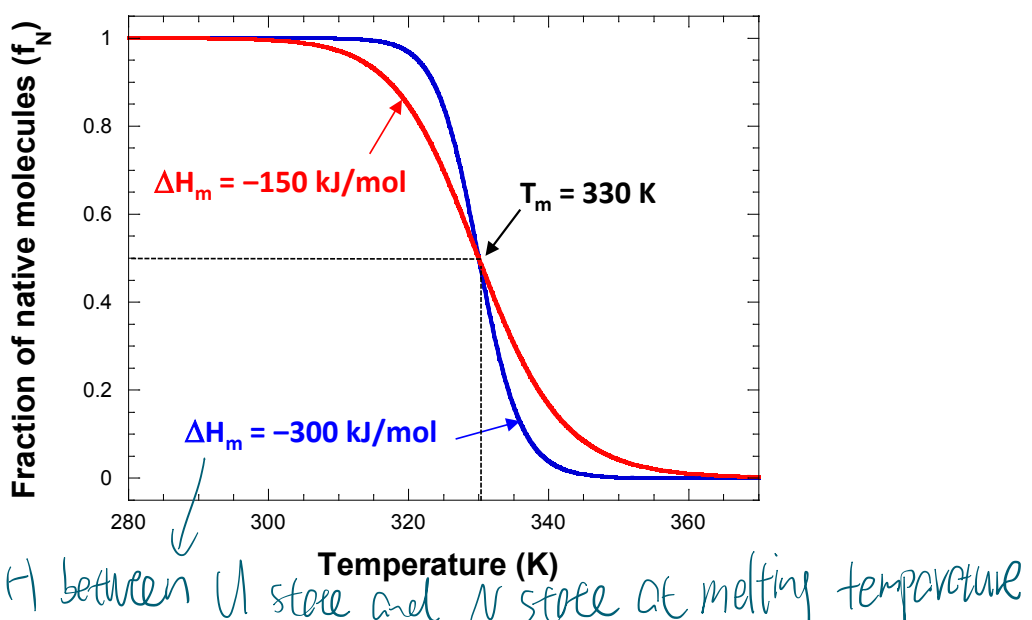


Figure 21: Thermal unfolding of two proteins with identical T_m , but different ΔH_m values (-150 and -300 kJ/mol, respectively). Both proteins reversibly unfold with increasing temperature according to the two-state model of folding. Protein unfolding is recorded via the change in a spectroscopic signal (typically the far-UV CD signal), and the recorded signal (S) is converted to the f_N , the fraction of native molecules ($f_N = (S - S_U) / (S_N - S_U)$) (see Figure 12).

It follows from the vant' Hoff equation (eq. 27, 28) that neither T_m nor ΔH_m contains information on the free energy of protein folding ΔG at temperatures other than T_m ! Figure 22 illustrates this and shows that T_m values cannot even be used as a qualitative measure to compare the stability of *different* proteins. It shows the dependence of ΔG on temperature for two proteins: a protein A isolated from a thermophilic organism with $T_m = 360$ K and a protein B isolated from a mesophilic organism with $T_m = 340$ K. Despite the higher T_m value of protein B, this does not mean that protein B is more stable than protein A at any temperature! On the contrary, protein A is three times more stable than protein B at 25°C in this specific example (-18.1 compared to -6.1 kJ/mol, respectively) due to the differences in ΔH_m and Δc_p between protein A and B.

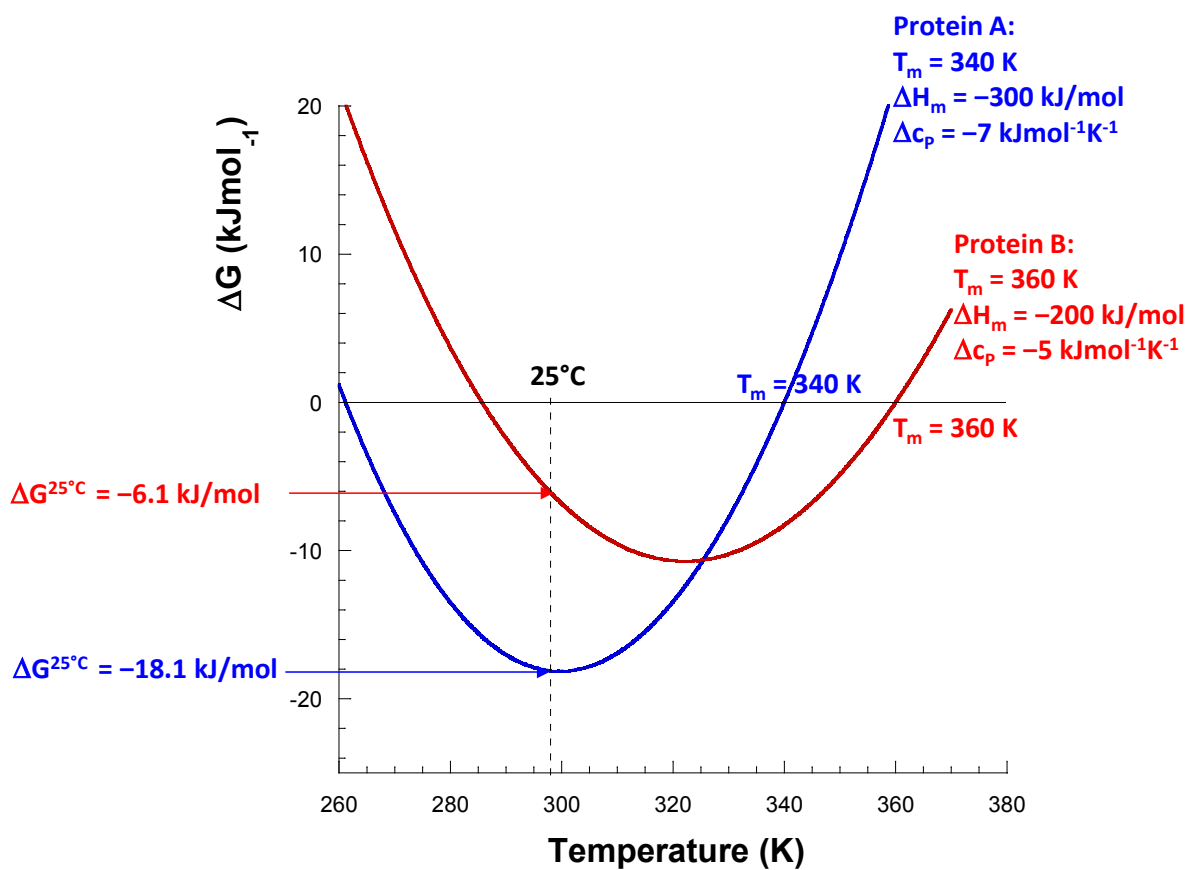


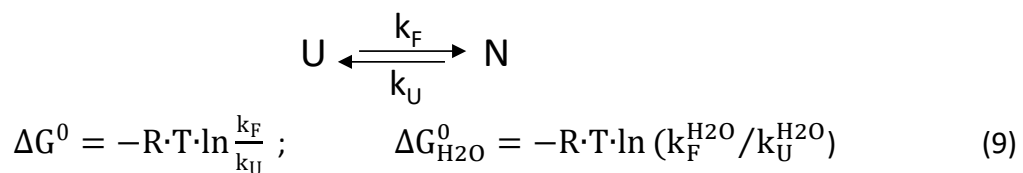
Figure 22: Higher melting temperature does not mean higher stability at any temperature. As an example, the stability profiles of a mesophilic (A) and thermophilic protein (B) are shown. The thermophilic protein is more stable at high temperatures and has a higher T_m , while the mesophilic protein is more stable at mesophilic temperatures.

5. Kinetics of protein folding

The folding funnel model in Figure 1 indicates that the energy landscape of protein folding may be rough and contain local minima that can be transiently populated by partially structured states during folding. In addition, Figure 1 shows that there may be parallel pathways leading to N in which U either folds directly to N or transiently populates a structured intermediate I.

5.1. Direct folding from U to N via a single transitions state

We first consider the simplest case that applies to many small one-domain proteins: The protein folds according to the two-state mechanism, and the energy landscape of folding is smooth so that no intermediates are populated and U folds to N via a single transition state. The folding equilibrium in the presence and absence of denaturant is thus characterized by only two microscopic rate constants, k_U and k_F :



In general, the kinetics of attainment of any two-state equilibrium in chemistry are influenced by both the forward and the reverse reaction, because both reactions contribute to the attainment of equilibrium. Applied to protein folding, this means that the observed rate constant of folding or unfolding, k_{obs} , is always the sum of k_F and k_U (eq. 29). Formally, folding and unfolding kinetics at any denaturant concentration will thus always yield only a single first-order rate constant, k_{obs} , and k_U and k_F cannot be determined directly.

$$k_{\text{obs}} = k_F + k_U \quad (29)$$

With increasing denaturant concentration [D], the rate constant of unfolding k_U increases exponentially and the rate constant of folding k_F decreases exponentially [5]. Thus, $\ln k_U$ and $\ln k_F$ linearly depend on denaturant concentration according to equations (30) and (31),

$$\ln k_F = \ln k_F^{\text{H}_2\text{O}} + m_F \cdot [D] \quad (30)$$

$$\ln k_U = \ln k_U^{\text{H}_2\text{O}} + m_U \cdot [D] \quad (31)$$

where $k_F^{\text{H}_2\text{O}}$ and $k_U^{\text{H}_2\text{O}}$ are the rate constants of folding at zero denaturant and m_F and m_U are the *kinetic m-values* of folding and unfolding, respectively, which are a measure of the denaturant-sensitivity of folding and unfolding (see Figure 23). Combination of equations (29–31) yields equation (32) that describes the dependence of $\ln k_{\text{obs}}$ on [D]:

$$\ln k_{\text{obs}} = \ln(k_F^{\text{H}_2\text{O}} \cdot e^{m_F \cdot [D]} + k_U^{\text{H}_2\text{O}} \cdot e^{m_U \cdot [D]}) \quad (32)$$

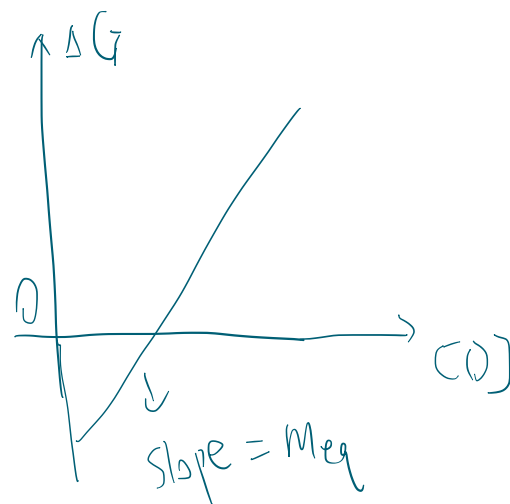
Equation (32) yields a V-shaped dependence of $\ln k_{\text{obs}}$ on denaturant concentration [12], which is also sometimes called “Chevron Plot”. Figure 23 shows a concrete example for a protein with an equilibrium unfolding transition at 3.0 M GdmCl, which folds with a rate constant of 0.5 s^{-1} at zero denaturant and has a free energy of folding of $\Delta G_{\text{H}_2\text{O}}^0 = -21 \text{ kJ/mol}$. At zero denaturant, unfolding is thus 4800-fold slower than folding (eq. 9). The V-shaped denaturant dependence of $\ln k_{\text{obs}}$ comes from the large differences between k_U and k_F outside of the transition region: At low denaturant concentrations (native conditions, folding branch of the V-plot), k_F is much larger than k_U so that k_U becomes negligible and $k_{\text{obs}} \approx k_F$. Conversely, k_F becomes negligible at high denaturant concentrations (unfolding branch of the V-plot) and $k_{\text{obs}} \approx k_U$. Thus, both unfolding and refolding experiments need to be performed for recording a V-plot. In the transition region (f_N values between 0.1 and 0.9 after attainment of the equilibrium), the k_{obs} values of the unfolding and refolding kinetics coincide (Figure 23 B and Figure 24). Figure 23 also shows that the lines of $\ln k_U$ and $\ln k_F$ intersect at the transition midpoint (3 M GdmCl), because $k_U = k_F$ at $[D]_{1/2}$.

V-Plot data also provide an additional tool to verify the two-state model of folding, because the linear extrapolation of the folding and the unfolding branch to zero denaturant yields $k_F^{\text{H}_2\text{O}}$ and $k_U^{\text{H}_2\text{O}}$ (Figure 23B). If the two state model is correct, the $\Delta G_{\text{H}_2\text{O}}^0$ value calculated from the $k_F^{\text{H}_2\text{O}}/k_U^{\text{H}_2\text{O}}$ ratio (eq. 9) must be identical to the $\Delta G_{\text{H}_2\text{O}}^0$ value obtained from equilibrium unfolding/refolding experiments (eq. 12, Figure 13).

The linear dependence of $\ln k_F$ and $\ln k_U$ on denaturant (eq. 30, 31) readily explains why ΔG^0 is linearly dependent on denaturant concentration! In fact, the kinetic m-values m_F and m_U are linked to the equilibrium m_{eq} value via equation (33). Note that m_U is always positive and m_F is always negative (Figure 23B).

$$m_{\text{eq}} = (m_U - m_F) \cdot RT = (|m_U| + |m_F|) \cdot RT \quad (33)$$

Equation (33) thus provides additional tool to verify the correctness of the two-state assumption.



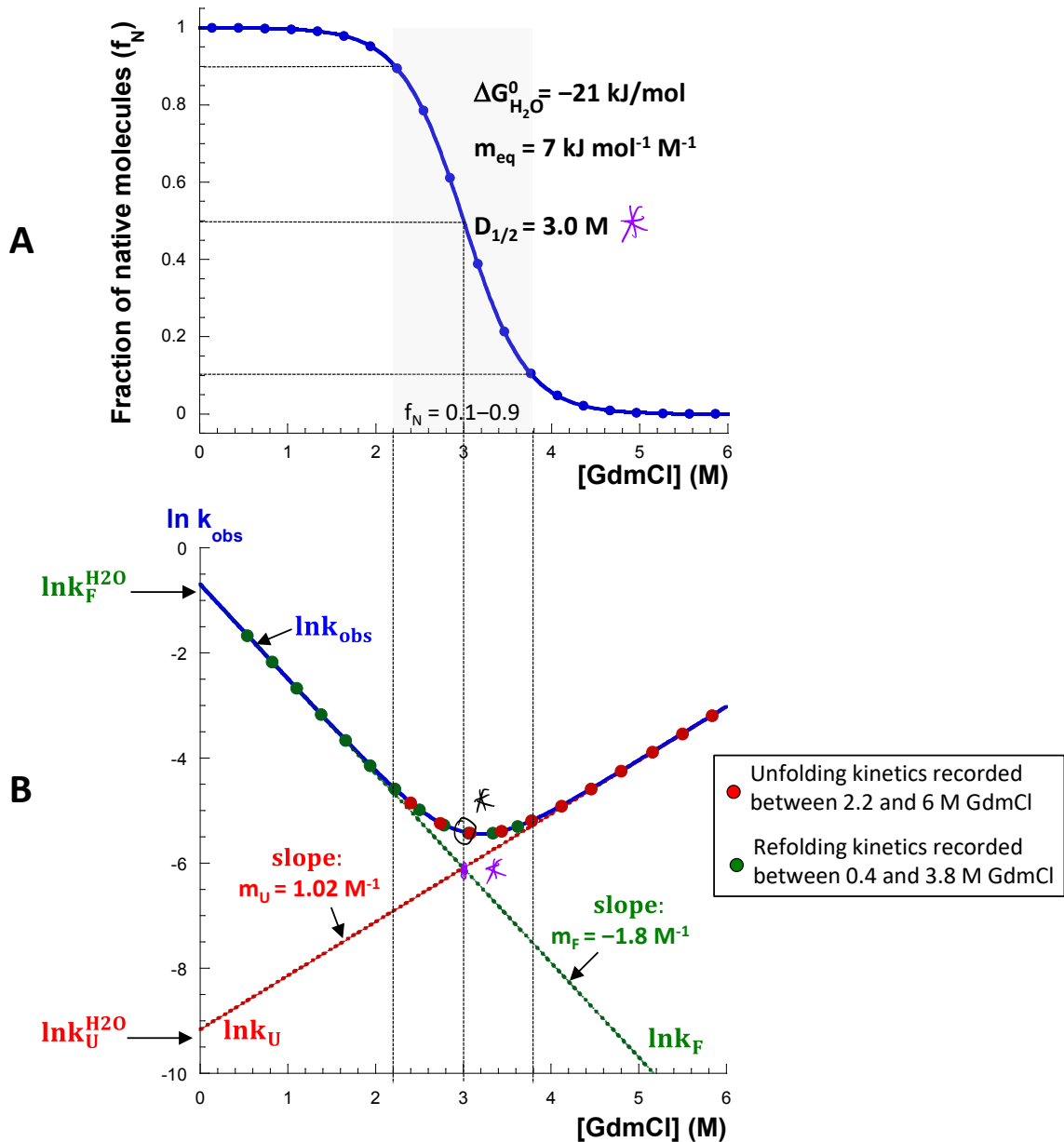


Figure 23: Unfolding/refolding kinetics of a protein that folds according to the two-state model (no kinetic intermediates are populated).

A: GdmCl-dependent equilibrium unfolding transition with the following parameters: $\Delta G_{H_2O}^0 = -21 \text{ kJ/mol}$; $m_{eq} = 7 \text{ kJ mol}^{-1} M^{-1}$, $D_{1/2} = 3 \text{ M}$ GdmCl. The gray area highlights the transition region in which the fraction of native molecules f_N varies between 0.1 and 0.9.

B: V-plot (also termed “Chevron Plot”) showing the dependence of the logarithm of the observed rate constant of folding and unfolding ($k_{obs} = k_F + k_U$) on GdmCl concentration (blue line). The green and red dotted lines show the linear dependence of $\ln k_F$ and $\ln k_U$ on GdmCl concentration with their kinetic m-values m_F and m_U , respectively. The dotted lines intersect at the transition midpoint (3.0 M GdmCl) where $k_F = k_U$. Note that k_{obs} can be obtained from either unfolding or refolding kinetics at GdmCl concentrations in the transition region (see overlapping data points in the transition region). $\ln k_F^{H_2O} = -0.693$; $k_F^{H_2O} = 0.5 \text{ s}^{-1}$; $\ln k_U^{H_2O} = -9.16$; $k_U^{H_2O} = 10.5 \cdot 10^{-4} \text{ s}^{-1}$.

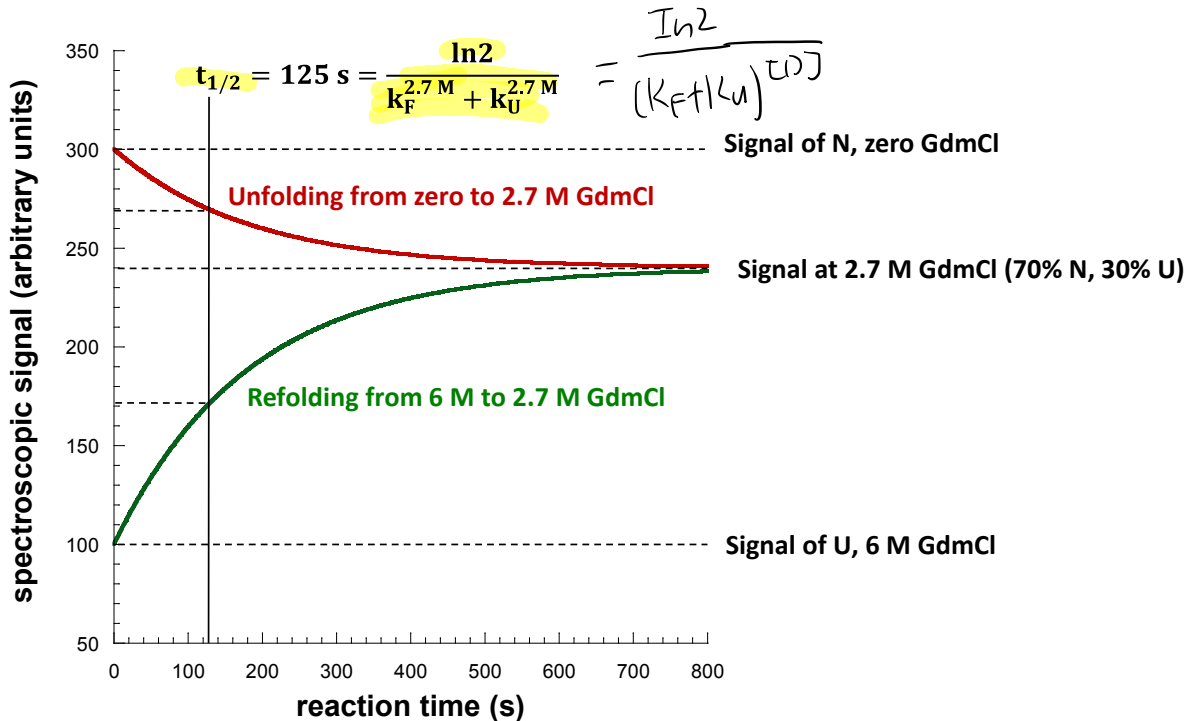


Figure 24: Kinetics of refolding (green line) and unfolding (red line) of the protein from Figure 23 in the transition region at 2.7 M GdmCl where 70% of the molecules are native and 30% of the molecules are unfolded after attainment of equilibrium. Both reactions show the same value of k_{obs} , corresponding to a half-life of 125 s. The spectroscopic signal of N is 300 a.u., and that of U is 100 a.u. the signal after attainment of equilibrium is 240 a.u.. At 2.7 M GdmCl, $k_F = 3.88 \cdot 10^{-3} \text{ s}^{-1}$, $k_U = 1.66 \cdot 10^{-3} \text{ s}^{-1}$, and $k_{\text{obs}} = 5.54 \cdot 10^{-3} \text{ s}^{-1}$.

V-Plots not only contain the same information on protein stability as equilibrium unfolding transitions (i.e., $\Delta G_{\text{H}_2\text{O}}^0$ and m_{eq}), but additional information on the dynamics of the folding equilibrium ($k_U^{\text{H}_2\text{O}}$ and $k_F^{\text{H}_2\text{O}}$) and the solvent accessibility of the transition state TS. For the latter, the values of m_U and m_F are analyzed. Analogous to the dependence of m_{eq} on the difference in accessible surface area between U and N ($\Delta \text{ASA}_{\text{UN}}$ (eq. 15)), the kinetic m-values m_F and m_U depend on differences in accessible surface area between U and TS ($\Delta \text{ASA}_{\text{U-TS}}$), and N and TS ($\Delta \text{ASA}_{\text{N-TS}}$), respectively. This is illustrated by Figure 25 that shows the energy diagram of a two-state folding reaction: As the reaction from U to TS determines the rate of folding (k_F), the denaturant-sensitivity of the rate of folding, m_F , depends on $\Delta \text{ASA}_{\text{U-TS}}$. Conversely, m_U depends on $\Delta \text{ASA}_{\text{N-TS}}$. TS is generally more compact than U and often already partially structured, so that $\text{ASA}_U > \text{ASA}_{\text{TS}} > \text{ASA}_N$.

Together, the comparison of the absolute values of m_F and m_U provides information about ASA_{TS} relative to ASA_N and ASA_U . For this purpose, the parameter α has been introduced, which is defined as follows (eq. 34) [13]:

$$\alpha = \frac{|m_F|}{|m_F| + |m_U|} \quad (34)$$

The following rules apply to the interpretation of the α -value:

- $0.5 < \alpha < 1$ ($|m_F| > |m_U|$): ASA_{TS} is more similar to ASA_N than to ASA_U . The transition state is relatively compact and more than 50% of the residues contribute to the stabilization of TS. *large MF K_F is more dependent on denaturant concentration*
- $0 < \alpha < 0.5$ ($|m_U| > |m_F|$): ASA_{TS} is more similar to ASA_U than to ASA_N . Less than 50% of the residues contribute to the stabilization of TS. *low MF ASA_U ASA_N*

V-plots have been determined for a quite large number of small proteins that obey the two-state model of folding. *It turned out the majority of proteins show α -values above 0.5.*

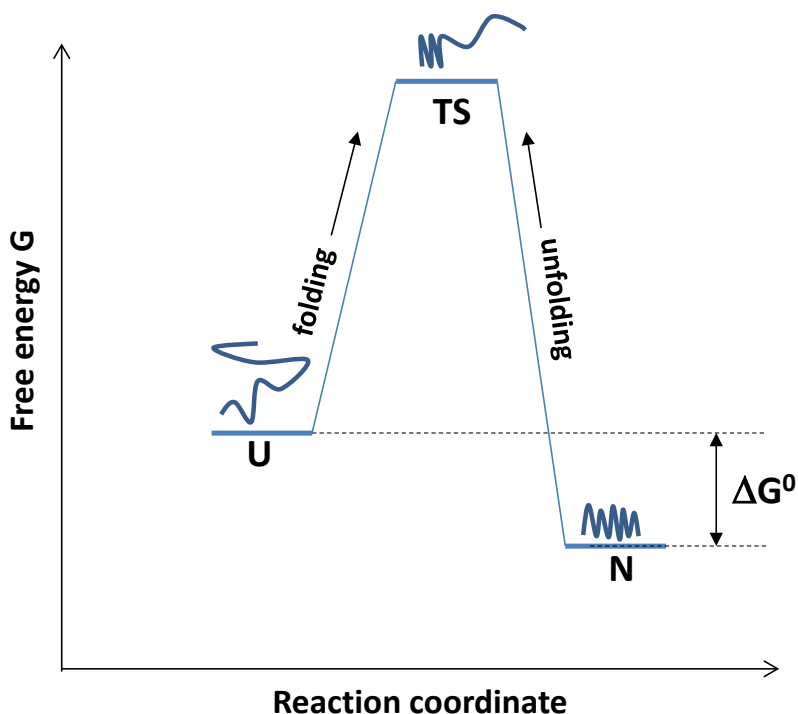


Figure 25: Energy diagram of two-state folding via a single transition state (TS).

expt high denaturant-dependence
of K_F low denaturant-dependence
of K_U

↓
partially folded
and its ASA is more
similar to N compared to U.
 $U \rightarrow TS$ transition has high
ASA
 $N \rightarrow TS$ transition has low
ASA

38

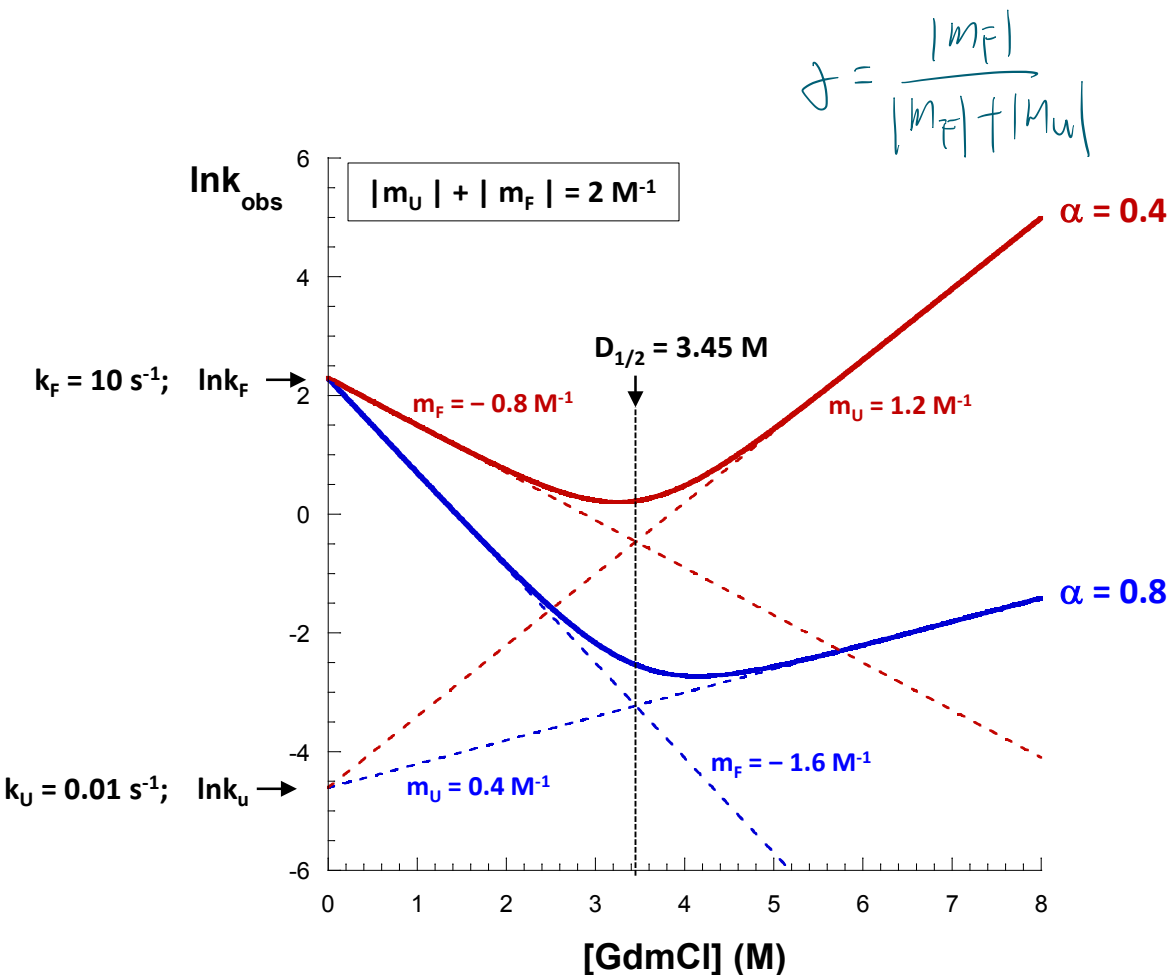
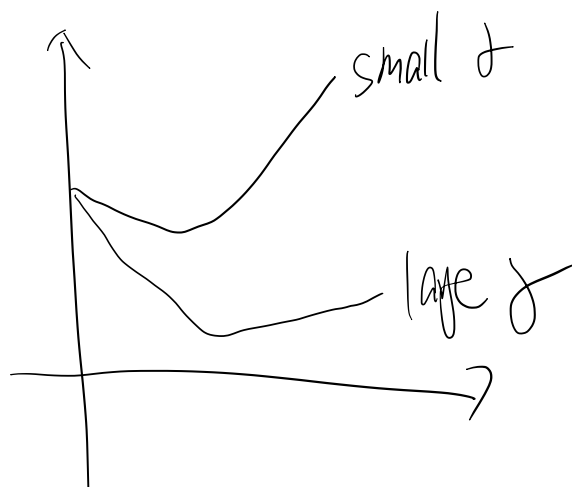


Figure 26: The shape of the V-Plot provides information on the difference in accessible surface area (ASA) between the transition state (TS) of folding relative to ASA of U and N. The figure shows a theoretical example of two proteins with identical $\Delta G_{\text{H}_2\text{O}}^0$ (-17.1 kJ/mol, $D_{1/2} = 3.45 \text{ M}$ GdmCl) and identical values of $k_F^{\text{H}_2\text{O}}$ (10 s^{-1}) and $k_U^{\text{H}_2\text{O}}$ (0.01 s^{-1}). The proteins however differ in the solvent accessibility of TS: For the protein with $\alpha = 0.8$ (blue line), ASA of TS is closer to ASA of N, while ASA of TS is closer to ASA of U for the protein with $\alpha = 0.4$ (red line).



Phi-value analysis for characterization of TS

How can one find out whether a specific amino acid side chain contributes to the structure and stability of TS? For this purpose, a method termed “**phi (ϕ) value analysis**” can be applied [14,15]. It is based on the observation that the α -value (i.e., the shape of the V-plot) is not affected when only a single residue in a protein is replaced. *In other words, the replacement of only a single amino acid in a protein generally has no influence on the structure and solvent accessibility of TS.* In phi value analysis, the specific residue of interest is replaced by alanine, and the V-plots of the wild type protein (WT) and the Ala variant are compared. *We assume that the Ala replacement has no influence on the free energy of U* and consider the following three cases:

\nearrow transition state

A: The replaced residue contributes to the stability of TS to the same extent as to the stability of N. Therefore, TS of the Ala variant (TS_{var}) is less stable (i.e., has a higher free energy) than TS of the WT (TS_{WT}), and N_{var} is destabilized relative to N_{WT} to the same extent, so that $\Delta G_N = \Delta G_{TS}$. The variant will thus fold slower than WT, but unfold with the same rate: $k_F^{H_2O}(\text{variant}) < k_F^{H_2O}(\text{WT})$ and $k_U^{H_2O}(\text{variant}) = k_U^{H_2O}(\text{WT})$.

B: The replaced residue does not contribute to the stability of TS and only contributes to the stability of N. Therefore, the stability of TS_{var} will be identical to TS_{WT} , and only N_{var} will be less stable than N_{WT} . Consequently, the variant will fold with the same rate as the WT, but unfold faster than WT:

$$k_F^{H_2O}(\text{variant}) = k_F^{H_2O}(\text{WT}) \text{ and } k_U^{H_2O}(\text{variant}) > k_U^{H_2O}(\text{WT}).$$

C: The replaced residue partially contributes to the stability of TS, but to a smaller extent compared to the stabilization of N by this residue ($\Delta G_{TS} < \Delta G_N$). Therefore, the variant will fold slower and unfold faster than the WT:

$$k_F^{H_2O}(\text{variant}) < k_F^{H_2O}(\text{WT}) \text{ and } k_U^{H_2O}(\text{variant}) > k_U^{H_2O}(\text{WT}).$$

The phi-value ϕ of an individual residue in a protein has been introduced as a parameter that quantified the residue's influence on the stability of TS and N. It is defined by equation (35):

$$\phi = \frac{\Delta G_{TS}}{\Delta G_N} \quad \text{See picture 42} \quad (35)$$

Based on the assumption that the influence on the free energy of U of a single amino acid replacement is negligible, the parameter ΔG_N can be calculated from the difference between the thermodynamic stability of the variant and the WT (eq. 36)

$$\Delta G_N = \Delta G_{var.} - \Delta G_{WT} \quad (36)$$

Where ΔG_{WT} and $\Delta G_{var.}$ to the free energies of folding in the absence of denaturant, $\Delta G_{H_2O}^0$, of the WT and the variant, respectively.

The parameter ΔG_{TS} can be calculated from the ratio between the rate constants of folding in the absence of denaturant of the wild type and the variant according to equation (37):

$$\Delta G_{TS} = R \cdot T \cdot \ln \frac{k_F^{H_2O}(WT)}{k_F^{H_2O}(var.)} \quad (37)$$

Therefore, the three different residues that were replaced in cases A–C will have the following phi-values:

Case A: $\phi = 1$;

Case 2: $\phi = 0$;

Case C: $0 < \phi < 1$.

Figures 27 shows the V-plots for the variants (A–C) compared to the V-plot of the WT, and Figure 28 shows the energy diagrams for the variants (A–C).

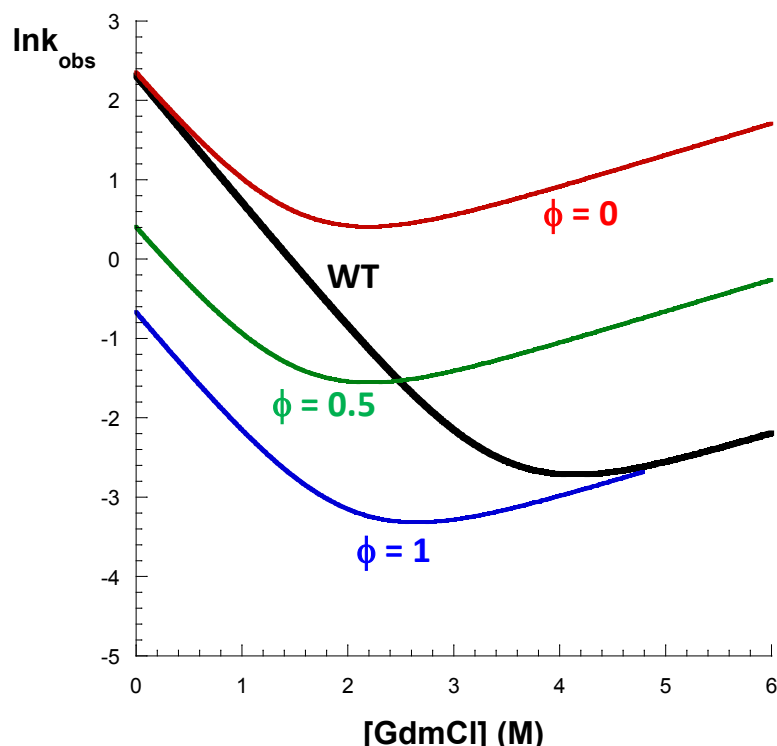


Figure 27: ϕ -value analysis with V-plots for three protein variants in which a different residue was replaced by Ala. All three variants are less stable than the wild type, which can be seen from their transition midpoints $[D_{1/2}]$ (intercept of the extrapolated folding and unfolding branches) that are shifted to lower GdmCl concentration relative to $[D_{1/2}]$ of the wild type. All variants have the same α -value as the wild type (WT). Linear extrapolation of the unfolding branches to zero GdmCl yields the respective values of $k_U^{H_2O}$.

Black solid line: V-plot of the WT protein.

Blue solid line: Case A, variant with $\phi = 1$. $k_U^{H_2O}$ is not affected by the amino acid replacement, but $k_F^{H_2O}$ is smaller than $k_F^{H_2O}$ of the WT.

Red solid line: Case B, variant with $\phi = 0$. $k_F^{H_2O}$ is not affected by the amino acid replacement, but $k_U^{H_2O}$ is larger than $k_U^{H_2O}$ of the WT.

Green solid line: Case C, variant with $\phi = 0.5$. Relative to the WT, the single amino acid replacement in variant C leads to a decrease in $k_F^{H_2O}$ and an increase in $k_U^{H_2O}$.

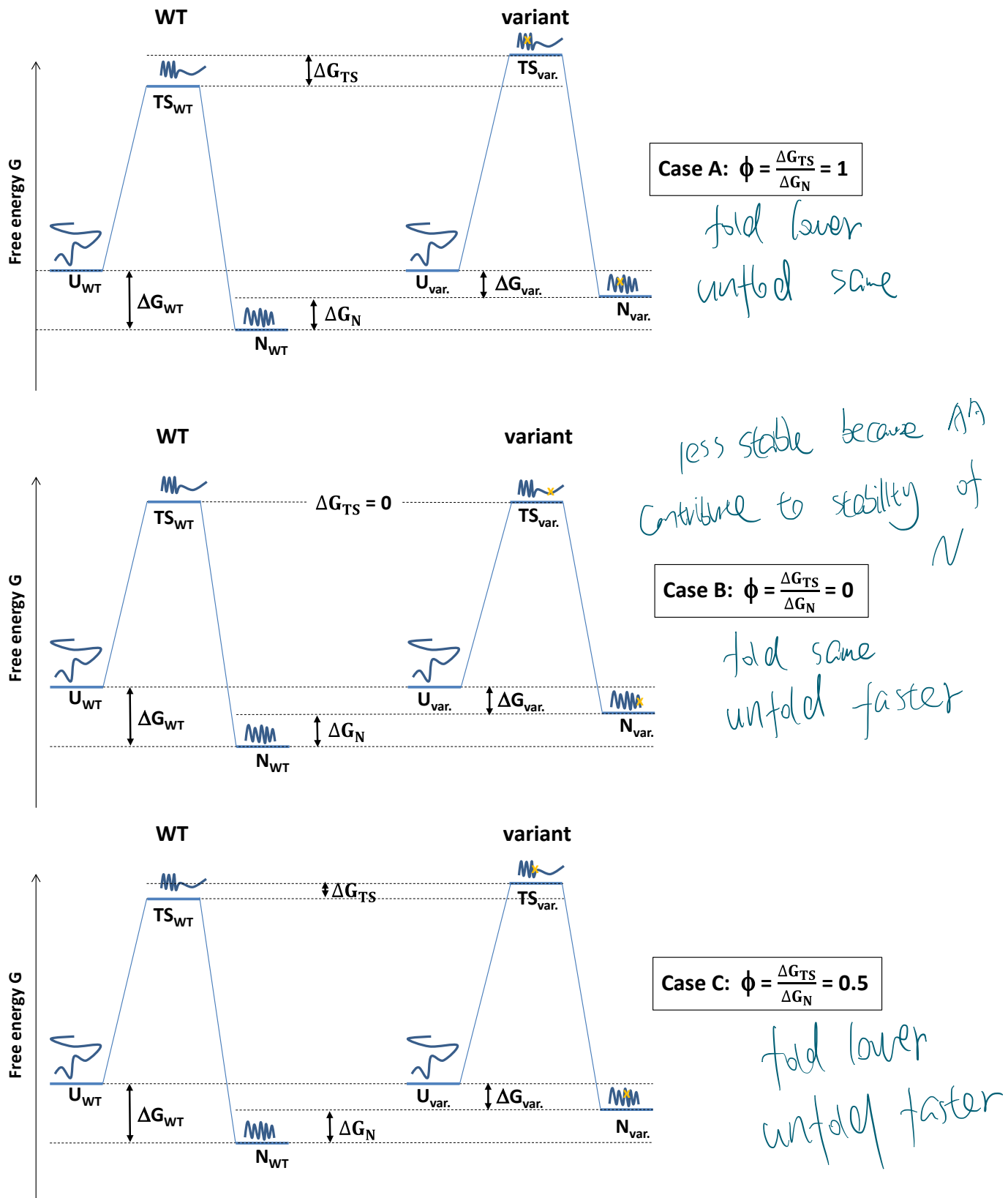


Figure 27: Energy diagrams for three variants of the same protein with single Ala replacements at different positions showing with ϕ -values of 1 (A), zero (B) and 0.5 (C). ΔG_{WT} and $\Delta G_{var.}$ correspond to the thermodynamic stabilities in the absence of denaturant of the WT and the variant, respectively.

Although TS of folding cannot be observed directly and thus cannot be characterized structurally, the systematic replacement of each individual residue in a protein and the recording of the phi-values of all residues allow, at least to a certain extent, the visualization of TS. For this purpose, the residues in the three-dimensional structure of the protein are color-coded according to their phi values, allowing the identification of regions in TS which have already formed native-like interactions. Although this analysis is biased because no structural information on TS is accessible, it is reasonable to assume that native-like interactions govern the folding pathway, and that the structure of TS is mostly stabilized by native-like interactions.

The speed limit of direct folding from U to N

As mentioned in chapter one, many small one-domain proteins show half-lives ($t_{1/2}$) of folding between 1 ms and 10 s (corresponding to $k_F^{H_2O}$ values between 1000 s^{-1} and 0.1 s^{-1} ; $t_{1/2} = \ln 2 / k_F^{H_2O}$). Direct on-line recording of their folding kinetics is therefore well accessible for spectrometers coupled to a stopped-flow mixing device (Figure 28). It has turned out that the logarithm of $k_F^{H_2O}$ decreases linearly with increasing contact order of the protein's three-dimensional structure (Figure 29). The contact order is defined as the average distance in the primary structure between all pairs of residues forming a contact in N, normalized to the length of the polypeptide chain (equation 37):

$$\text{contact order} = \frac{\text{average distance in the amino acid sequence between all pairs of residues forming a contact in N}}{\text{total number of residues in the protein}} \cdot 100\% \quad (37)$$

Proteins that exclusively contain α -helices as regular secondary structures have low contact orders due to the main chain hydrogen bonds between the carbonyl group of residue i and the NH group of residue $i+4$ in α -helices. In contrast, β -sheet proteins with complex β -sheet topologies have much higher contact orders because β -strands that are very distant in the amino acid sequence come together and form β -sheets with inter-strand hydrogens bonds. Thus, there is a tendency that α -helical proteins fold faster than β -sheet proteins.

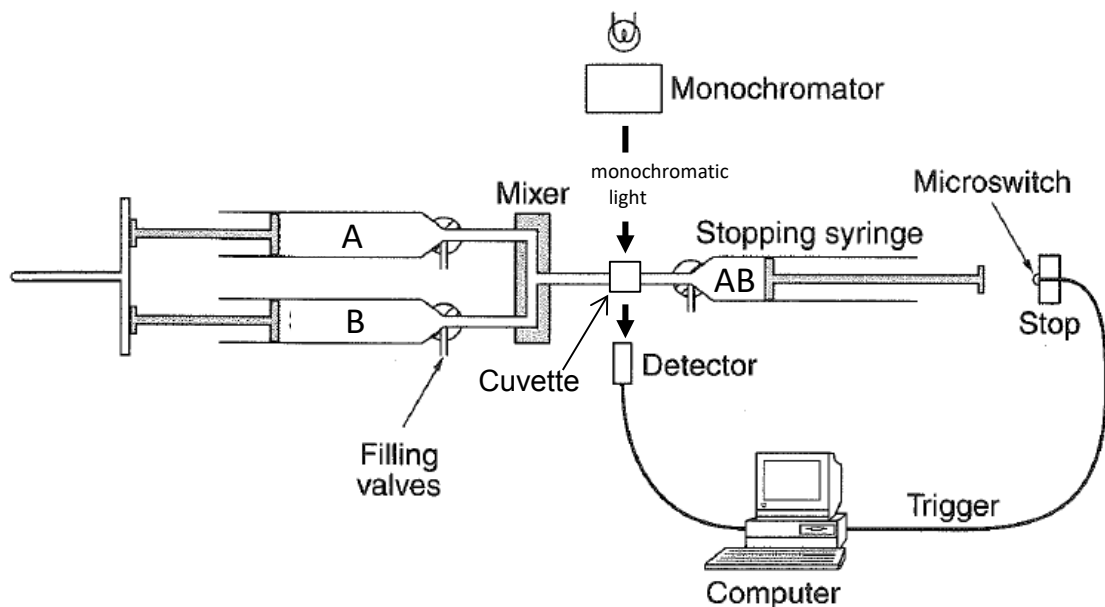


Figure 28: Stopped-flow apparatus for recording fast reactions. The reaction is started by pressing the stamps of the syringes containing solutions A and B into the mixer. The AB mixture is pressed into the stopping syringe until the stamp of the stopping syringe hits the microswitch that starts the recording of the spectroscopic signal of the AB mixture in the cuvette. When the flow in the system stops, the AB mixture in the cuvette is about 1–2 milliseconds old (dead time of the experiment), and the signal change after this dead time is recorded. Note that the mixing ratio for the solutions A and B can be varied by using syringes with different diameters. Adapted from A. Fersht, *Structure and Mechanism in Protein Science*, 1999, Freeman, New York.

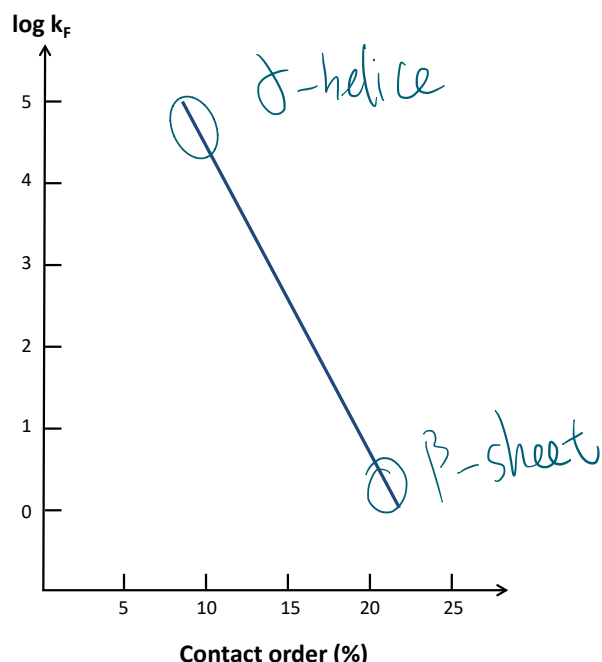


Figure 29: As a rough approximation, the logarithm of the rate constant of folding decreases linearly with increasing contact order.

The fastest known protein folding reactions show half-lives of about 10–100 µs and have been recorded for small polypeptides with 30–50 residues. This raises the question of the speed limit of protein folding. Spectroscopic triplet-triplet energy transfer reactions that require a direct physical contact between donor and acceptor have shown that it takes about 100 ns for formation of a single contact between side chains that are about 10 residues apart in the sequence of an unfolded peptide. Formation of all native contacts in the fastest folding proteins thus takes about 2–3 orders of magnitude longer. Essentially all proteins that show very high folding rates with half-lives of 10–100 µs are α -helical proteins with similar, low contact orders. Among these very fast folders, there is a tendency towards slower folding with increasing protein size.

5.2. Folding intermediates and their consequences for protein folding kinetics

We now consider cases where the energy landscape of folding is not smooth but rough (Figure 1) so that the polypeptide chain can fall into local minima populated by partially structured, kinetic intermediates. As kinetic intermediates are always less stable than N, they are generally not populated to an extent that they can be detected after the attainment of the folding equilibrium. However, kinetic intermediates can be detected during the folding reaction from U to N. Two main types of kinetic intermediates can be distinguished:

- Molten globule (MG)-like intermediates that lack tertiary structure but nevertheless are already relatively compact and already contain secondary structure elements.
- Structured intermediates that already contain a significant amount of tertiary structure. Structured intermediates are more stable and more similar to N than MG-like intermediates.

Kinetic intermediates generally make the folding reaction slower. For the vast majority of proteins that accumulate kinetic intermediates during folding, one can say that the more structured (the more stable) an intermediate is, the more it slows the folding reaction, because the activation energy for leaving an intermediate state and reacting further to N typically increases with increasing stability of the intermediate (Figure 30). Note that the states U, MG and I in the two-dimensional representation of Figure 30 do not represent a single structurally well-defined state, but an ensemble of different states with very similar energy that can be formally treated as a single state.

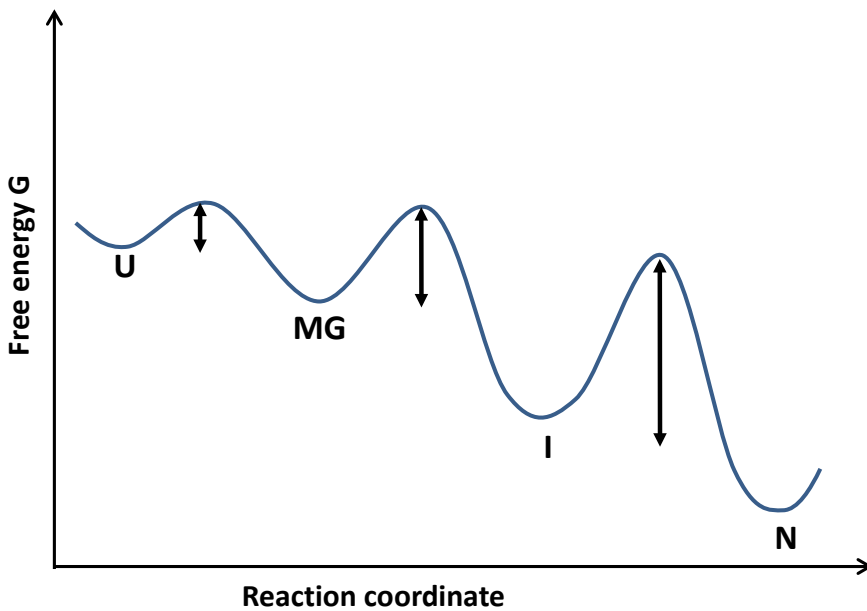


Figure 30: The activation energy ($\uparrow\downarrow$) required to leave a partially structured state on the folding pathway from U towards N generally increases with the stability of the intermediate.

We first consider a simple case where a MG-like state is transiently populated during the folding reaction. As the activation energy required for the reaction from U to MG is very low, MG-like states are formed very rapidly on the microsecond time scale and the kinetics of formation of MG are too fast for being detectable by stopped-flow kinetics (dead time: 1–2 ms). The rate-limiting transition state for the folding reaction is therefore the transition state for the reaction from MG to N (Figure 31C). As MG-like states form extremely rapidly during protein refolding at low denaturant concentrations and are formed much faster than the MG \rightarrow N reaction, the observed folding reaction stays an apparent first-order reaction. Nevertheless, the transient population of a MG-like intermediate can be detected if MG differs in its spectroscopic properties from U and N. If this is the case, the signal at $t = 0$ in a refolding experiment recorded by stopped flow mixing will not be the signal of U but that of MG. Consequently, the **amplitude** of the signal change recorded during the refolding reaction will deviate from the amplitude expected for the direct folding from U to N. Figure 31 shows a specific example and demonstrates that the analysis of the amplitude of the signal change during the folding reaction is a very important tool for verifying or excluding collapsed, MG-like intermediates during folding. As MG-like intermediates are only slightly more stable than U and much less stable than structured intermediates, they do not significantly affect (slow) the folding reactions. In addition, due to their low stability, they accumulate only at very low denaturant concentrations.

The role of rapidly forming MG-like intermediates in protein folding is still poorly understood. Specifically, it is not clear whether they are productive on-pathway intermediates for the folding of certain proteins, or whether they are just collapsed states that many polypeptides form after initiation of refolding by rapid dilution to low denaturant concentration.

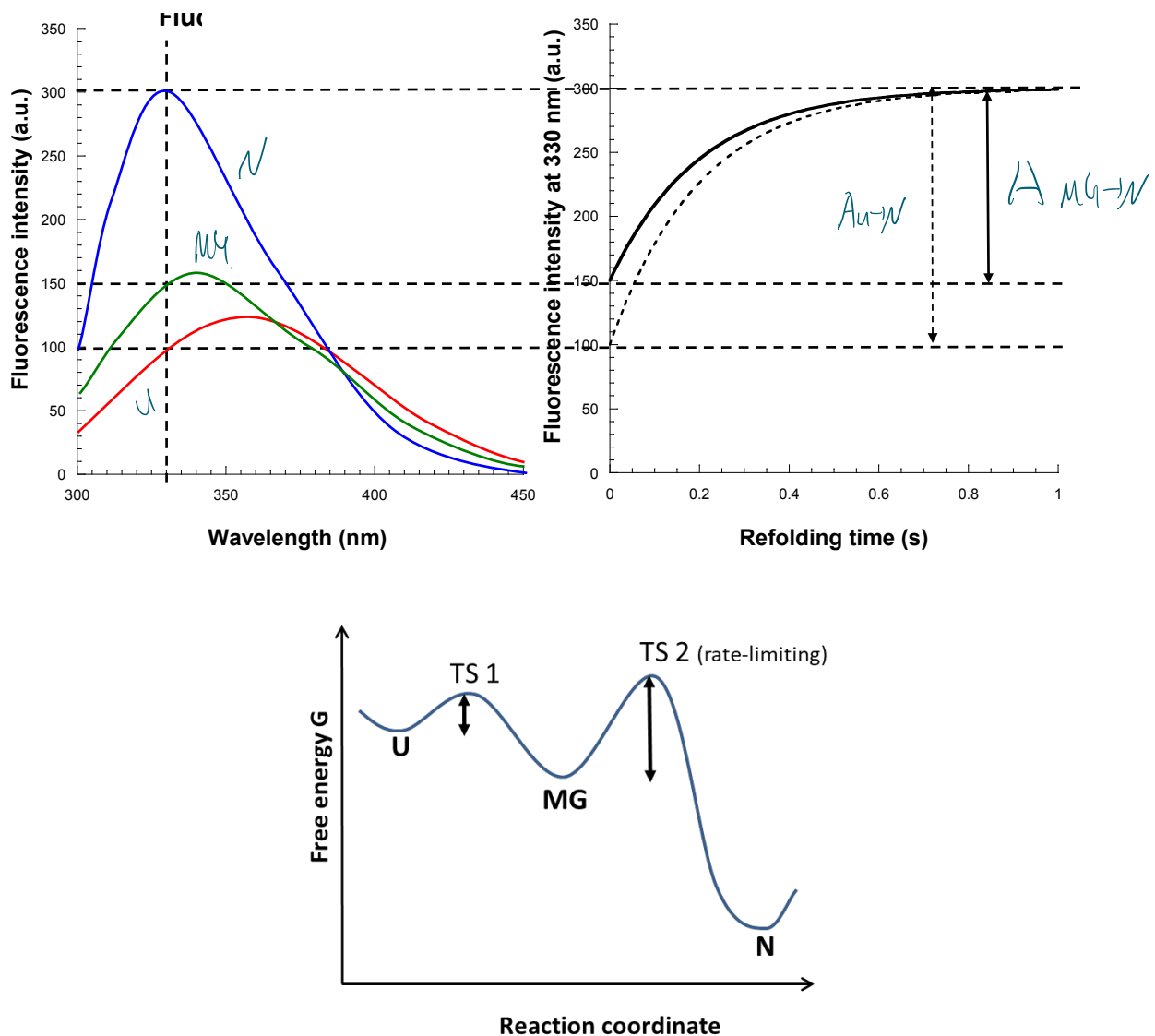


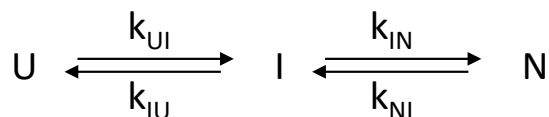
Figure 31: A rapidly forming molten-globule (MG) intermediate during protein folding can be detected when MG differs in its spectroscopic properties from U and N.

A: Fluorescence spectra of U, MG and N, showing that all three species can be well distinguished via the fluorescence signal at 330 nm.

B: Stopped-flow refolding kinetics recorded via the fluorescence intensity at 330 nm (solid line), showing that the fluorescence does not start at the signal of U but with the signal of MG. MG thus formed rapidly during the dead time of the stopped-flow experiment. The existence of MG is evident from a smaller amplitude of the fluorescence trace ($A_{MG \rightarrow N}$) compared the amplitude ($A_{U \rightarrow N}$) expected for the direct reaction from U to N (dotted line).

C: Energy diagram of the $U \rightarrow MG \rightarrow N$ mechanism at low denaturant concentrations. The transition state TS 2 is the rate-limiting transition state.

We now consider the case where a **structured kinetic intermediate I** accumulates during protein folding that is more stable than a MG state but less stable than N [13]. We assume that the intermediate is on-pathway and can directly react to N (it is generally difficult to distinguish between on- and off-pathway intermediates, but it has turned out that most structured intermediates in folding are on-pathway). If the folding pathway of all molecules proceeds via I, the kinetic mechanism can be described by the following scheme with four rate constants:



In general, kinetic intermediates can only be detected if they are more stable than the educt and less stable than the product of the reaction [13]. The **intermediate then causes the appearance of an additional kinetic phase**, i.e., product formation can longer be described by simple first-order kinetics (see below). In contrast, if the **intermediate is less stable than both the educt and the product of the reaction**, the kinetics of product formation will be indistinguishable from a two-state system without intermediate.

As kinetic intermediates in protein folding are less stable than N, they **can only be detected at low denaturant concentrations**. This is because the $U \leftrightarrow I$ equilibrium is already on the side of U at medium denaturant concentrations where N starts to unfold. The intermediate I will thus also have a higher energy than U at high denaturant concentrations where U is more stable than N. This is illustrated by the free energy profiles in Figure 32:

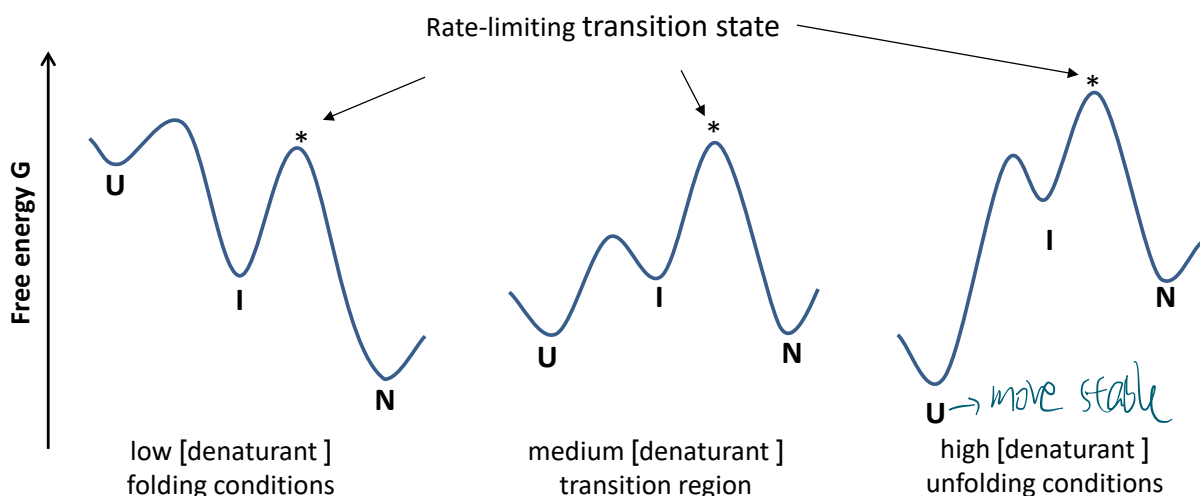


Figure 32: Energy diagram for a protein folding reaction in which a structured intermediate I is populated that is more stable than U but less stable than N at zero or low denaturant concentration (left panel). The intermediate I can however not be observed at medium (transition region) or high denaturant concentrations (unfolding conditions) where **I is always less stable than U and N** (middle and right panel). If the reaction from I to N is rate-limiting for formation of N at low denaturant concentrations and significantly slower than the U to I reaction, the folding reaction at low denaturant concentrations appears like a single first-order reaction.

We now consider the refolding reaction of a protein that accumulates a kinetic intermediate at very low denaturant concentration where the reverse reactions (k_{IU} and k_{NI}) are negligibly slow so that the kinetics of formation of N can be described with an irreversible, consecutive mechanism ($U \rightarrow I \rightarrow N$). Figure 33 shows that the occurrence of I can be immediately recognized by a lag phase in the formation of N if $k_{UI} \approx k_{IN}$. However, the lag phase apparently disappears and the kinetics of formation of N can no longer be distinguished from a mono-exponential $U \rightarrow N$ reaction if the formation of I is more than 100-fold faster than the $I \rightarrow N$ reaction ($k_{UI} \geq 100 k_{IN}$).

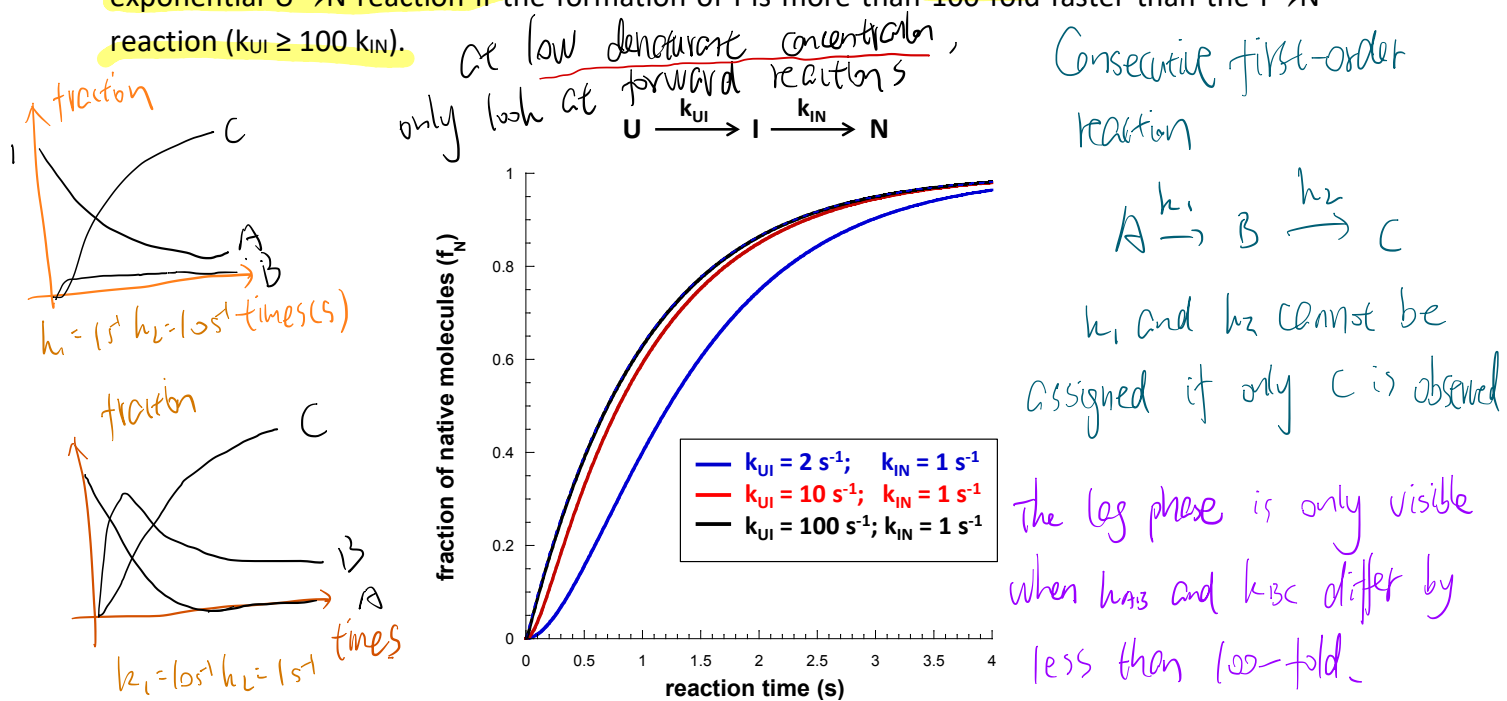


Figure 33: Influence of the rate of the $U \rightarrow I$ reaction on the kinetics of formation of N. A lag phase in the formation of N is only detectable if $k_{UI} \approx k_{IN}$. If $k_{UI} >> k_{IN}$, the kinetics cannot be distinguished from a first-order $U \rightarrow N$ reaction.

As the $U \rightarrow I$ reaction generally has a lower activation energy than the $I \rightarrow N$ transition (Figure 30), the observed folding kinetics at low denaturant concentration are indeed often apparently mono-exponential, so that is impossible to judge from a single, mono-exponential refolding trace whether the folding mechanism is two-state or proceeds via a kinetic intermediate. However, the presence of a kinetic intermediate becomes immediately evident when the *entire* V-plot is analyzed: As I is not populated in the transition region and under unfolding conditions (Figure 32), the shape of the V-plot does not deviate from a two-state mechanism at medium and high denaturant concentrations. However, at low denaturant concentrations where I is transiently populated during refolding, the folding limb of the V-plot deviates from a two-state mechanism because the intermediate slows the folding reaction! With decreasing denaturant concentration, the observed (apparent) first-order rate constant of folding thus continuously decreases compared to a pure two-state mechanism, as illustrated in Figure 34. An important consequence of the formation of I during folding at low denaturant concentration is that the free energy of folding at zero denaturant can no longer be determined from the ratio between the extrapolated, apparent rate constant at zero denaturant of the bent folding limb and the extrapolated unfolding rate constant at zero denaturant. Consequently, the only possibility to distinguish between a two-state and a three-state mechanism of folding is the analysis of the entire V-Plot.

V-Plot: Shows fluorescence intensity (I, N, U) versus refolding time. Handwritten notes indicate: "Fluorescence intensity" and "refolding time". Below the plot, it says: " \Rightarrow More obvious to observe the kinetics" and "49".

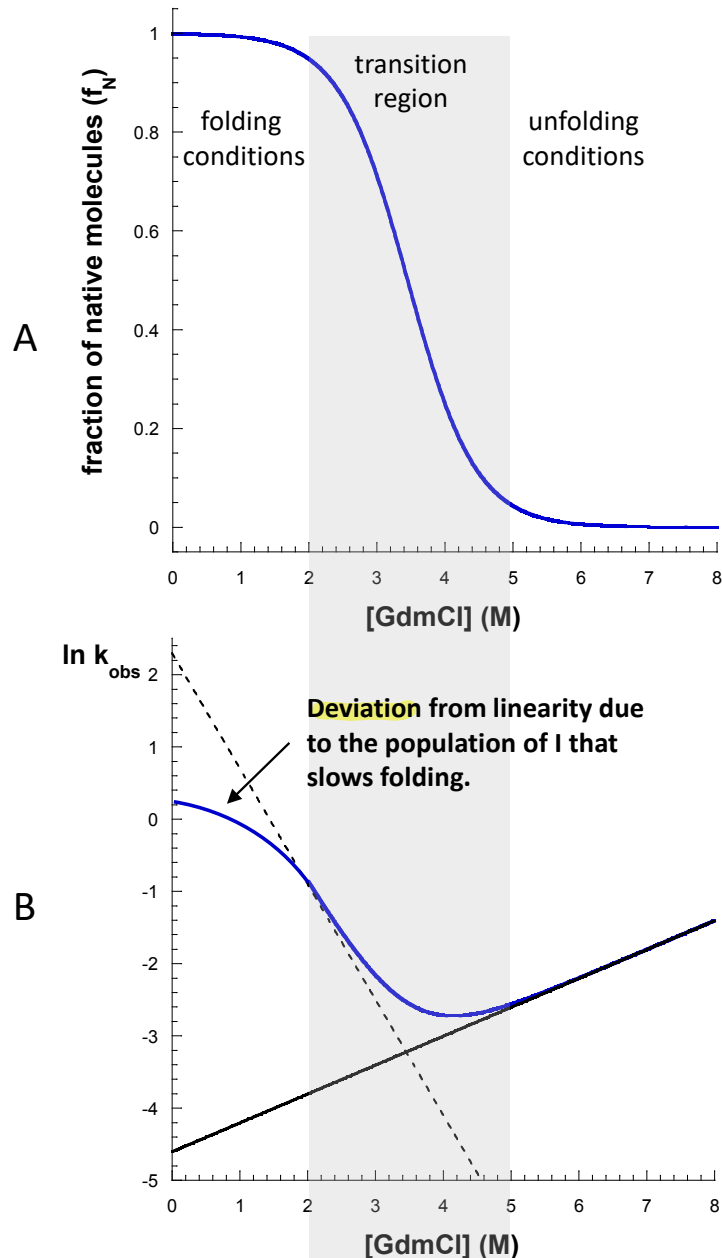
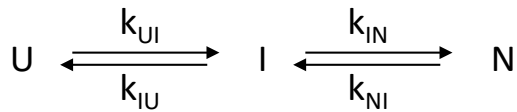


Figure 34 A: The formation of a structured, kinetic intermediate at low denaturant concentrations slows folding, causes a deviation from the linear dependence of $\ln k_u$ on denaturant concentration and lowers protein stability at zero or low denaturant concentration.

A: Equilibrium unfolding transition of protein that folds according to a $U \leftrightarrow I \leftrightarrow N$ mechanism. As I is not populated in the transition region, the equilibrium transition cannot be distinguished from a two-state $U \leftrightarrow N$ mechanism.

B: The population of I at low denaturant concentrations slows the folding reaction, but does not affect k_u .

For the quantitative evaluation of the V-plot of a protein that folds via a kinetic intermediate (Figure 34B) and the correct calculation of $\Delta G_{H_2O}^0$, the dependence of the logarithm of each of the four microscopic rate constants on denaturant concentration needs to be considered (equations 38–41):



$$\ln k_{UI} = \ln k_{UI}^{H_2O} + m_{UI} \cdot [D] \quad (38)$$

$$\ln k_{IU} = \ln k_{IU}^{H_2O} + m_{IU} \cdot [D] \quad (39)$$

$$\ln k_{IN} = \ln k_{IN}^{H_2O} + m_{IN} \cdot [D] \quad (40)$$

$$\ln k_{NI} = \ln k_{NI}^{H_2O} + m_{NI} \cdot [D] \quad (41)$$

Fitting of the V-plot for protein folding via a kinetic intermediate according to equations (38–41) is performed numerically. Analogous to a two-state mechanism (eq. 33), the equilibrium m-value (m_{eq}) can be deduced from the sum of the absolute values of all kinetic m-values according to equation (42):

$$m_{eq} = (|m_{UI}| + |m_{IU}| + |m_{IN}| + |m_{NI}|) \cdot RT \quad (42)$$

Kinetic intermediates are typically significantly less stable than N so that their population is in most cases negligible under physiological conditions (zero denaturant) after attainment of the folding equilibrium. Note however that this does not mean that kinetic intermediates disappear completely when the folding equilibrium is reached. For example, if I is 11.7 kJ less stable than N, a small fraction of 1% of the protein molecules will still populate the I state at equilibrium and zero denaturant. The stability of I relative to U and N relative to I can be calculated from the fitted values of $k_{UI}^{H_2O}$ and $k_{IU}^{H_2O}$, and $k_{IN}^{H_2O}$ and $k_{NI}^{H_2O}$, respectively.

Deviations from the ideal two-state V-plot are also observed for proteins that fold via a high-energy intermediate that is less stable than U and N at any denaturant concentration. In such a case, the high energy intermediate cannot be trapped and characterized experimentally, but detected indirectly via a curvature in the folding or unfolding limb of the V-plot when the rate-limiting transition state (TS1 or TS2) changes as a function of denaturant concentration, because TS1 and TS2 show different denaturant sensitivity. Figure 34 B shows an example for a protein that folds via a high-energy intermediate where TS1 is the rate-limiting transition state at zero or low denaturant concentrations, and TS2 is the rate-limiting transition state at high denaturant concentrations. The consequence of this switch of the rate-limiting transitions state leads to a kink in the unfolding limb of the V-plot at high denaturant concentrations. This example shows that recording of folding kinetics can provide information on the existence of high-energy intermediates. In this context, it is noteworthy that a pure two-state folding mechanism (only a single TS, straight folding and unfolding limbs) cannot be distinguished from a three-state mechanism with a high-energy intermediate that is less stable than U and N when the rate-limiting transition state (TS1 or TS2) is the same over the entire range of denaturant concentrations.

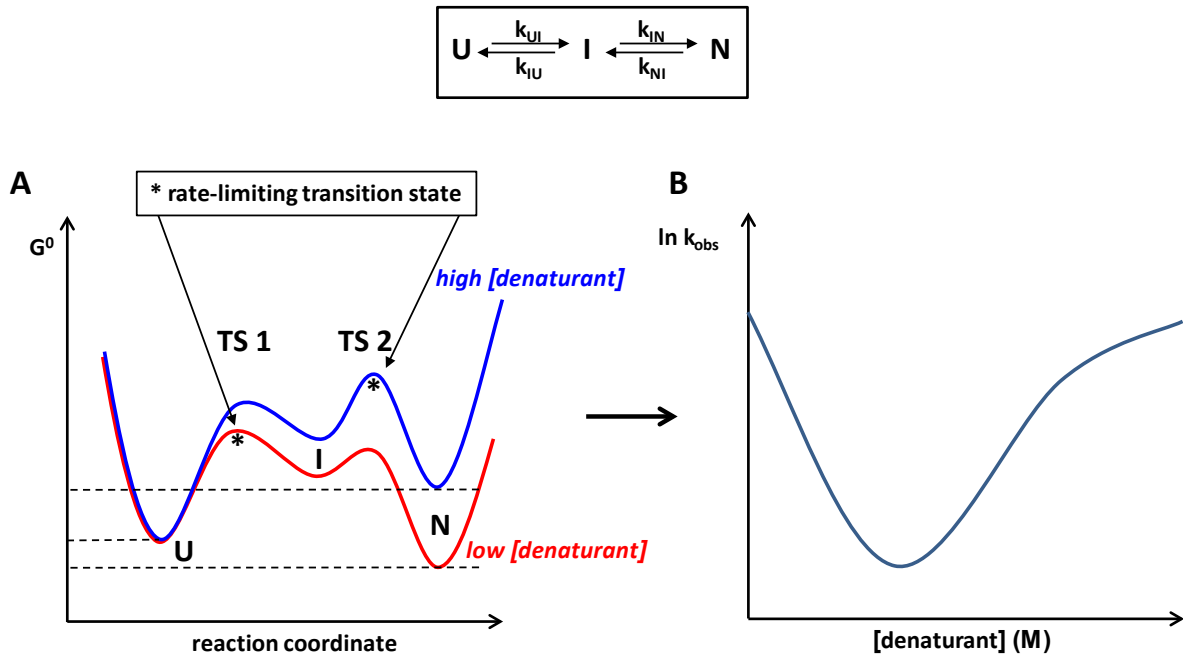
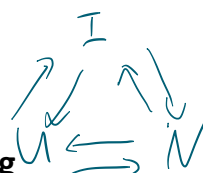


Figure 34 B: High energy intermediates I that are less stable than U and N under all conditions can also lead to deviations from the ideal V-plot when the rate-limiting transition state changes with increasing denaturant concentrations.

A: Energy diagram of a protein for which the rate-limiting transition state of folding/unfolding is TS1 at low and TS2 at high denaturant concentrations.

B: V-plot of the protein from (A), with a curvature in the unfolding limb caused by the switch from TS1 to TS2 as the rate-determining transition state.

Triangular folding model



Two states and three states
coexist

6. Slow reactions in protein folding

6.1. Proline cis/trans isomerization as the rate-limiting step in protein folding

Due to the double bond character of the peptide bond, it can only adopt two different conformations, *trans* and *cis*, which can be interconverted by a 180° rotation around the bond between the main chain carbonyl C atom and the amide nitrogen (Figure 35 A). The *trans* conformation is energetically highly favored due to the steric clashes in the *cis* conformation between the substituents of the C^α atoms on the same side of the peptide bond (Figure 34). In unstructured peptides or in the denaturant-induced unfolded state of proteins, the *cis/trans* equilibria of the peptide bonds are thus far on the *trans* side, with only about 0.1% of the molecules in *cis* under equilibrium conditions. However, there is an exception to this rule if the more C-terminal residue is a proline [16,17]: Proline is the only amino acid with a secondary amine group so that the main chain nitrogen of proline belongs to its 5-membered ring. The consequence is that there are also steric clashes in the *trans* conformation of Xaa-Pro peptide bonds (Xaa = any amino acid) in unfolded polypeptides between the C^δ methylene group of the proline ring and the substituents of the preceding C^α atoms. As the *trans* conformation is almost as unfavorable as *cis*, the equilibrium population of *cis* in Xaa-Pro

peptide bonds is much higher than in non-prolyl peptide bonds. For non-aromatic amino acids Xaa preceding Pro, the *cis* population varies between 6 and 14%, and is even higher for aromatic residues (Xaa=Phe: 23%; Tyr: 24%, Trp: 38%) [18]. In the following, we assume an average of 10% *cis* for the Xaa-Pro peptide bonds in unfolded proteins.

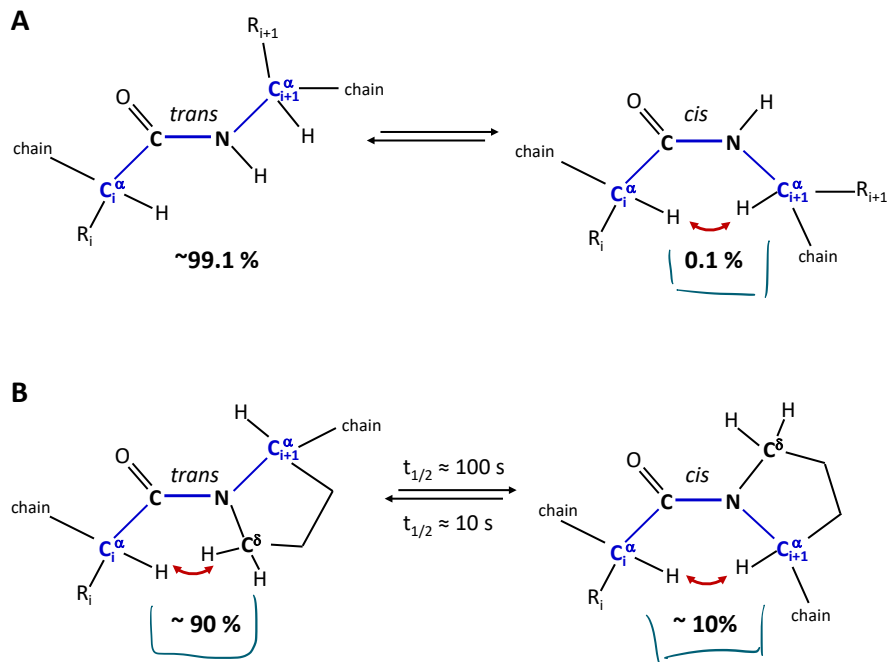


Figure 35: The *cis/trans* equilibrium of peptide bonds in short, unstructured peptides or in the denaturant-induced unfolded state of proteins. A: Non-prolyl peptide bonds. B: Peptide bonds where the more C-terminal amino acid is a proline. The red arrow indicates the energetically unfavorable steric hindrance for *cis* peptide bonds and *trans* Xaa-prolyl peptide bonds. R_i and R_{i+1} : side chains of residues i and i+1:

In non-prolyl peptide bonds, the *cis* conformation is roughly 20 kJ/mol less stable than *trans*. Therefore, *cis* non-prolyl peptide bonds are normally not found in three-dimensional structures of folded proteins, because it would cost too much energy and evolutionary effort to compensate for the incorporation of such an unfavorable *cis* peptide bond by additional interactions stabilizing N. The situation is however different for Xaa-Pro peptide bonds [16,17], because the incorporation of a *cis* Xaa-bond costs only about 5–6 kJ/mol which can easily be compensated by the overall free energy of protein folding with values up to –80 kJ/mol. This is the reason why nature has exploited the possibility to incorporate *cis* Xaa-Pro peptide bonds into three-dimensional protein structures. Indeed, about 6% of all Xaa-Pro peptide bonds in the known three-dimensional protein structures are in the *cis* conformation [18]! As proline is an amino acid with average frequency (5%), it follows that there is an about 50:50 chance that a protein of 100 amino acids contains one *cis* Xaa-Pro bond, and the probability of the occurrence of a *cis* Xaa-Pro bond increases with increasing mass of the protein.

For recording protein folding kinetics *in vitro*, the *cis/trans* equilibrium at each Xaa-Pro peptide bond in the unfolded state has important consequences, because the equilibrium is intrinsically slow: The *trans-to-cis* reaction typically shows a half-life of $\sim 100\text{ s}$ at 25°C with a

high activation energy barrier of about 80 kJ/mol (Figure 35), and the *trans*-to-*cis* reaction still has a half-life of ~ 10 s at 25°C. This leads to the following considerations:

- Proteins with a *cis* Xaa-Pro peptide bond in N cannot fold rapidly (on the millisecond time scale) when the refolding reaction starts will all Xaa-Pro peptide bonds of U are in *trans*, because the formation of a *cis*-Xaa-Pro bond proceeds with a half-life of ~ 100 s. Such slow folding rates favor protein aggregation during folding by unspecific hydrophobic interactions between exposed hydrophobic residues due to the long lifetime of U. Indeed, a specific class of enzymes termed peptidyl-prolyl-*cis/trans* isomerasases (PPIases, also termed proline isomerasases) catalyze the *cis/trans* isomerization of Xaa-Pro bonds and, together with molecular chaperones, contribute to the suppression of aggregation during folding *in vivo* and improve the yields of *in vivo* folding [20].
- A *cis/trans* equilibrium at each Xaa-Pro peptide bond in the unfolded state of a protein is attained already after several minutes of incubation at high denaturant concentration. This leads to a heterogeneity of the unfolded state, and this heterogeneity affects both the folding kinetics of proteins that contain and do not contain a *cis* Xaa-Pro bond in N.

The following example illustrates the consequences for protein folding kinetics:

We consider a small one-domain protein that has only a single proline residue that adopts the *cis* conformation the native state (N^{cis}). After unfolding of the protein at high denaturant concentration and several minutes of incubation, 10% of the unfolded molecules will still have the Pro in *cis* (U^{cis}) and 90% of the unfolded molecules will have the Pro in *trans* (U^{trans}). If N^{cis} can only be formed from U^{cis} and if $U^{cis} \rightarrow N^{cis}$ occurs rapidly with $t_{1/2} = 100$ ms, the refolding kinetics will be composed of 10% fast folding molecules that fold with a half-life of 100 ms, and 90% slow folders that fold with an apparent half-life of 100 s because the U^{trans} must first react to U^{cis} before these molecules can fold (Figure 36 A). If the single proline residue of the protein was however in *trans* in the native state (N^{trans}), then 90% of the molecules would fold rapidly with $t_{1/2} = 100$ ms, and 10% would fold slowly with a half-life of 10 s because N^{trans} can only be formed from U^{trans} and because the $U^{cis} \rightarrow U^{trans}$ reaction has a half-life of 10 s (Figure 36 B).

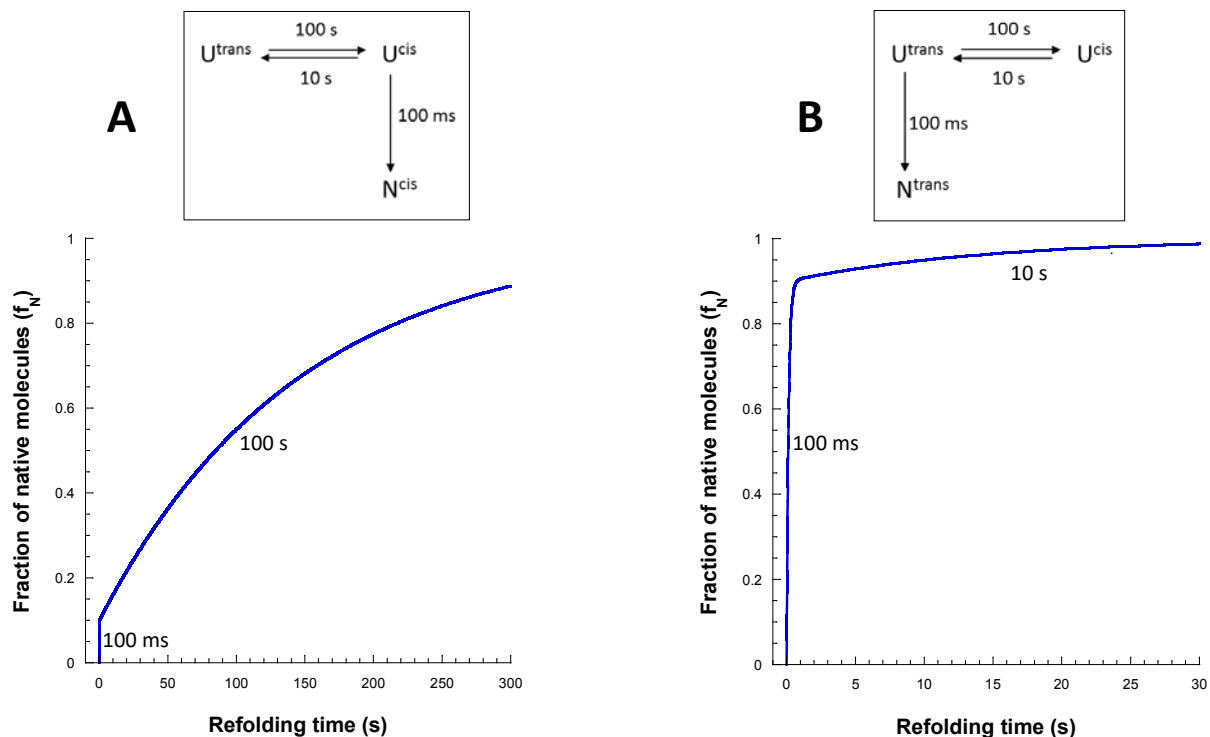


Figure 36: Influence of the *cis/trans* equilibrium of Xaa-Pro peptide bonds on the heterogeneity of U and protein refolding kinetics. A: Refolding kinetics of a protein containing only a single proline that adopts the *cis* conformation in N. B: Refolding kinetics of a protein containing only a single proline that adopts the *trans* conformation in N. Reaction half-lives at low denaturant concentration are indicated.

In more general terms, the *cis/trans* equilibria at each Xaa-Pro peptide bond in U lead to a mixture of fast and slow folding molecules.

The fraction of slow folding species can become considerably high even if N lacks *cis* Xaa-Pro peptide bonds! Due to the average frequency of 5.0% for proline in protein sequences, a 100-residue protein will have 5 proline residues on the average. If all five prolines are in *trans* in N, the probability that all 5 prolines are still in *trans* after unfolding by denaturant is $\sim 0.9^5 = 0.59$. Thus, only 59% of the molecules will be able to fold rapidly, while 41% of the molecules will fold slowly because they will have at least one nonnative *cis* proline in U when refolding is initiated. The situation is even more dramatic if one of the 5 prolines is in *cis* and 4 are in *trans* in N: then the probability that all five prolines in U are in the same conformation as in N is $0.1 \cdot 0.9^4 = 0.066$. Thus, only about 7% of the molecules will fold rapidly and the rest will fold slowly because at least one of the prolines needs to rearrange in U before folding can start.

What are now the consequences of the *cis/trans* isomerization of prolines in U for the determination of $\Delta G_{H_2O}^0$ by denaturant-induced equilibrium unfolding/refolding transitions (chapter 3)? Two scenarios are conceivable: First, if a protein unfolds and refolds faster at $[D_{1/2}]$ than the isomerization prolines in U, the prolines in all molecules will have the native conformation (*cis* or *trans*) when refolding starts. Second, if refolding at $[D_{1/2}]$ is slower than proline isomerization, nonnative prolines will accumulate in U under equilibrium conditions at

$[D_{1/2}]$. However, such a proline isomerization in U under equilibrium conditions has no influence on the symmetrical shape of equilibrium unfolding/refolding transitions, because the protein always exists as a mixture of N and U and the different proline conformers of U can be treated as a single state.

Proline isomerization in U can however make the recording the folding limb of V-Plots (refolding at low denaturant concentration) difficult. Note that the apparent rate constants of folding (k_F) recorded in V-plots represent only the folding rates of the fast folding species in which all prolines are in the native conformation when refolding is started. This means that the folding rates of the slow-folding species are not considered in the V-plot! The fraction of slow folding species can however become very high when i) a protein has many proline residues, even if they are all in *trans* in N, and ii) when a protein has a *cis* proline in N. In the latter case the fraction of fast folding molecules drops below 10% (see above), which makes the recording of the folding rate of the fast folding species very difficult and often impossible. This is exactly the reason why small proteins with a low content of prolines and lacking *cis* prolines have been chosen as model proteins for studying the mechanism of protein folding with V-plots.

In summary, the accumulation of slow-folding molecules with nonnative Xaa-Pro peptide bonds after protein unfolding at high denaturant concentration is an inevitable artefact of *in vitro* protein folding experiments, in which refolding is started by dilution from high to low denaturant concentration. In addition, only the fast-folding species are relevant for analyzing the folding mechanism with V-plots. Notably, the accumulation of slow-folding molecules with nonnative Xaa-Pro bonds is the main reason why the yields of *in vitro* refolding are often very low compared to folding *in vivo*. This is particularly true for larger proteins with a high number of prolines and proteins with *cis* prolines in N: The longer lifetime of U in slow folding species favors unspecific aggregation during refolding *in vitro*, while molecular chaperones prevent unspecific aggregation and folding catalysts like PPIases accelerate the folding of protein with *cis* prolines *in vivo*. Strategies to improve *in vitro* refolding yields are i) refolding at low protein concentrations to suppress unspecific aggregation and ii) refolding at low temperatures and low salt concentrations to weaken unspecific hydrophobic interactions.

6.2. Disulfide bond formation as the rate-limiting step in protein folding

Structural disulfide bonds are a typical feature of secretory proteins. In most secretory proteins, structural disulfide bonds increase protein stability by destabilization of U and not by stabilization of N! The destabilization of U is caused by the decrease in chain entropy of U through the loop introduced by the disulfide (Figure 37 A). The loss of chain entropy increases with increasing loop size, so that disulfide bonds between cysteine pairs that are distant in the polypeptide sequence are often more stabilizing than disulfide bonds between cysteines close in the sequence. The fundamental difference between the folding of proteins with disulfide bonds and proteins lacking disulfides is that proteins with disulfide bonds in N cannot form spontaneously. Instead, disulfide bond formation is a *redox reaction* that can only occur when

a polypeptide interacts with an oxidant that accepts the two electrons released upon disulfide formation (Figure 37 B) [21]. Therefore, disulfide bond formation is always rate limiting for folding if a protein has structural disulfide bonds!

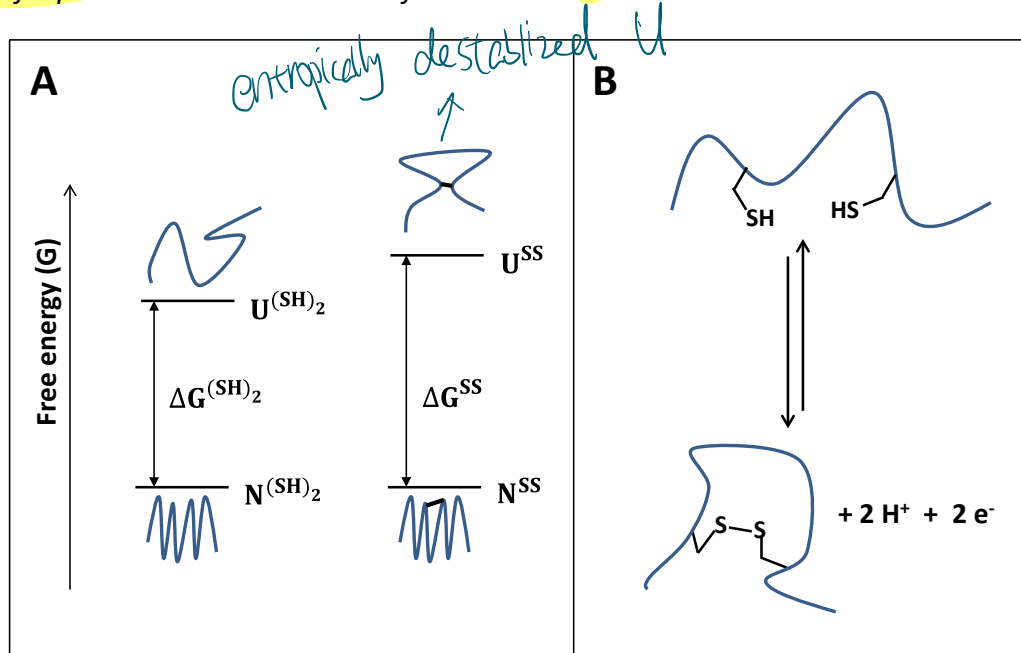


Figure 37: Structural disulfide bonds stabilize secretory proteins by decreasing the chain entropy of U (A). However, they cannot form spontaneously unless the polypeptide chain interacts with an oxidant that accepts the two electrons generated upon disulfide bond formation. $\Delta G^{(SH)_2}$ and ΔG^{SS} : thermodynamic stability of the reduced and oxidized (disulfide bonded) protein.

The final oxidant of disulfide bonds in eukaryotes and in bacteria growing under aerobic conditions is molecular oxygen. However, direct oxidation of cysteine pairs by oxygen is very slow, so that disulfide bond formation *in vivo* is always catalyzed by enzymes of the family of thiol/disulfide oxidoreductases. Each member of this enzyme family has at least one reactive cysteine pair that can form a disulfide bond. This disulfide bond is then transferred to thiol pairs of the folding secretory protein by disulfide exchange (Figure 38). Disulfide exchange reactions involve the nucleophilic attack of the enzyme's disulfide bond by a cysteine thiolate of the substrate protein, which leads to the transient formation of a covalent mixed disulfide between substrate and enzyme. The mixed disulfide is then attacked by the thiolate of a second cysteine of the polypeptide substrate, which generates a disulfide bond in the substrate and the reduced, dithiol form of the enzyme:

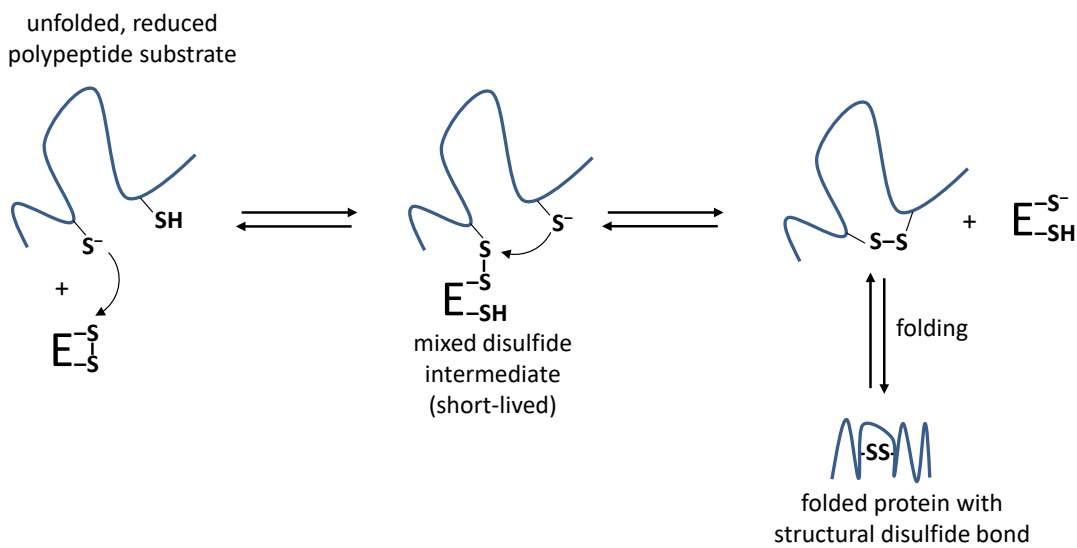


Figure 38: Mechanism of formation of structural disulfide bonds *in vivo* via disulfide exchange with the oxidized (disulfide) form of a thiol/disulfide oxidoreductase (E). Thiol/disulfide oxidoreductases have particularly reactive active-site cysteines with lowered pK_a values (4–7) compared to the normal pK_a of a cysteine thiol of ≈ 9. As structural disulfides are generally buried in folded proteins, their cysteines are only accessible for disulfide exchange with the enzyme when the protein is still unfolded. Disulfide formation thus must precede folding.

All members of the thiol-disulfide oxidoreductase family catalyzing disulfide bond formation are located in oxidizing cellular compartments. In eukaryotes, disulfide bond formation is catalyzed by protein disulfide isomerase (PDI) in the endoplasmic reticulum (ER). PDI is an essential enzyme in all eukaryotes. The transfer of a disulfide bond from PDI to a polypeptide substrate can already occur during secretion to the ER, but also after completion of translocation and signal sequence cleavage (Figure 39). The transfer of a disulfide from the active site of PDI to a substrate generates the reduced (dithiol) form of PDI, which needs to be reoxidized to its disulfide form for the next catalytic cycle. The reoxidation of PDI occurs via disulfide exchange with the ER membrane-associated enzyme Ero1p. Ero1p requires FAD as cofactor, which allows the transfer of oxidizing equivalents from oxygen to a cysteine pair on the surface of Ero1p under formation of hydrogen peroxide (Figure 39). Consequently, molecular oxygen is the oxidant required for disulfide bond formation in any eukaryotic, secretory protein. PDI not only catalyzes disulfide bond formation, but also the isomerization (rearrangement) of wrong (non-native) disulfide bonds in substrate proteins. This activity is particularly important for correct folding of proteins with multiple disulfide bonds, because the probability of forming nonnative disulfides increases dramatically with the number of disulfide bonds in a secretory protein.

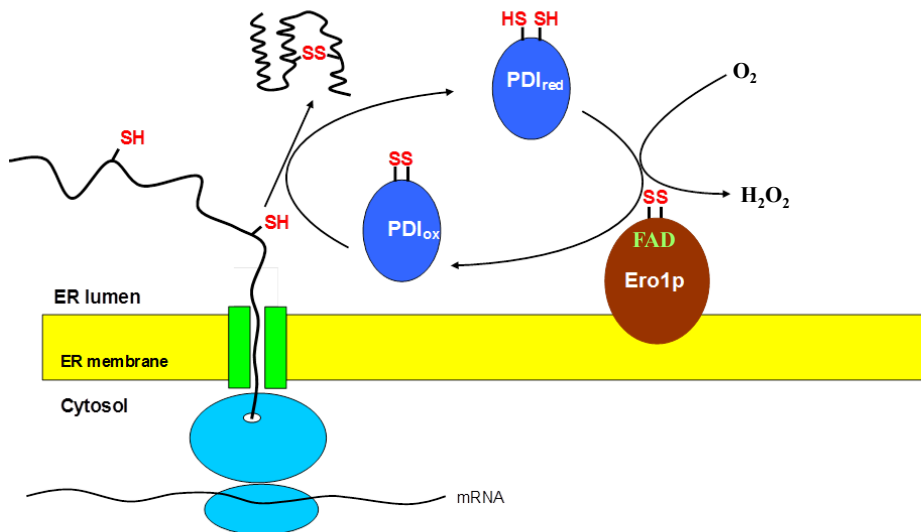


Figure 39: Disulfide bond formation in the endoplasmic reticulum. Disulfide bonds are introduced into secretory proteins by protein disulfide isomerase (PDI). This can either happen co-translationally/co-translocationally as depicted in the figure, or post-translocationally. Reduced PDI is converted back to oxidized PDI by disulfide exchange with Ero1p, which in turn is reoxidized by molecular oxygen under formation of hydrogen peroxide. Ero1p has an essential FAD cofactor that is required for transferring electrons from its active-site cysteine pair to oxygen.

The inter-membrane space of mitochondria is the second cellular compartment of eukaryotes in which proteins with structural disulfide bonds occur. The mechanism of catalyzed disulfide bond formation is similar to that in the ER [23]. The protein Erv1 is functionally equivalent to Ero1P and, like Ero1p, can convert oxidizing equivalents of oxygen to a disulfide bond on the surface of the protein. The functional equivalent of PDI is a small protein termed Mia40, receives a disulfide bond through disulfide exchange with Erv1 and passes it on to substrates (Figure 40).

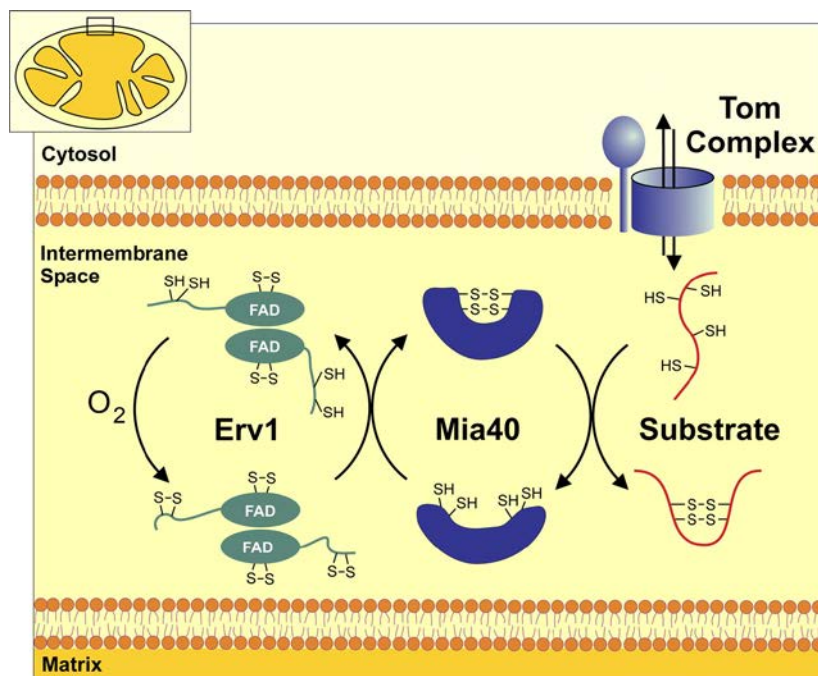


Figure 40: Disulfide bond formation in proteins of the inter-membrane space of mitochondria. Disulfide bonds are introduced into substrate proteins via disulfide exchange with the oxidoreductase Mia40. Mia40 is oxidized by molecular oxygen via Erv1, an FAD-dependent oxidoreductase that is a functional homolog of Ero1p in the endoplasmic reticulum (Adapted from Herrmann & Köhl, *J. Cell. Biol.* 176, 559, 2007).

In Gram-negative bacteria, proteins with structural disulfides only occur in the periplasmic space. Here, the pathways of disulfide bond formation and isomerization are distinct [24]. The dithiol oxidase DsbA introduces disulfide bonds, and the disulfide isomerase DsbC catalyzes the rearrangement of wrong disulfides introduced by DsbA. Notably, the pathway of disulfide formation via DsbA is more complex in bacteria compared to the ER and involves components of the respiratory system. Specifically, the disulfide bond of DsbA is regenerated by oxidation of reduced DsbA by ubiquinone, a reaction catalyzed by the membrane protein DsbB. The electrons are then transferred from ubiquinol to molecular oxygen via terminal oxidases under aerobic conditions. Under anaerobic conditions, menaquinone reoxidizes DsbA, and the reduced menaquinol passes the electrons on to alternate electron acceptors such as fumarate (Figure 41).

DsbA randomly introduces disulfide bonds into proteins with multiple disulfide bonds. This may generate completely oxidized substrate proteins with nonnative disulfide bonds that cannot rearrange their disulfide bonds spontaneously. The intramolecular isomerization of disulfide bonds is only possible when at least one of the nonnative disulfide bonds is reduced again so that free thiol groups of the substrate can attack nonnative disulfide bonds and dissolve them. The reduction of nonnative disulfides is catalyzed by the disulfide isomerase DsbC, which however needs to be kept reduced for being active as a catalyst in an otherwise strongly oxidizing compartment. This is achieved with the specific reduction of DsbC by the membrane protein DsbD. DsbD has the unique ability of passing on electrons from thioredoxin in the cytoplasm to DsbC in the periplasm. Eventually, the reducing equivalents for DsbC come from NADPH, because thioredoxin reductase catalyzes the reduction of thioredoxin by NADPH (Figure 41).

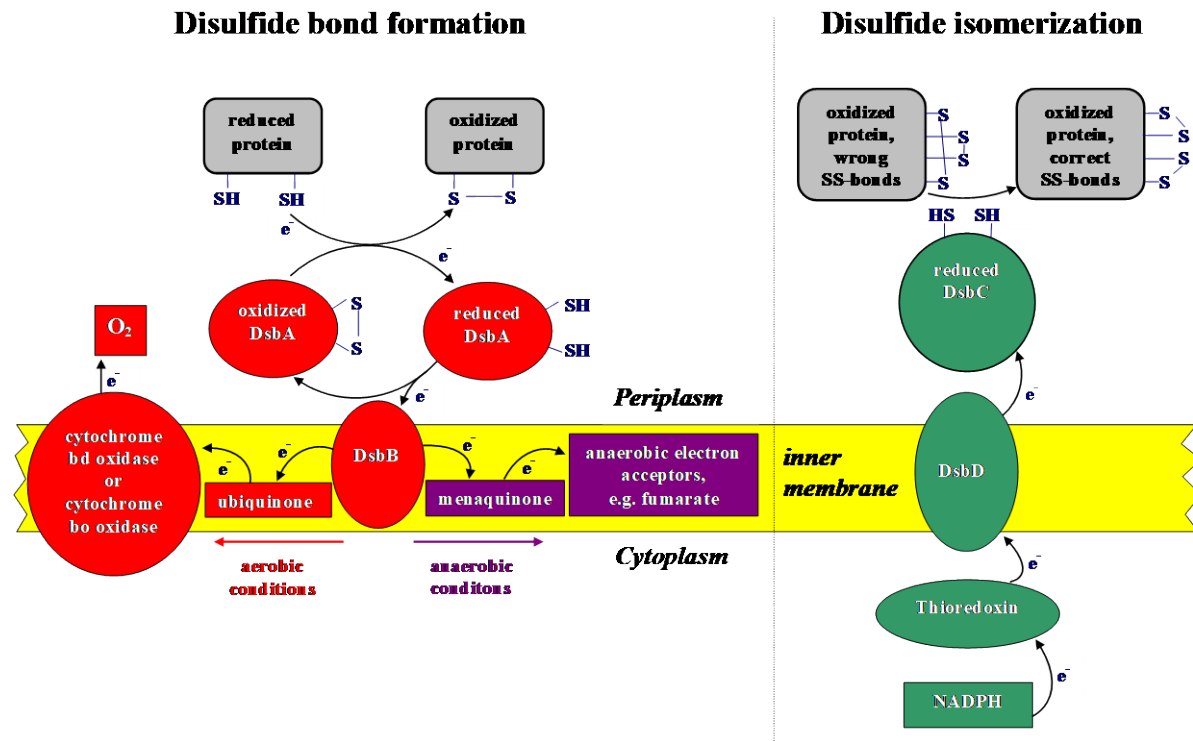


Figure 41: Disulfide bond formation in the periplasm of Gram-negative bacteria (*Escherichia coli*) is composed of an oxidative and reductive pathway.

Left panel: Disulfide bonds are introduced into folding proteins in the periplasm by the dithiol oxidase DsbA. The reoxidation of DsbA by ubiquinone from the respiratory pathway is catalyzed by the membrane protein DsbB. Under aerobic conditions, the reduced ubiquinol transfers its electrons to molecular oxygen via terminal cytochrome oxidases. Under aerobic conditions, DsbA is reoxidized by menaquinone with the transfers its electrons to alternate electron acceptors.

Right panel: Disulfide bond isomerization in proteins with multiple disulfide bonds is catalyzed by DsbC. DsbC is kept in its catalytically active, reduced state by the membrane protein DsbD, which receives its electrons via thioredoxin from cytoplasmic NADPH. The arrows always indicate the transfer of two electrons.

Disulfide bond formation *in vitro*: Oxidative refolding of proteins

The fact that disulfide bonds can only form in oxidizing cellular compartments, but not in the reducing environment of the cytoplasm, has important consequences for the recombinant production of secretory proteins. There are two possibilities to obtain recombinant proteins with intact disulfide bonds from *Escherichia coli*, the most frequently used host organism for recombinant protein production: First, the N-terminus of the recombinant protein can be fused to a bacterial signal sequence that mediates transport of the protein to the periplasm and DsbA/DsbC-catalyzed disulfide bond formation *in vivo*. The soluble, folded protein can then be purified from the periplasmic extract with conventional chromatographic techniques. The yields of the correctly folded, disulfide bonded recombinant protein in the periplasm can often be increased by co-expression of DsbA or DsbC and, in the case of proteins with multiple disulfide bonds, by addition of glutathione (GSH, see below) to the growth medium [25]. The second possibility is the production of the secretory protein without signal sequence in the cytoplasm where the protein cannot fold and will form insoluble aggregates. These insoluble aggregates are also termed “inclusion bodies” and can accumulate in surprisingly large quantities, with protein yields of several 100 mg per liter of bacterial culture (Figure 42).

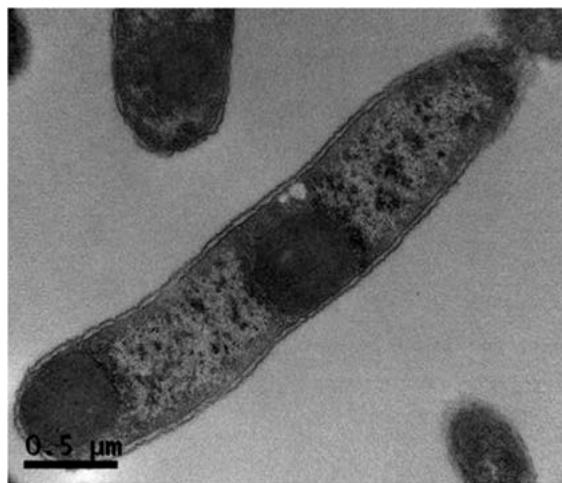
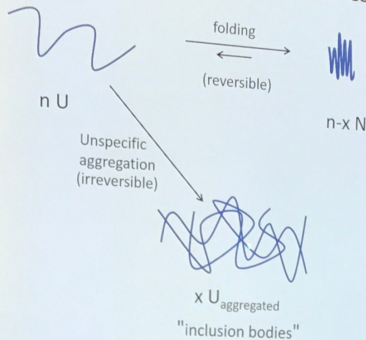


Figure 42: Electron micrograph of ab *E. coli* cells in which a recombinantly expressed protein does not fold and forms large amounts of insoluble aggregates termed “inclusion bodies” (dark spots) (adapted from Soundrarajan et al, Sci. Rep. 6, 20661, 2016).

After cell lysis, the inclusion bodies can be separated from all soluble proteins with a simple centrifugation step and are then be dissolved by high concentrations of GdmCl. Subsequently, the reduced, unfolded proteins need to be refolded *in vitro* under conditions that allow disulfide bonds formation [26]. The refolding reaction is initiated by rapid dilution with buffer solutions containing a *thiol/disulfide redox system*. Note that any disulfide exchange reaction requires the nucleophilic attack of a thiolate anion on a disulfide. As the pK_a of cysteine thiols is around 9, the rates of disulfide exchange reactions strongly decrease with decreasing pH. The pH values used in oxidative refolding reactions are typically kept between 8 and 9 to

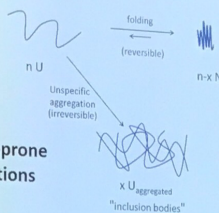
Competition between protein folding and aggregation



Parameters that determine the YIELD of protein folding

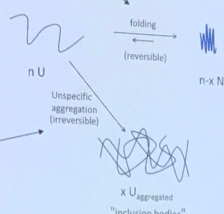
In vitro protein folding yields of aggregation-prone proteins can be increased by choosing conditions that disfavour unspecific, intermolecular hydrophobic interactions:

- Low temperature
- Low ionic strength
- Low protein concentration (*in vivo*: weaker expression)



Molecular chaperones and folding catalysts suppress unspecific aggregation during protein folding *in vivo*

- **Protein folding catalysts** make folding faster and lower the life time of the aggregation-prone, unfolded state.
There are two families of folding catalysts:
 - Proline cis/trans isomerases
 - Dithiol oxidases and protein disulfide isomerase



- **Molecular chaperones** prevent unspecific aggregation by transient binding to unfolded or partially folded polypeptides.

guarantee sufficient population of the thiolate anion forms of all free thiols. The most frequently used redox system for oxidative refolding of proteins *in vitro* is composed of a mixture of glutathione (GSH) and glutathione disulfide (GSSG). In most eukaryotic organisms and in many bacteria, GSH is highly abundant and, together with GSSG, serves as a redox buffer that regulates the redox state of the cell and protects it from oxidative damage. GSH is a tripeptide composed of γ -glutamate, cysteine and glycine, in which the γ -carboxylate of the glutamate forms an isopeptide bond with cysteine. GSSG is composed of two disulfide-linked molecules of GSH (Figure 43).

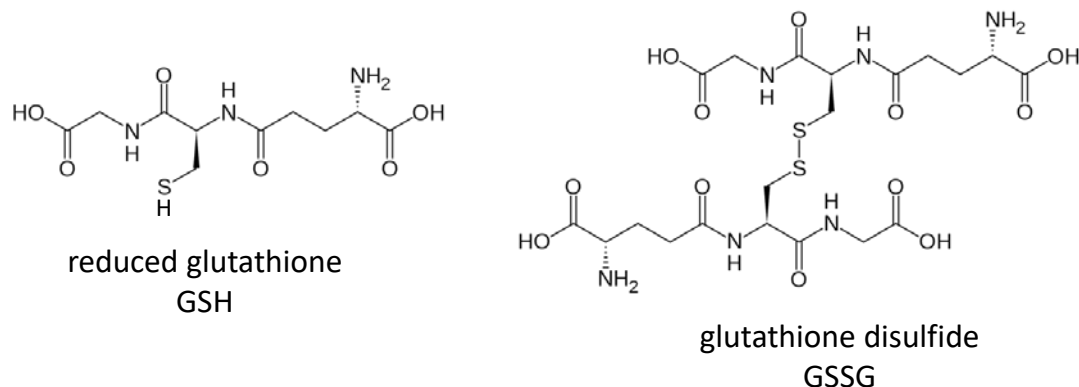


Figure 44: Covalent structures of the glutathione (GSH) and glutathione disulfide (GSSG)

Figure 45 shows that three types of reactions can be distinguished during oxidative refolding of a protein in the presence of GSH/GSSG redox buffers:

- **Disulfide bond formation:** GSSG is used as the oxidant for cysteine pairs in the protein. The disulfide bond of GSSG is attacked by a free thiolate of a cysteine in the protein, and a mixed disulfide intermediate between glutathione and the protein is formed. This mixed disulfide is then attacked intramolecularly by a second thiolate of the protein, which generates the disulfide bond in the protein and two equivalents of GSH (Figure 45, top panel).
- **Intramolecular disulfide rearrangement:** Once the first disulfide bond is formed in the protein, it can be attacked intramolecularly by any other free thiolate. This intramolecular equilibrium between different disulfide forms favors formation of the most stable, native disulfides.
- **Catalysis of disulfide isomerization of completely oxidized proteins with wrong disulfide bonds by GSH:** If all thiol pairs in the protein become completely oxidized by GSSG and non-native disulfides accumulate, the non-native disulfides can no longer rearrange spontaneously to the native disulfide configuration if the polypeptide lacks an unpaired thiol that could attack a nonnative disulfide. Rearrangement of wrong disulfides is then only possible if at least one disulfide is reduced by an external reductant (GSH). If the protein to be refolded has a high number of disulfide bonds, the probability that nonnative disulfides accumulate is particularly high, and oxidative

refolding becomes more efficient if more GSH is included to dissolve nonnative disulfides. Indeed it has turned out that the highest refolding yields of proteins with multiple disulfide bonds are often obtained with an excess of GSH over GSSG (e.g. 5 mM GSH and 1 mM GSSG). Note that structural disulfides in proteins do not only stabilize the tertiary structure of the protein, but in turn are also stabilized by the tertiary structure. This makes *native* disulfides in folded proteins particularly stable against reduction by GSH, so that an excess of GSH over GSSG does not prevent the formation of all native disulfide bonds and folding to the native state.

Whether secretion to the periplasm or oxidative refolding from inclusion bodies *in vitro* leads to higher yields of recombinant protein with disulfide bonds needs to be determined empirically. In the case of proteins with multiple disulfide bonds, it is often found that oxidative refolding *in vitro* is the more efficient method. This is due to the high amounts of reduced, unfolded protein that can be obtained from solubilized inclusion, so that even low yields of *in vitro* refolding may eventually lead to higher amounts of the folded protein per liter of bacterial culture compared to periplasmic secretion.

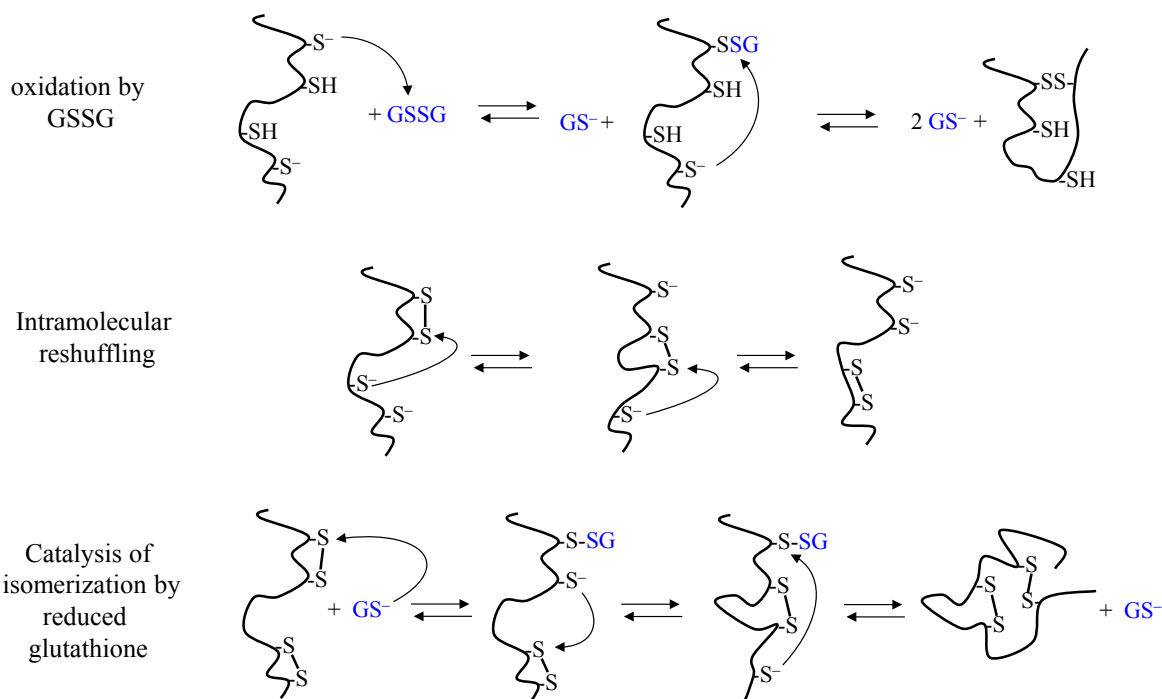


Figure 45: Mechanism of oxidative refolding of secretory proteins *in vitro* with glutathione redox buffers. Three types of reactions can be distinguished: *in vitro* with GSH/GSSG

Top: Disulfide bond formation via disulfide exchange with glutathione disulfide (GSSG).

Middle: Intramolecular disulfide reshuffling.

Bottom: Catalysis of disulfide isomerization in fully oxidized polypeptides with scrambled disulfides by reduced glutathione (GS⁻).

7. Analysis of complex folding reactions: Test for native molecules by interrupted refolding experiments.

As discussed in chapter 1, the energy landscape of protein folding may be rough, and there can be parallel pathways leading to N (Figure 3). For example, it may be that a fraction of the molecules can fold directly and rapidly to N, while the other fraction folds slower via the transient population of a kinetic intermediate (Figure 46 A). In such a case, it is not trivial to elucidate the folding mechanism in quantitative terms if the spectroscopic signal of I and the fractions of the molecules folding directly to N or via I are unknown. In addition, the fraction of fast and slow folding species is often difficult to determine when the folding rate of a fraction of the molecules is limited by proline *cis/trans* isomerization (chapter 6.1). Even in the simpler case of a consecutive folding mechanism discussed in chapter 5.2 (see also Figure 46 B), it may not be possible to determine the concentration of N during folding if I and N cannot be distinguished spectroscopically.

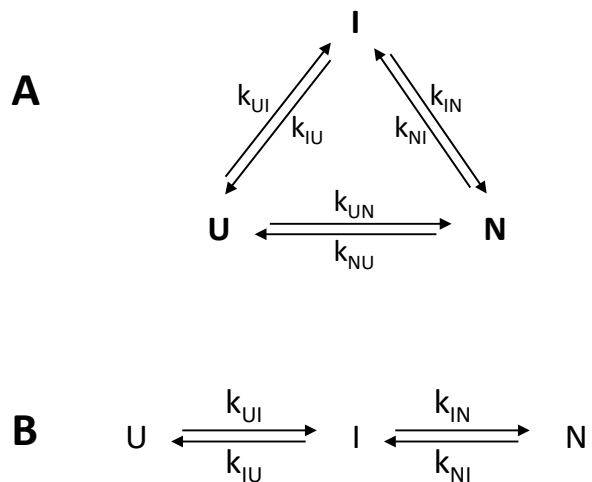


Figure 46: Folding mechanisms that are difficult to elucidate. A: Triangular folding mechanism with parallel pathways to N. N is formed either directly from U, or U first folds to a kinetic intermediate that reacts further to N. B: Even a simpler, consecutive pathway that is followed by all molecules may be difficult to characterize if I and N cannot be distinguished spectroscopically.

The solution to this problem is a method that allows the detection of the concentration of N at any time during the refolding reaction, termed *interrupted refolding* [27]. Let us discuss the application of this method in the context of a specific example (Figure 47): We consider a protein follows a consecutive folding mechanism in which all molecules follow the same $U \rightarrow I \rightarrow N$ pathway, and I is formed from U with half-life of 1 s and N is formed from I with a half-life of 10 s at low denaturant concentration. In addition, we assume that I, by coincidence, has the same spectroscopic properties as N and thus cannot be distinguished from N. Thus, only the $U \rightarrow I$ reaction is visible when the folding reaction is monitored and the $I \rightarrow N$ reaction is spectroscopically silent. The spectroscopic trace will thus appear like a direct $U \rightarrow N$ reaction although the formation of N is delayed by the slower $I \rightarrow N$ reaction (Figure 47).

↗ enzyme
 ↓
 65
 of intermediate
 In enzymatic reaction, the activity
 may be same as N state molecules.

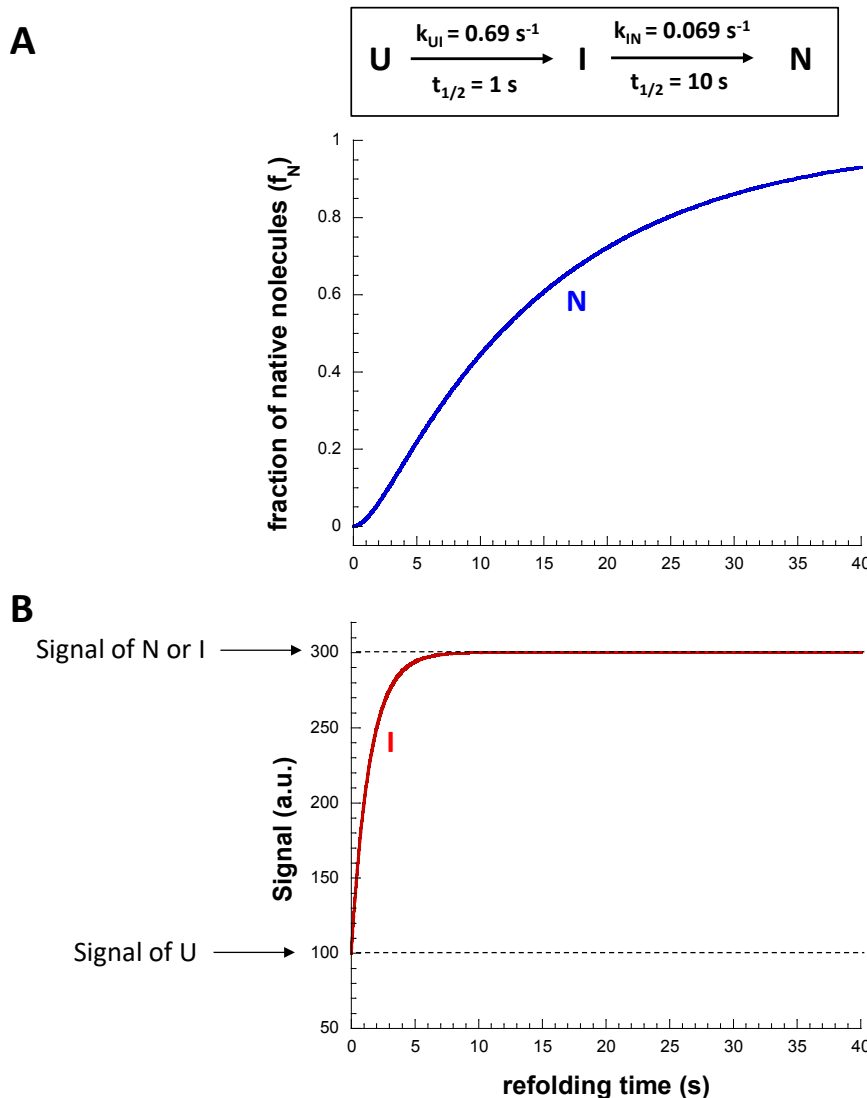


Figure 47. Example of a folding reaction in which the change in the spectroscopic signal does not report on the formation of native molecules.

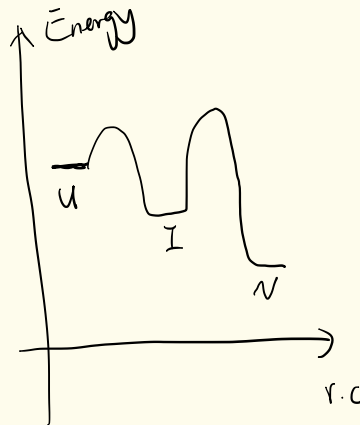
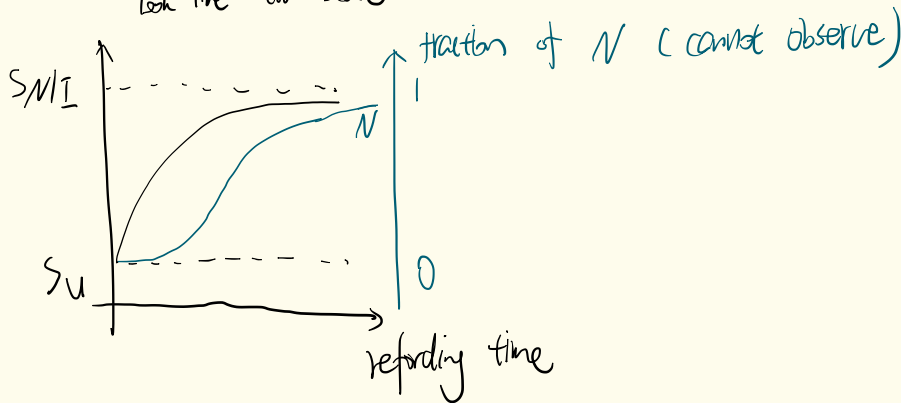
A: We consider a sequential folding mechanism $U \rightarrow I \rightarrow N$ in which the half-life of the $U \rightarrow I$ reaction is 1 s and the half-life of the $I \rightarrow N$ reaction is 10 s. The formation of N (blue solid line) shows a lag-phase and a half-life of ~ 11.5 s.

B: Observed spectroscopic signal change during refolding (red solid line) for the case that the $I \rightarrow N$ reaction is spectroscopically silent, with a signal of 100 a.u. for U and 300 a.u. for I or N. Note that the observed kinetics for the $U \rightarrow I$ reaction perfectly follow first-order kinetics, suggesting that N forms with a half-life of 1 s. However, N is formed much slower, which can only be detected with interrupted refolding experiments (see Figure 48).

Interrupted refolding experiments allow the determination of the fraction of native molecules at any time during a folding reaction! They are based on the fact that N is the most stable state of a protein, and that any other conformation is less stable against unfolding and unfolds faster. Figure 48 A shows the workflow of interrupted refolding: The refolding reaction is interrupted after different refolding times by addition of high concentrations of denaturant, and the corresponding unfolding reactions are monitored. The final denaturant concentration in the unfolding reaction is chosen such that it is high enough to achieve complete unfolding.

where if I and N cannot be distinguished spectroscopically?

look like two state



→ "N test" or interrupted refolding experiment



fast

slow
add high [GdnCl]
so that all molecules
will eventually be
unfolded

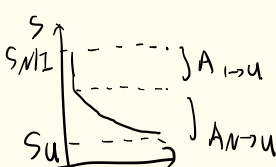


example: after refolding the t with 50% I
spectroscopic signal

50% N

$$\begin{aligned} S(t) = & S_u + A_{I \rightarrow u} e^{-k_{I \rightarrow u} t} \\ & + A_{N \rightarrow u} e^{-k_{N \rightarrow u} t} \end{aligned}$$

select $[GdnCl]$ such
that N unfolds with $t_{1/2} \approx 100s$



In our specific example (Figure 47), the unfolding reactions monitored after different times of refolding will be composed of two phases: A fast phase corresponding to the rapid unfolding of intermediates and a slow phase corresponding to the unfolding of native molecules present after the respective refolding time (Figure 48 B). The observed signal change in each unfolding reaction can be described by the sum of two exponential functions (equation (43)),

$$S = S_U + A_{\text{fast}} \cdot e^{-k_{\text{fast}} \cdot t} + A_{\text{slow}} \cdot e^{-k_{\text{slow}} \cdot t} \quad (43)$$

where S is the observed spectroscopic signal, t is the unfolding time, S_U is the signal of U (final signal after complete unfolding), and k_{fast} and k_{slow} are the rate constants of unfolding of I and N , and A_{fast} and A_{slow} are the amplitudes of the fast and the slow phase, respectively.

The concentration of N prior to the initiation of unfolding is directly proportional to A_{slow} , and the fraction of N after refolding time t ($f_N(t)$) before the start of unfolding can be calculated from the ratio between A_{slow} and the unfolding amplitude after completion of refolding ($A_{\text{slow}} / 100\% N$) according to equation (44):

$$A_{\text{slow}} \sim [N]; \quad f_N(t) = \frac{A_{\text{slow}}(t)}{A_{\text{slow}} 100\% N} \quad (44)$$

Figure 49 A shows unfolding traces recorded after different times of refolding: After short refolding times, the majority of the molecules is in state I and unfolds rapidly (high A_{fast} value), and the small fraction of already formed native molecules unfolds slowly (small A_{slow}). With increasing refolding time, A_{fast} then decreases and A_{slow} increases. The kinetics of formation of N during refolding are then obtained by plotting A_{slow} or f_N against refolding time (Figure 49 B).

Note that interrupted refolding experiments are the only possibility to monitor the formation of N if the folding mechanism is more complex than simple two-state folding! A particular advantage of interrupted refolding is that it is independent of the spectroscopic method used to monitor unfolding, and independent of the spectroscopic properties of U , I and N .

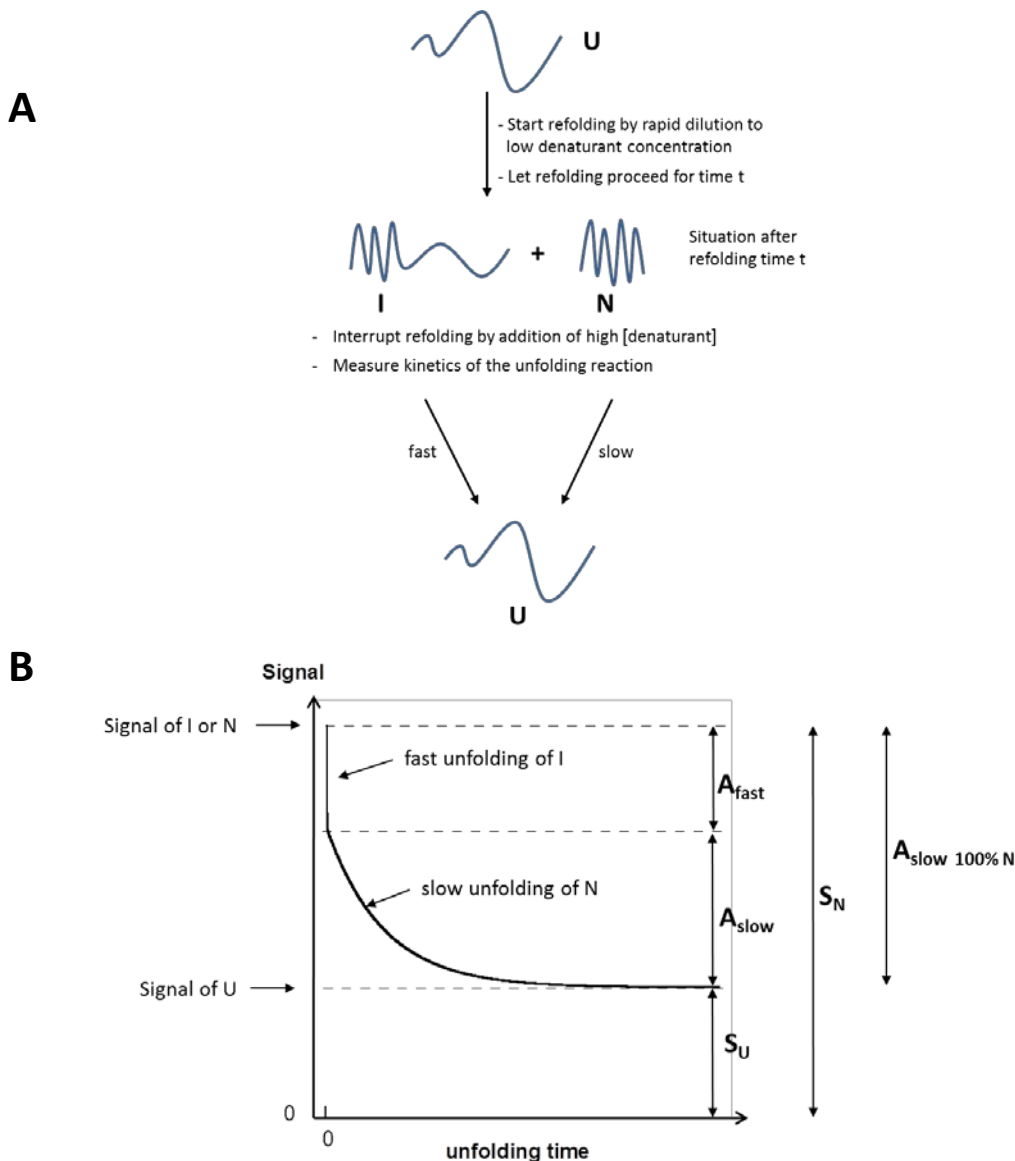


Figure 48: Determination of the concentration of **N** at any time during a protein folding reaction by interrupted refolding experiments (N-tests):

A: Principle and experimental protocol of interrupted refolding experiments.

B: Example of the recorded signal change of the unfolding reaction for the case that unfolding was interrupted when the refolding reaction consisted of a mixture of 60% **N** and 40% **I**, assuming and $\text{U} \rightarrow \text{I} \rightarrow \text{N} \rightarrow \text{U}$ mechanism in which **I** and **N** have identical spectroscopic signals.

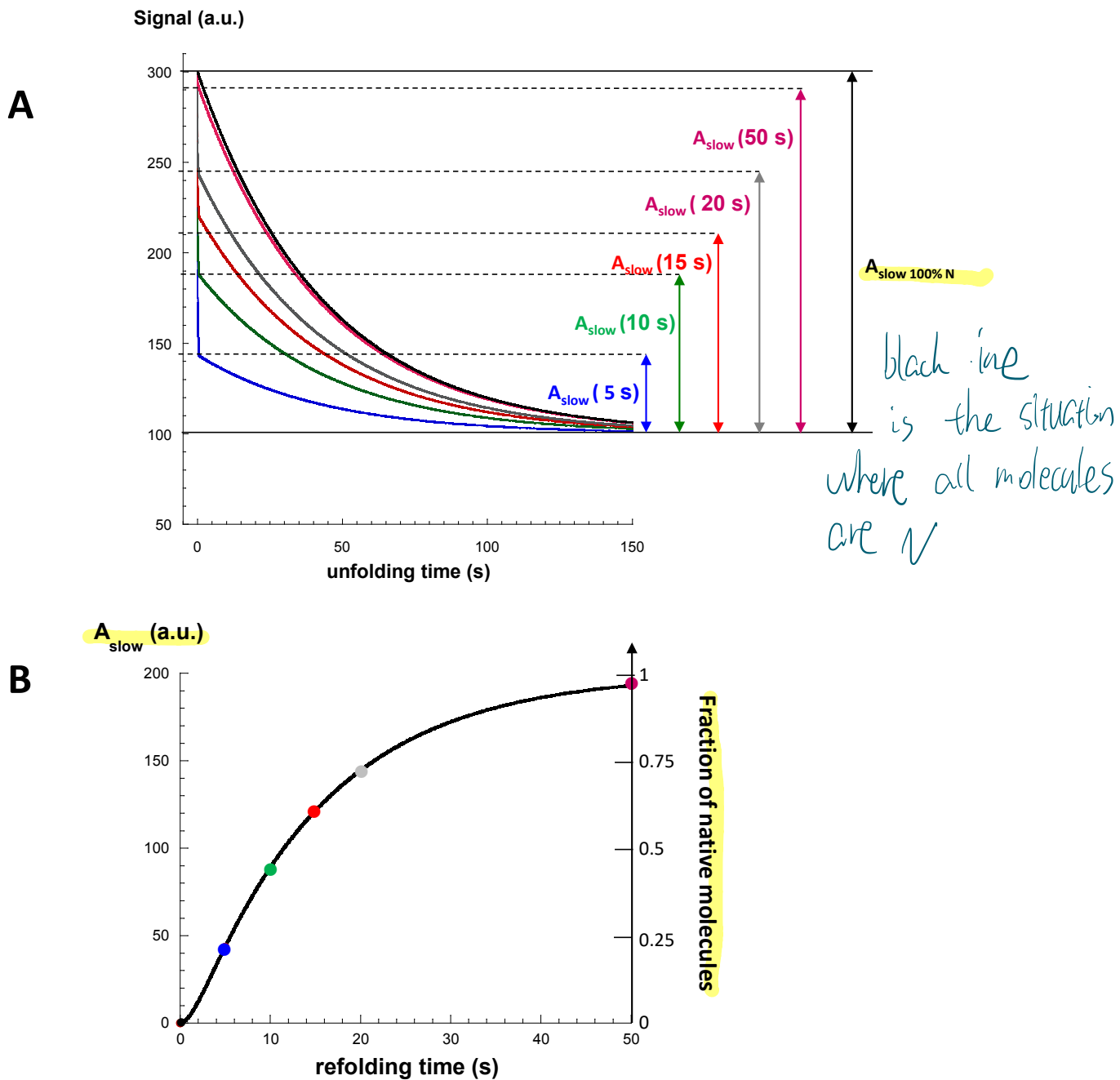


Figure 49: Quantification of native molecules during the refolding reaction in Figure 48 by interrupted refolding.

A: Spectroscopic signal change recorded after interrupting refolding by addition of high denaturant concentration. At the chosen denaturant concentration, N unfolds with a half-life of 30 s, and I unfolds with a half-life of 0.1 s. The spectroscopic signal of U is 100 arbitrary units (a.u.), and the signal of N or I is 300 a.u.. Unfolding traces are shown for unfolding reactions started after 5, 10, 15, 20, or 50 s of refolding ($t = 0$ is the time when denaturant was added).

B: The amplitudes of the slow unfolding phases (A_{slow}) recorded in A were plotted against the respective refolding time prior to addition of the denaturant and fitted to a sequential $\text{U} \rightarrow \text{I} \rightarrow \text{N}$ mechanism (solid black line). Normalization of the data to the maximum value of A_{slow} yields the fraction of N after the respective refolding times (right y-axis).

8. References

- [1] Anfinsen CB, 1973, Principles that govern the folding of protein chains *Science* 181, 223-230.
- [2] Dill KA and MacCullum JL., 2012, The protein folding problem, 50 years on. *Science* 338, 1042-1046.
- [3] Levinthal C, 1969, Are there pathways for protein folding? *J. Chim. Phys.* 65, 44-45.
- [4] Schmid FX, 2005, Spectroscopic techniques to study protein folding and stability. *Protein folding handbook* (Buchner J, Kieffhaber T eds), Wiley, pp. 22-44.
- [5] Tanford C, 1968, Protein denaturation. A. Characterization of the denatured state. B. Transition from native to denatured state. *Adv. Protein Chem.* 23, 121-282.
- [6] Pace CN, Grimsley GR and Scholz JM, 2005, Denaturation of proteins by urea and guanidine hydrochloride. *Protein folding handbook* (Buchner J, Kieffhaber T eds), Wiley, pp. 45-69.
- [7] Myers, JK, Pace CN and Scholz MJ (1995) Denaturant m values and heat capacity changes: Relation to changes in accessible surface areas of protein unfolding. *Protein Sci.* 4, 2138-2148.
- [8] Jaenicke R, 1987, Folding and association of proteins, *Prog. Biophys. Mol. Biol.* 49, 117-237.
- [9] Becktel WJ and Schellman, JA, 1987, Protein stability curves, *Biopolymers* 26, 1859-1877.
- [10] Makhatadze GI, 2005, Thermal unfolding of proteins studied by calorimetry. *Protein folding handbook* (Buchner J, Kieffhaber T eds), Wiley, pp. 70-98.
- [11] Privalov PL. 1979, Stability of proteins. Small globular proteins. *Adv.Protein. Chem.* 33, 167-241.
- [12] Jackson SE and Fersht, AR, 1991, Folding of chymotrypsin inhibitor 2: 1. Evidence for a two-state transition, *Biochemistry* 30, 10428.
- [13] Fersht, AR, 1999, Structure and Mechanism in Protein Science, Freeman, New York.
- [14] Matouschek, A, Otzen, DE, Itzaki, LS, Jackson, SE and Fersht, AR, 1995, Movement of the position of the transition state in protein folding. *Biochemistry* 34, 13656-13662.
- [15] Li, AJ and Daggett, V, 1996, Characterization of the transition state of protein unfolding by use of molecular dynamics: Chymotrypsin inhibitor 1. *Proc. Natl. Acad. Sci. USA* 92, 10869.

- [16] Brandts, JF, Halvorson, HR and Brennan M, 1975, Consideration of the possibility that the slow step in protein denaturation reactions is due to cis-trams isomerism of proline residues. *Biochemistry* 14, 4953-4963.
- [17] Fischer G and Schmid FX, 1990, The mechanism of protein folding. Implications of in vitro refolding models for de novo protein folding and translocation in the cell, *Biochemistry* 29, 2205-2212.
- [18] Reimer U, Scherer G, Drwello M, Kruber S, Schutkowski M and Fischer G, 1998, Side chain effects on peptidyl-prolyl cis/trans isomerization. *J. Mol. Biol.* 279, 229-260.
- [19] Jabs A, Weiss MS, and Hilgenfeld R. 1999, Non-proline cis peptide bonds in proteins. *J. Mol. Biol.* 286, 291-304.
- [20] Schmidpeter PA and Schmid FX, 2015, Prolyl isomerization and its catalysis in protein folding and function. *J. Mol. Biol.* 427, 1609-1631.
- [21] Glockshuber R, 1999, Protein folding. Where do the electrons go? *Nature* 401, 30-31.
- [22] Oka OB and Bulleid NJ, 2013, Forming disulfides in the endoplasmic reticulum. *Biochim. Biophys. Acta* 1833, 2425-2429.
- [23] Herrman JM and Köhl R, 2007, Catch me if you can! Oxidative protein trapping in the intermembrane space of mitochondria. *J. Cell. Biol.* 176, 559-563.
- [24] Kakodura H and Beckwith J, 2010, Mechanisms of oxidative protein folding in the bacterial cell envelope. *Antiox. Redox Signal.* 13, 1231-1246.
- [25] Maskos K, Huber-Wunderlich M and Glockshuber R, 2003, DsbA- and DsbC-catalyzed oxidative folding of proteins with complex disulfide patterns in vivo and in vitro. *J. Mol. Biol.* 325, 495-513.
- [26] Weissman JS and Kim PS, 1991, Reexamination of the folding of BPTI: Predominance of native intermediates. *Science* 253, 1386-1393.
- [27] Schmid FX, 1983, Mechanism of folding of ribonuclease A. Slow refolding is a sequential reaction via structural intermediates. *Biochemistry* 22, 4690-4696